

Saldaeva, Elena (2010) Through thickness air permeability and thermal conductivity analysis for textile materials. PhD thesis, University of Nottingham.

Access from the University of Nottingham repository:

<http://eprints.nottingham.ac.uk/13140/1/537646.pdf>

Copyright and reuse:

The Nottingham ePrints service makes this work by researchers of the University of Nottingham available open access under the following conditions.

- Copyright and all moral rights to the version of the paper presented here belong to the individual author(s) and/or other copyright owners.
- To the extent reasonable and practicable the material made available in Nottingham ePrints has been checked for eligibility before being made available.
- Copies of full items can be used for personal research or study, educational, or not-for-profit purposes without prior permission or charge provided that the authors, title and full bibliographic details are credited, a hyperlink and/or URL is given for the original metadata page and the content is not changed in any way.
- Quotations or similar reproductions must be sufficiently acknowledged.

Please see our full end user licence at:

http://eprints.nottingham.ac.uk/end_user_agreement.pdf

A note on versions:

The version presented here may differ from the published version or from the version of record. If you wish to cite this item you are advised to consult the publisher's version. Please see the repository url above for details on accessing the published version and note that access may require a subscription.

For more information, please contact eprints@nottingham.ac.uk



**The University of
Nottingham**

Through thickness air permeability
and thermal conductivity analysis
for textile materials

GEORGE GREEN LIBRARY OF
SCIENCE AND ENGINEERING

Elena Saldaeva

Thesis submitted to The University of Nottingham
for the degree of Doctor of Philosophy

January 2009

To my dear parents who have been around all these years to support, protect and
inspire me for all the achievements I have done.

This is my way to thank them and say how much I adore my lovely mum and dad.

Huge thanks to my beloved parents-in-law for their endless love and support.

I am very lucky to have you in my life. Love you.

To my wonderful men, husband Mayank and our son Arthur. You have been with me
every step of the way, through good times and bad. Thank you for all the
unconditional love, guidance, and support that you have always given me, helping me
to succeed and instilling in me the confidence that I am capable of doing anything I
put my mind to. I love you!

Посвящаю моим любимым родителям, которые на протяжении этих лет
поддерживали, оберегали меня и придавали мне уверенности в своих силах. Я
вас очень сильно люблю, мои папуля и мамуля.

Моему маленькому герою, моему сыночку Артурчику. Ты сделал мою жизнь
ярче и осмысленней.

Моему любимому Маянку, воплотившему мои мечты в реальность.

Main tahe dil se apne patidev ki shukragujar hoon jis ki maded se main ye theses
pura kar saki, yah main unhe samarpit karti hoon.

ABSTRACT

Woven fabrics have found enormous application in our daily life and in industry because of their flexibility, strength and permeability. The aim of this work was to create a general model for through thickness air permeability and thermal conductivity for different types of textile fabrics because of their applications in industries and everyday life. An analytical model to predict through thickness air permeability was developed. The objective was to create a model which will take into consideration the two primary mechanisms of air flow in fabrics: through the gaps between yarns and through the yarns. Through thickness air permeability was measured according to British Standard BS EN ISO 9237:1995. Several fabrics were tested including plain weave, twill weave and satin weave fabrics. The analytical model is a combination Kulichenko and Van Langenhove's analytical model which predicts the permeability through gaps between yarns with Gebart's model to predict permeability within yarns. Analytical predictions were compared to the experimental data.

Computational modelling of through thickness air permeability using Computational Fluid Dynamics CFD software is presented in this thesis. The Polymer Composites Research Group in the University of Nottingham has created a textile schema, named TexGen. The prerequisites of this software were to be able to model various types of textile structures. A CFD model using CFX 11.0 was developed to be able to predict fabric permeability.

In addition, an analytical model was developed for fabrics deformed by shear, compaction and tension. Experimental work for through thickness air permeability of sheared fabric was used to verify predicted results.

An analytical model for thermal conductivity of fabrics was developed including the influence of moisture content on thermal conductivity. Two existing approaches for single-layer fabrics are described and compared: rule of mixtures and thermal resistance approach. A method for thermal conductivity prediction for multiple layer fabrics is presented. The results are compared to the experimental data and analysed.

Through thickness air permeability and thermal conductivity analysis for textile materials

Some predicted results were in excellent and good agreement with experimental data whereas other predicted results were in poor agreement with experimental data as they were dramatically affected by the assumptions made in the analytical model.

ACKNOWLEDGEMENTS

The work described in this thesis would not have been possible without the help and support of various individuals and organisations. I extend my foremost gratitude to my supervisors, Professor Andrew Long, Dr. Michael Clifford and Dr. Hua Lin, for sharing their vision and knowledge as well as for their patience with me. Their valuable suggestions, comments and continued support made me work hard and enthusiastically. Their experience and knowledge introduced me to the technicalities of high level academic writing as well as research method.

I would also like to thank the Head of the Department of Mechanical, Materials and Manufacturing Engineering, Professor Paul Shayler, for the use of the Department facilities. The technical support given by Roger Smith and Geoff Tomlinson is gratefully thanked. I would also like to thank Dr. David Allinson and Dr. Matthew Hall from School of Built Environment for the use of laboratory facilities as well as for constant help and support. The support of the project partners: Unilever UK Central Resources, OCF PLC, Croda Chemicals Europe Ltd, University of Manchester, Heriot-Watt University, ScotCad Textiles Ltd, Carrington Career and Workwear Ltd, Moxon Ltd, Airbags International, Technitex Faraday Ltd. Special thanks to Mr. Simon Watson and Mr. Noel Ruddock from Unilever for help with understanding CFX 11.0 software.

Thank you to all my colleagues at the Polymer Composites Research Group in the University of Nottingham who made my time here enjoyable and unforgettable. I felt real support and friendly attitude to me. I am also grateful to all my friends from Russia, France, India and America for their support throughout of these years. Special thanks to my dearest friend Sheela who was very supportive and encouraging throughout of these years.

Last but not least, I want to thank and dedicate this work to my parents, Valery Saldaev and Ludmila Lisenko, whose endless love, support and understanding made this long route easier. I would not have enough strength and courage to undertake this project without your love. My warmest thank to my boys, my man Mayank and our son Arthur, for being here for me throughout of this journey, brightening my days and

Through thickness air permeability and thermal conductivity analysis for textile materials

always making me laugh. My warmest love to my dearest parents-in-law, Pradeep and Anshu Shukla who believed in me and help me all the way through. My dear ones, your love made me believe in myself.

CONTENTS

Abstract.....	i
Acknowledgements.....	ii
Nomenclature.....	ix
Glossary.....	xi
1 Introduction	
1.1 Textile fabrics.....	1
1.2 Thesis framework.....	2
1.3 Overview of thesis.....	3
2 Literature review on permeability and thermal conductivity of porous fabrics	
2.1 Introduction.....	5
2.2 Multiscale nature of fabric.....	6
2.3 Permeability prediction using analytical models.....	8
2.4 Permeability prediction using computational models.....	16
2.5 Experimental approach and Forchheimer equation.....	23
2.6 Permeability prediction for deformed fabrics.....	29
2.7 Thermal conductivity prediction using analytical models.....	35
2.8 Current developments.....	56
3 Permeability prediction of textiles using analytical methods	
3.1 Introduction.....	58

- 3.2 Development of analytical model for through thickness air permeability of fabrics.....59
 - 3.2.1 Analytical model of air flow through gaps.....59
 - 3.2.2 Analytical model of air flow through yarns.....61
 - 3.2.3 Analytical model of air flow through whole fabric.....62
- 3.3 Experimental measurement of through thickness permeability
 - 3.3.1 Air permeability.....63
 - 3.3.2 Oil permeability.....64
- 3.4 Results and analysis.....67
- 3.5 Conclusion.....74

- 4 Permeability modelling of through fabric thickness using TexGen and CFD
 - 4.1 Introduction.....76
 - 4.2 Modelling approach
 - 4.2.1 Geometric modelling of unit cell using TexGen software.....77
 - 4.2.2 Computational modelling of unit cell using CFX 11.0.....79
 - 4.3 Sensitivity study.....82
 - 4.4 Results and analysis.....84
 - 4.5 Advantages and disadvantages of CFD approach.....90
 - 4.6 Conclusions.....90

- 5 Through thickness air permeability prediction for deformed fabrics
 - 5.1 Introduction.....92
 - 5.2 Development of analytical model for through thickness air permeability of deformed fabrics.....93
 - 5.2.1 Pure shear.....93

5.2.2	Compaction.....	96
5.2.3	Tension.....	97
5.3	Experimental measurement of through thickness permeability of deformed fabrics.....	98
5.4	Results and analysis.....	99
5.4.1	Experimental results.....	99
5.4.2	Predicted results using analytical model.....	100
5.4.3	Comparison between predicted results and experimental data.....	106
5.5	Conclusions.....	107
6	Thermal conductivity of fabrics	
6.1	Introduction.....	108
6.2	Experimental measurements of fabric thermal conductivity	
6.2.1	Experimental set-up.....	109
6.2.2	Experimental results and analysis.....	111
6.3	Development of analytical model for thermal conductivity of fabrics.....	114
6.4	Comparison between measured and predicted results.....	117
6.5	Experimental measurement of moisture content for fabrics	
6.6.1	Experimental set-up.....	119
6.6.2	Experimental results and analysis.....	120
6.6.3	Study of influence of moisture content on thermal conductivity of fabrics.....	121
6.6	Conclusions.....	123
7	Discussion and conclusions	
7.1	Introduction.....	125
7.2	General discussion.....	126

7.3 Recommendations for the future work.....	129
7.4 Conclusions.....	130
References.....	132
Appendix A Publications.....	143
Appendix B Image J.....	144
Appendix C TexGen.....	149
Appendix D CFX 11.0 Software.....	158

NOMENCLATURE

A	Area	mm^2
B	Permeability	m^2
d	Yarn width	mm
d_h	Hydraulic pore diameter	m
d^{max}	Maximum width reduction of warp yarn	mm
g	Acceleration due to gravity	m/s^2
k	Thermal conductivity	$\text{W}/(\text{m}\cdot\text{K})$
k_K	Kozeny constant	-
L^{def}	Length of deformed gap	mm
L	Looseness factors	-
m_e	Number of yarns in warp direction	ends/100mm
m_p	Number of yarns in weft direction	picks/100mm
M_f	Fabric area density	kg/m^3
p	Pressure	Pa
ΔP	Pressure drop	Pa
Q	Flow rate	mm^3/s
r	Fibre radius	mm
R	Thermal resistance	$\text{K}\cdot\text{m}\cdot\text{W}^{-1}$
s	Yarn spacing	mm
S	Resistance to flow	$\text{K}\cdot\text{m}\cdot\text{W}^{-1}$
t	Thickness	m
τ_{ij}	Shear stresses	Pa
v	Velocity	m/s
V_f	Fibre volume fraction	-
V_a	Yarn packing fraction	-
W^{def}	Width of deformed gap	mm

GREEK SYMBOLS

α	Porosity	-
β	Forchheimer coefficient	-
Δ	Half of distance between two fibres	mm
μ	Dynamic fluid viscosity	Pa·s
ρ	Fibre density	kg/m ³
θ_L	Locking angle	degrees
θ_s	Shear angle	degrees
w	Water content	-

SUBSCRIPTS

A	Air
e	Warp
f	Fabric
F	Fibre
g	Gap
h	Hydraulic
i	i-th conduction element
L	Locking
m	Material
p	Weft
s	Spacing
UC	Unit cell
w	Width
W	Water
x	Along
y	Yarn
z	Perpendicular

SUPERSCRIPTS

<i>0</i>	Initial
<i>an.</i>	Analytical
<i>CFD</i>	Computational Fluid Dynamics
<i>def</i>	After deformation
<i>exp.</i>	Experimental
<i>max</i>	Maximum value
<i>pred.</i>	Predicted

GLOSSARY

<i>Bleaching</i>	Process which improves whiteness by removing natural colouration and remaining trace impurities from the cotton; the degree of bleaching necessary is determined by the required whiteness and absorbency.
<i>CFD</i>	Computational Fluid Dynamics. One of the branches of fluid mechanics that uses numerical methods and algorithms to solve and analyze problems that involve fluid flows.
<i>CFX 11.0</i>	A commercial Computational Fluid Dynamics (CFD) program, used to simulate fluid flow in a variety of applications.
<i>Compaction</i>	Process when the weight compresses the fabric, causing it to lose pore space.
<i>Desizing</i>	Process of removing the size material from the yarns in woven fabrics.
<i>Dyeing</i>	Process of imparting colors to a textile material in loose fibre, yarn, cloth or garment form by treatment with a dye often referred to as thread or

yarn.

Fabric

A flexible material consisting of a network of natural or artificial fibres.

Forchheimer equation

Extended Darcy's law which applies for a sufficiently high flow velocity.

Mercerizing

Process during which the fabric is treated with caustic soda solution to cause swelling of the fibres.

Moisture content

Quantity of water contained in a material.

Permeability

A measure of the ability of a material to transmit fluids.

Porosity

A measure of the void spaces in a material.

Scouring

Chemical washing process carried out on cotton fabric to remove natural wax and non-fibrous impurities (eg the remains of seed fragments) from the fibres and any added soiling or dirt.

Shear

Occurrence of a shear strain, which is a deformation of a material substance in which parallel internal surfaces slide past one another.

Shear angle

The reduction in angle between the warp and weft yarns from their original configuration to their sheared configuration.

TexGen

Software which models the geometry of a fabric

unit cell.

Thermal conductivity Property of a material that indicates its ability to conduct heat.

Through thickness permeability Permeability in direction perpendicular to the yarns.

Warp Set of lengthwise yarns.

Weave A method of interlacing yarns or yarns to form a fabric.

Weft Yarn which is drawn under and over parallel warp yarns to create a fabric.

Yarn An assembly of fibres to form a continuous length that is suitable for use in making textile fabrics.

CHAPTER 1

INTRODUCTION

1.1 TEXTILE FABRICS

Textile fabrics are relatively thin, flexible, porous sheet materials. Most of them can bend and fold easily. Textile fabrics consist of yarns, which in turn consist of fibres. Textile fabrics can be loose or tight depending on the amount of pores in their structure. Woven fabrics are that in which yarns are interlaced at an angle to each other.

Because of their flexibility, strength and permeability, woven fabrics have found enormous application in our daily lives and in industry for example, sports clothing, clothing protecting from rain, wind and heat, airbags for road vehicles, geotextiles etc. In the garment industry, fabric comfort is a most important property. Clothing comfort includes three main aspects: psychological, which is related to fashion, tactile which includes fabric surface and mechanical properties, and thermal comfort related to the ability of a fabric to control the temperature of the skin through heat and moisture transfer [1]. The comfort of fabrics depends on several factors: heat and water vapour transport, sweat absorption and drying, permeability or impermeability, weight etc. In addition, fabric comfort depends on the properties of each fabric layer and the combination of all the worn layers. To create a high performance fabric cloth, a designer considers fashion and other technical factors: fibre nature and size, surface modification of fibres, hydrophobic (repelling water) or hydrophilic (absorbs water) membranes fused to a textile layer, weaving pattern, and abrasion of the fabric surface. In addition, for technical fabrics like airbags, permeability and thermal conductivity properties are very important due to their application. During vehicle collision, airbags can experience a rapid rise in heat when they inflate. It is important to know how permeability changes with pressure as airbags fabrics may experience a very high pressure changes in a very short period of time. Inflating of the airbag happens in 0.04s with the force of $3.33 \times 10^4 \text{N}$ [84]. In addition, airbags fabrics will deform during inflation which leads to a change in permeability.

Experimental work as well as analytical and computational approaches have been used to predict different fabric comfort parameters. Permeability is one of the comfort factors which has been widely studied since last century. Permeability is the ability of a material to transmit fluids. It was first described by Darcy's law [2]. It is important for both clothing and airbag fabrics because in the case of clothing, permeability supports comfort of the person wearing it, keeping the body cool or warm whenever it is needed. In the case of airbags, permeability is important for the inflation and deflation of the airbag. Another important comfort parameter is thermal conductivity, which indicates the ability of material to conduct heat. It is important to be able to predict thermal conductivity of clothing fabrics as it will help to achieve optimal body temperature. For airbag fabrics it is important to know thermal conductivity as inflation can lead to a rise in temperature which may cause changes in properties of airbag fabrics. The first clothing model that described the mechanism of transient diffusion of heat and moisture transfer into an assembly of hygroscopic (attracts water from environment through absorption or adsorption) textile materials was introduced and analyzed by Henry in 1939 [61]. Recently CFD modelling has become more popular to predict fabric permeability and thermal conductivity as it can give good predictions without simplifying assumptions used in analytical models (more details see Chapter 2).

1.2 PROJECT FRAMEWORK

The work described in this thesis was performed within the Technology Strategy Board project "Materials modelling: Multi-Scale Integrated Modeling for High Performance Flexible Materials", which was supported by several industrial partners: Unilever UK Central Resources, OCF PLC, Croda Chemicals Europe Ltd, ScotCad Textiles Ltd, Carrington Career and Workwear Ltd, Moxon Ltd, Airbags International, Technitex Faraday Ltd. It also included three research groups from different universities: University of Nottingham, University of Manchester and Heriot-Watt University. The main objectives of the project related to this thesis are: develop 'unit cell models' for a variety of weaves; generate computational models automatically using the Nottingham TexGen schema; develop a CFD model to predict through thickness air permeability; model thermal conductivity of fabrics; through thickness permeability, thermal conductivity and moisture content measurement and validation of the unit cell model; develop a model to predict permeability of deformed

Through thickness air permeability and thermal conductivity analysis for textile materials

fabrics; to model the behaviour of flexible materials in a 3D manner, taking into account the dynamic changes of performance related properties with physical changes during use; mechanical measurements and validations of yarn model; model mechanical properties of yarn and unit cell using Finite Element (FE) method.

Following the project objectives, the aim of this thesis was to create a general model for through thickness air permeability and thermal conductivity including moisture content using analytical and computational methods for different types of textile fabrics. An analytical model for deformed (shear, compaction and tension) fabrics was developed. Experimental work was carried out for fabric permeability (air and oil) and thermal conductivity to verify predicted results.

1.3 OVERVIEW OF THE THESIS

This thesis presents research carried out into predicting through thickness permeability and thermal conductivity of textile structures. An analytical model to predict through thickness air permeability (which includes both permeability through yarns and permeability between yarns) has been developed. The objective was to create a model which will take into consideration these two mechanisms of air flow in fabrics. Analytical predictions were compared to experimental data. Several fabrics were tested including plain weave, twill weave and satin weave fabrics. A CFD model was also developed using TexGen and CFX 11.0. In addition, an analytical model was developed for deformed fabrics. The main deformation mechanisms included shear, compaction and tension. Experimental work for through thickness air permeability of sheared fabric was used to verify predicted results. An analytical model for thermal conductivity of fabrics was developed including the influence of moisture content. The structure of the thesis is outlined below.

Chapter 2 provides a literature review on air permeability and thermal conductivity prediction. The fundamental theory relating to flow through porous media and the definition of permeability is presented. Experimental, theoretical and computational work on permeability of undeformed and deformed fabrics and thermal conductivity is presented. Gaps in previous research on the prediction of textile through thickness permeability and thermal conductivity are identified.

Chapter 3 describes the development of an analytical model to predict through thickness air permeability which takes into account the influence of both permeability through gaps and permeability through yarns on the overall fabric permeability. An experimental measurement technique is described and predicted results are compared to the experimental data.

Chapter 4 presents computational modelling of through thickness air permeability using CFD (CFX 11.0 software). TexGen software is used for geometric modelling whereas CFX 11.0 is used to simulate through thickness permeability. The results of the simulation are compared to the analytical and experimental data.

Chapter 5 discusses through thickness permeability for deformed fabrics. Shear, compaction and tension in two directions were chosen as deformation mechanisms. An analytical model is developed based on that presented in Chapter 2. Experimental verification is performed for sheared fabric.

In Chapter 6, thermal conductivity of fabrics is discussed. A detailed description of experiments is provided. Analytical methods to predict thermal conductivity for one layer and for multiple layers are developed. The analytical method takes into account the influence of moisture content on the thermal conductivity of fabrics. Predicted results are compared to experimental data.

Chapter 7 presents an overall discussion and conclusions of the work and recommendations for future work.

CHAPTER 2

LITERATURE REVIEW ON PERMEABILITY AND THERMAL CONDUCTIVITY OF FABRICS

2.1 INTRODUCTION

In this thesis several different fabrics have been studied with different applications such as clothing, airbags etc. Comfort is a most important property of clothing. Comfort has been studied widely since last century [1]. Permeability and thermal conductivity are two main material parameters for clothing comfort characterisation. Literature regarding permeability and thermal conductivity prediction for textile fabrics is reviewed in this chapter. Darcy's law [2], which describes flow through porous media, is the central theory used to describe permeability. Predictive permeability models potentially offer an accurate and robust alternative to experimental methods. In order to predict fabric permeability, research has advanced into studies at the mesoscopic and microscopic levels. Research is based on understanding the influence of fundamental factors such as porosity, yarn permeability and gap permeability on fabric permeability. For some simple cases, a mathematical model such as Gebart's equation [3], which shows the influence of porosity on permeability through an array of filaments, gives reasonably accurate results. Computational analysis is another approach adopted to predict permeability, usually based on the use of CFD software. A number of such models are reviewed in the following sections.

Permeability prediction for deformed fabrics is of interest because of applications of some fabrics such as airbags. Airbags can be sheared and compacted during their use and it is very important to know how much their permeability changes due to deformation. Hence studies related to the effects of fabric deformation on permeability are reviewed.

Thermal conductivity of fabrics is another important parameter of fabric comfort. Most of the work in this area consists of experimental studies. However, there is some research based on analytical prediction of fabric thermal conductivity, which is also described in this chapter.

2.2 MULTISCALE NATURE OF FABRICS

Despite the tremendous amount of fabric permeability data published in the literature, the range of textile fabrics available on the market is too large for characterisation based on experiments alone. Reliable measurements of permeability are difficult even for relatively simple fabric geometry. It is even more difficult to accurately measure permeability of deformed fabrics. The variable nature of fabrics also means that a large number of measurements are needed to characterise just one fabric. Clearly, such an approach is highly time consuming and is not viable in the long term. There is a need for a predictive permeability model to complement experimental data. The key to permeability prediction is an understanding of the architecture of fabrics. There are three length scales. Firstly the microscopic scale which is concerned with individual fibres in a yarn, their geometric parameters such as diameter and shape as well as their arrangement inside the yarn. The second scale is mesoscale which is concerned with unit cell behaviour. It takes into consideration the yarns' geometric parameters such as width, length and height, the geometry of gaps between yarns and their interlacing pattern. Finally, the macroscopic level scale describes a textile sheet or a garment taking into consideration the deformation of the fabric due to body shape or their application. Figure 2.1 presents the scales described above [4, 5].

By studying the flow at different length scales individually, one can better understand the interaction between the flow and the fabric. For example, starting with microscopic flow between the fibres, one can relate flow behaviour to that at the mesoscale or unit cell level. At the mesoscopic level, permeability through pores influences the overall permeability of a unit cell, however, permeability through yarns must also be taken into consideration. Using unit cell analysis, one can then deduce a permeability value which is used in macroscopic simulations to account for the complicated interactions between the fluid and the fabric structure [6]. Similar considerations apply for prediction of thermal conductivity.

Variability in textile permeability can be incorporated into the flow simulations for optimised prediction by using mesoscale analysis to deduce a range of permeability values for use in the macroscopic simulations. Essentially, a fabric is defined by its structure and the interaction between yarns is the main cause of variability of the

Through thickness air permeability and thermal conductivity analysis for textile materials

fabric. Only by looking at the mesoscopic level can one analyse the effect of fabric architecture on permeability variability [6].

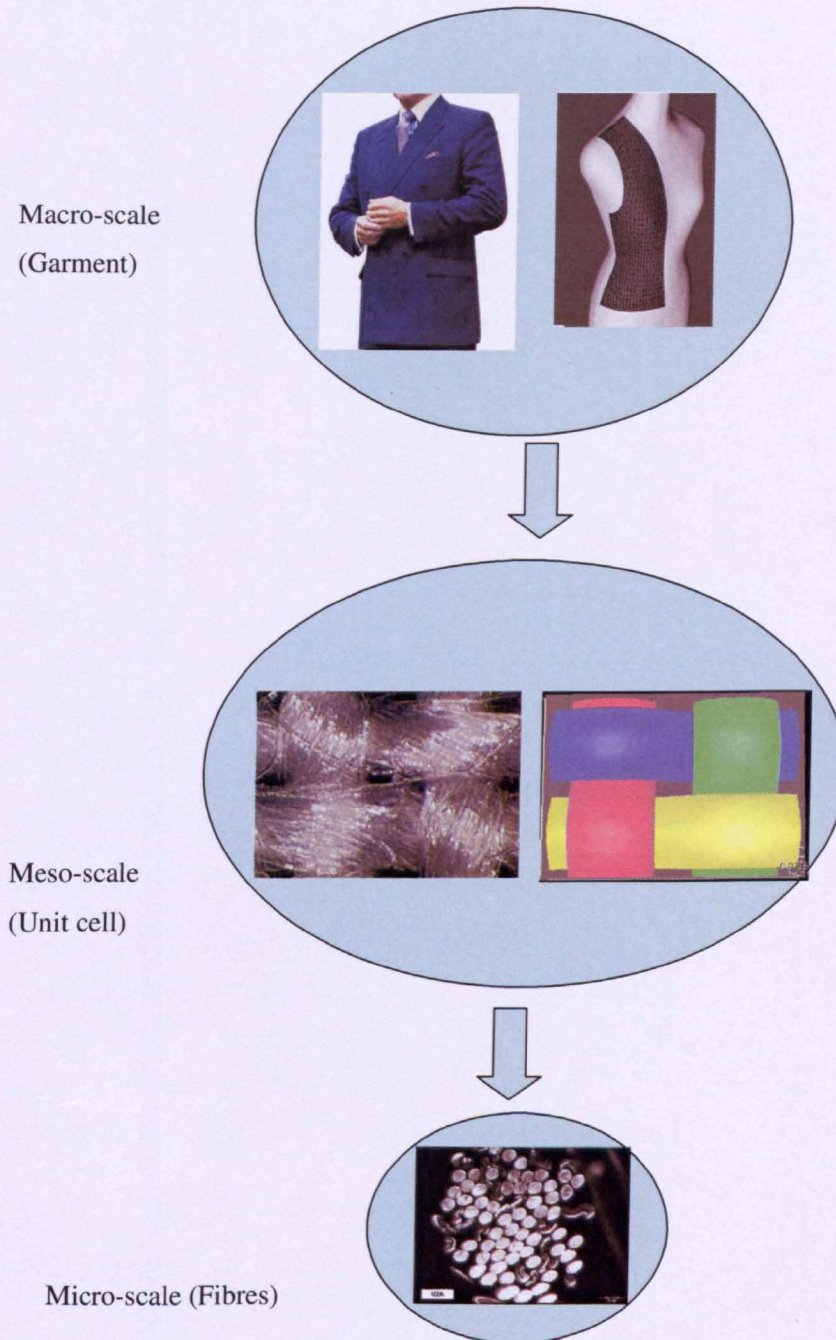


Figure 2.1 Three length scales of fabric architecture [4, 5]

Predictive permeability models can be separated into two general approaches: analytical and computational. The analytical approach leads to a closed form equation for calculating permeability, relating permeability to certain characteristics of the porous medium such as porosity or fibre diameter. These are usually derived by analysing the physical aspects of the flow process through the porous medium. Closed form solutions are invariably more suited to describe microscopic flow where it is easier to mathematically describe the arrangements of the fibres. The computational approach is based on equations for the flow through a unit cell that describes the architecture of the fabric. Such approaches are more adaptable than closed form solutions and can be used to study mesoscopic flow through fabrics.

2.3 PERMEABILITY PREDICTION USING ANALYTICAL MODELS

The ease or otherwise of the passage of fluid through a textile is of importance for a number of fabric end uses such as industrial filters, tents, sail cloths, parachutes, waterproof materials, clothing textiles, nappies and automobile airbags [7]. However, there are more studies related to composites manufacture than on textile fabrics in the literature. Permeability is of interest for composites researchers because of the methods which are using for composites production such as RTM (Resin Transfer Molding) and LCM (Liquid Composite Molding).

As a result of studying flow through porous media, Darcy [2] established the linear dependence of velocity on pressure drop. The first studies of the air permeability of fabrics conducted by Rubner [2] were based on Darcy's law. It was based on the experimental results for the flow of water through beds of sand. Darcy's law is a simple mathematical statement which neatly summarizes several familiar properties of groundwater flowing in aquifers, including [2]:

- if there is no pressure gradient over a distance, no flow occurs (this is the hydrostatic condition),
- if there is a pressure gradient, flow will occur from high pressure towards low pressure (opposite the direction of increasing gradient—hence the negative sign in Darcy's law),
- the greater the pressure gradient (through the same formation material), the greater the discharge rate, and

- the discharge rate of fluid will often be different — through different formation materials (or even through the same material, in a different direction) — even if the same pressure gradient exists in both cases.

Darcy's law can be written as follows:

$$v = \frac{-B}{\mu} \Delta P \quad (2.1)$$

where v is the average fluid velocity, μ is the fluid viscosity, B is the permeability of the porous medium, ΔP is the pressure gradient.

Darcy's law is only valid for slow, viscous flow; fortunately, most groundwater flow cases fall in this category. Typically any flow with a Reynolds number less than one is clearly laminar, and it would be valid to apply Darcy's law. Experimental tests have shown that flow regimes with values of Reynolds number up to 10 may still be Darcian [2]. However, Reynolds number for flow through textile fabrics is not always in the range of Darcy's law. In such situations it is reasonable to use Forchheimer equations, which is described later in this chapter.

Many analytical models have been proposed to predict permeability. These can be divided according to flow going through different parts of fabrics. Flow through fabrics can be split into two main mechanisms: flow through gaps between yarns and flow through yarns.

One very well known equation which relates the permeability B to porous media properties was derived by Kozeny [2]. Kozeny viewed the porous bed as an assemblage of channels of various cross-sections and expressed the permeability as in equation (2.2) [2]:

$$B = c \frac{\alpha^3}{S^2 T} \quad (2.2)$$

where α is the porosity of the porous medium, S is the specific surface of the channel, T is the tortuosity factor and c is a proportionality parameter which depends on the shape of the channels (Kozeny constant).

Kozeny's equation has been used extensively and modified by other researchers. Carman introduced the specific surface exposed to the fluid S_0 ($S_0 = S(1-\alpha)$) and experimentally determined a range of Kozeny constants for a variety of packing schemes and geometries of reinforcements. The result is known as the Kozeny-Carman equation [8]:

$$B = c \frac{\alpha^3}{5S_0^2(1-\alpha)^2} \quad (2.3)$$

where c is Kozeny constant, S_0 is surface area, α is porosity and B is permeability.

This equation holds for flow through packed beds with particle Reynolds numbers up to approximately 1.0, after which point frequent shifting of flow channels in the bed causes considerable kinetic energy losses. Their model was developed for in-plane flow parallel to the porous medium.

Gebart [3] conducted 2-D simulations for the flow of Newtonian fluid perpendicular to and parallel with unidirectional filaments. Gebart looked at two types of packing array: quadratic and hexagonal (see Figure 2.2). Gebart obtained the following permeabilities [3]:

- Quadratic packing:

Permeability along the filament B_x is:

$$B_x = \frac{8r^2}{57} \frac{(1-V_f)^3}{V_f^2} \quad (2.4)$$

Permeability perpendicular to the filaments B_z is:

$$B_z = \frac{16}{9\pi\sqrt{2}} \left(\sqrt{\frac{V_f^{\max}}{V_f}} - 1 \right)^{5/2} r^2 \quad (2.5)$$

- Hexagonally packing:

Permeability along the filaments B_x is:

$$B_x = \frac{8r^2}{53} \frac{(1-V_f)^3}{V_f^2} \quad (2.6)$$

Permeability perpendicular to the filaments B_z is:

$$B_z = \frac{16}{9\pi\sqrt{6}} \left(\sqrt{\frac{V_f^{\max}}{V_f}} - 1 \right)^{5/2} r^2 \quad (2.7)$$

where V_f and d_f are the yarn solid volume fraction (SVF) and the filament diameter, respectively, r is the radius.

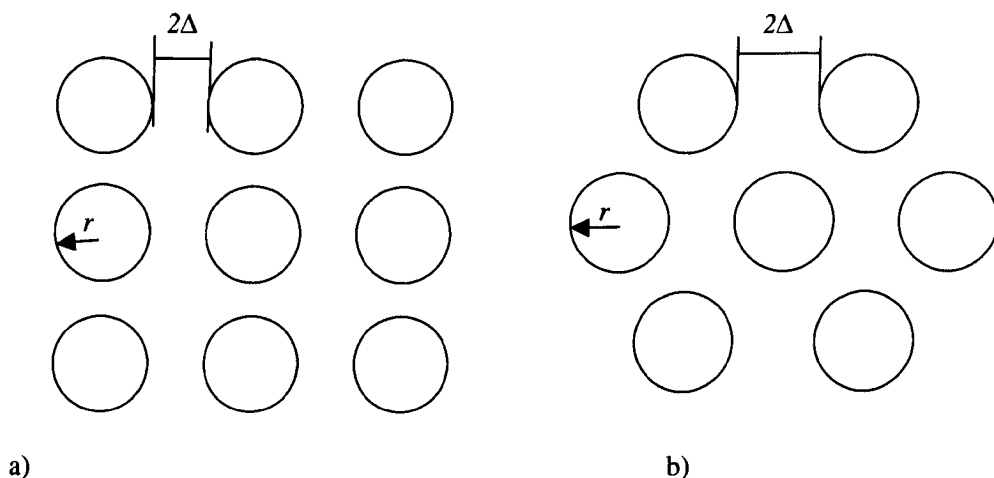


Figure 2.2 Idealized unidirectional reinforcement for quadratic (a) and hexagonal (b) fibre packing [3].

Gebart assumed the idealized unidirectional reinforcement with two types of packing (quadratic and hexagonal), whereas, in reality for textile fabrics fibres are in random order inside the yarns. Gebart's model had good agreement with experimental results when fibre volume fraction was lower than 0.5 [3].

Studies by Kulichenko and Van Langenhove [7, 10] to analyse through thickness air flow for textiles showed that their mathematical model for air permeability worked well when the flow goes through gaps between yarns only, for example, for loose fabrics. Kulichenko's analytical model [7] calculates velocity of the flow through gaps using the following equations:

$$v_g = \frac{v_f}{\alpha} \quad (2.8)$$

$$v_f = \frac{\Delta P}{80\mu} \frac{d_s^2 \alpha}{t} \quad (2.9)$$

where v_g is the velocity through gaps, v_f is the velocity through entire system, d_h is the hydraulic pore diameter and α is the through thickness porosity

Kulichenko developed a model of the “ideal soil” pore system, a system of parallel capillaries. They assumed that the flow is laminar. The pore cross-section size and shape is constant over the entire length. His model alone cannot be used for textile fabrics as it does not take into account flow inside the yarns.

Other closed-form modifications to Darcy’s law have been developed to relate volume fraction and geometric or empirical constants such as the maximum packing fraction to the permeability of a periodic medium. Cai and Berdichevsky [11, 12] used the self-consistent method and finite element simulations to estimate the permeability of an aligned fibre bundle. The self-consistent method gave formulae for both longitudinal and transverse permeabilities as a function of fibre volume fraction. The finite element simulation presented the solutions of various periodic fibre packings (Figure 2.3). They assumed that a circular insertion was placed into the homogeneous porous medium filled in space [11].

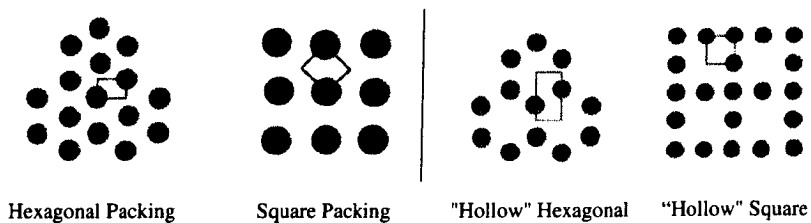


Figure 2.3 Fibre assembly and representative unit cells for different packing structures [11]

They came up with the following equations for longitudinal and transverse permeabilities [11]:

- Longitudinal permeability:

$$B_x = \frac{1}{8V_f} \left[\ln \frac{1}{V_f^2} - (3 - V_f)(1 - V_f) \right] \quad (2.10)$$

- Transverse permeability:

$$B_z = \frac{1}{8V_f} \left(\ln \frac{1}{V_f} - \frac{1-V_f^2}{1+V_f^2} \right) \quad (2.11)$$

The results for square and hexagonal fibre packings were found to be in good agreement with the previous work described in the literature. It was shown that the permeability was not only related to the fibre volume fraction or porosity, but was also greatly influenced by the packing structure or micro-level disturbance. However, there was no comparison with experimental results. Later, they improved their model by assuming that an insertion was open space surrounded by densely packed fibres [12]. This improvement allowed them to describe effectively the permeability of dense structures containing distributed voids. The insertion was placed in a homogeneous medium with an unknown permeability. They considered Stokes and Darcy flow for different regions. Boundary and interface conditions as well as two consistency conditions, including the total amount of the flow and the dissipation energy, were applied accordingly. This improved model captured the flow characteristics of a fibre bundle. In the longitudinal flow case, the openings within the bundle due to the disturbance dominated the flow path. In the transverse flow case, the gaps between neighbouring fibres governed the flow resistance. The derived expressions for the transverse permeability contained two variables, the average fibre volume fraction and the maximum packing efficiency as presented in Equation (2.12) [12].

$$B_z = 0.231 (\ln \sqrt{V_a/V_f}) \left[\frac{(1 - \sqrt{V_f/V_a})^{3/2}}{(V_f/V_a)} \right] \quad (2.12)$$

Predictions had good agreement with experimental data available in the literature [12]. However, their model was made for a bundle of fibres and was not applied to real fabrics.

Bruschke and Advani studied fluid flow across regular arrays of cylinders [13]. A closed form solution was developed by matching the analytical solution using the lubrication approach for low porosities and the analytical cell model solution for high porosities. The results of the closed form solutions agreed well with the numerical

solution obtained by solving the Stokes equations in square and hexagonal arrangements of cylinders for Newtonian fluids. They assumed no-slip boundary conditions on the surface of the cylinder, symmetry conditions on the top and bottom surfaces and constant pressure boundary conditions on the left and right surfaces. Closed form expressions which they developed can be used only for low porosities up to about 40%. The cell model for high porosities, however, assumed that the disturbance in the fluid model by one cylinder does not affect the flow field of any of the surrounding cylinders. In addition, packing configuration does not have any influence in this model. As a conclusion, neither of their two models can predict the permeability over the full porosity range successfully [13].

Van der Westhuizen and Du Plessis [14] used phase-average Navier-Stokes equations to calculate the permeability of representative unit cells. Their model did not assume any particular arrangement of fibres for longitudinal permeability, but used the maximum packing capacity for different arrangements of fibres to create an effective volume fraction for transverse permeability. A simplistic extension of the solution was proposed to account for pinch-off effects during crossflow through the fibre bed. They assumed that the fibre bed was solid. The flow was assumed laminar. Their model found good agreement with the experimental data. However, they were modelling in-plane permeability without considering through thickness cases.

Wang [15] developed a similar relation for an array of rectangularly-packed fibres. He assumed the slow viscous flow through an array of rectangular fibres. He solved it by the efficient method of Eigen function expansion and domain decomposition. The normalised permeability was determined for square fibres and strips in rectangular arrays. However, there was no comparison to any experimental results. Table 2.1 summarises some of these semi-empirical models as compared by Senoguz et al. [2].

Table 2.1 Fabric permeability relationships developed by various researches [2]

Author	In-plane permeability	Through thickness permeability
Gebart [3]	$B_x = \frac{8r_f^2 (1 - V_f)^3}{53 V_f^2}$	$B_z = \frac{16}{9\pi\sqrt{6}} \left(\sqrt{\frac{V_A}{V_f}} - 1 \right)^{2.5} r_f^2$
Cai and Berdichevsky [11]	$B_x = \frac{r_f^2}{8V_f} \left[\ln \frac{1}{V_f^2} - (3 - V_f)(1 - V_f) \right]$	$B_z = \frac{r_f^2}{8V_f} \left[\ln \frac{1}{V_f} - \frac{1 - V_f^2}{1 + V_f^2} \right]$
Berdichevsky and Cai [12]	$B_x = 0.111 \frac{r_f^2}{V_f} \ln \frac{1}{V_f} \exp[-1.54V_f - 2.82V_f^2]$	$B_z = 0.229r_f^2 \left(\frac{1.814}{V_A} - 1 \right) \left[\frac{1 - \sqrt{V_f/V_A}}{V_f/V_A} \right]^{-2.5}$
Bruschke and Advani [13]	Not applicable	$B_z = \frac{r_f^2 (1 - l^2)^2}{3\sqrt{3} l^3} \left(3l \frac{\arctan(\sqrt{(1+l)/(1-l)})}{\sqrt{1-l^2}} + \frac{l^2}{2} + 1 \right)^{-1}$ $l^2 = \frac{2\sqrt{3}}{\pi} (1 - \epsilon)$
Van der Westhuizen and Du Plessis [14]	$B_x = r_f^2 \frac{(5.299 - 2.157\epsilon)\epsilon^2}{48(1 - \epsilon)^2}$	$B_z = r_f^2 \frac{\pi(1 - V_f^*)(1 - \sqrt{V_f^*})^2}{24V_f^{*1.5}}$ $V_f^* = 2.22V_f^2 - 122V_f + 0.56$

Phelan and Wise [16] studied transverse flow in aligned fibrous porous media. They developed a semi-analytical model based on lubrication analysis to predict the effect of tow shape and intra-tow permeability on the overall bed permeability for flow through rectangular arrays of porous elliptical cylinders. The Brinkman equation was used to define flow inside the porous structures, and the Stokes equation to model flow between the structures. The model predictions were verified by comparing with finite element calculations. Their model showed that the influence of intra-tow permeability on overall bed permeability increases with inter-tow packing, and increasing degree of tow ellipticity. Their main assumption is that the transverse component of the velocity is negligible, which allowed them to simplify the governing equations. They compared intra-tow permeability predictions with the experimental data of Sadiq et al. [17] which used tows made of nylon rods to construct porous media. Their prediction found reasonable agreement with experimental data. Comparing predicted results to the computational model they obtained good agreement for the porous medium with a porosity of more than 25%.

The research presented in Chapter 3 combines Kulichenko and Van Langenhove analytical model which predicts the permeability through gaps between yarns with Gebart's model to predict permeability within yarns. These two models have been chosen as a basis for the model developed in this thesis because they take into account all important fabric parameters and at the same time are simple and easy to use. The resulting analytical model is applied to ten textiles used for airbags and clothing application.

2.4 PERMEABILITY PREDICTION USING COMPUTATIONAL MODELS

The permeability of woven fabric has been studied extensively. Most of this work, however, is experimental and many of the studies are designed for specific applications, due to the complexity of the geometries of such fabrics. Conducting a computational study on woven fabrics, especially multifilament, requires considerable computing power even for idealized geometries. For this reason, there are many studies based on monofilament geometries made of porous materials. In such studies, the flow field is divided into two zones of intra-yarn and inter-yarn, with different flow behaviour modelled in each zone. Assuming the yarn to be represented by a

Through thickness air permeability and thermal conductivity analysis for textile materials

porous domain greatly reduces computational requirements, but requires accurate information regarding the yarn's permeability [32].

High-volume applications require efficient software tools for process simulation and performance prediction. Such software tools are commercially available; for example, LCMflot™ [18] and LIMS™ [19] have been used for many years to predict filling patterns in Resin Transfer Molding (RTM) whilst ABAQUS™ [20] is used regularly to predict deformations under load. The difficulty lies in obtaining the required local material properties. The permeability data required by the above software is usually measured experimentally. Permeability can be also investigated using a CFD software package such as FLUENT™ [21] or CFX 11.0 [22]. Recently, TexGen software [23] has been used to create fabric geometry models suitable for different fabric structures such as plain weave or twill weave, which addresses the big issue of generating an accurate computational domain.

Lomov et al. presented an integrated modelling and design tool for textile composites based on hierarchical principles of textile modelling [24]. They implemented this approach in the WiseTex software, which models the internal structure of textiles. The architecture of the code implementing the model corresponds to the hierarchical structure of textile materials. The model of the textile geometry serves as a base for meso-mechanical and permeability models for composites. The Object Oriented Programming (OOP) technique is ideally suited to implement the hierarchical nature of textiles represented in Table 2.2 [28]. They predict the permeability of resin flow through the reinforcement during mould filling operation. However, they do not mention predictions for through thickness permeability. In addition, their model was very computationally expensive.

Table 2.2 Hierarchy of structure and models of textile composites [24]

Structure	Elements	Models
Yarn (tow)	Fibres	Fibre distribution in the yarn and its change under load/strain Mechanical properties of the yarn
Fabric (woven, knitted)	Yarns	Geometry of yarns in the fabric and its change under load/strain Mechanical behaviour of the fabric repeat under complex loading
Composite unit cell	Fabric Matrix	Mechanical properties Permeability tensor

Robitaille et al. presented an algorithm that generates geometric descriptions of unit cells of textiles and composite materials [25]. The purpose of these geometric descriptions was to act as domains for calculations performed at the scale of the unit cell. The algorithm defined both the volume of the tows and the empty volumes that extend between the tows within the calculation domain, for general textiles. Typical applications of the geometric definitions include the calculation of local permeability values for textile preforms and investigation of local stress distribution in textile composites. There are some restrictions in this model such as the boundaries of the calculation domain must form a rectangular volume with two faces parallel to the plane (x, y) . The 3D algorithm consisted of two main operations: the creation of the basis volumes that present the empty volumes defined between tows and the creation of the basis volumes that represent the tows. Their tool was created to predict the properties at the unit cell scale, however there were no comparison of their model to any other computational models or experimental data.

Belov et al. [26] developed an integrated design tool (IDT) for meso-scale analysis with the capability of linking to macro-scale simulation tools. This tool is used as a pre-processor for meso-mechanical and permeability models for textile composites. The core of the IDT was a model of textile geometry, which provides a generic description of a wide range of textile reinforcements. It is presented in Figure 2.4

[26]. The permeability analysis was carried out in a number of steps. The first step was characterising the reinforcement, which includes analysis of internal structure, data on fibre and yarns etc. This step culminated with creating the geometry using the WiseTex software. Next step was related to the deformability of the reinforcement. The compressibility and shear were of primary importance. This step was approached by the experimental evaluation of reinforcement behaviour in compression, extension and shear. All these data were linked to the flow simulation tool called FlowTex which calculates the permeability tensor. This used a numerical approach based on the lattice Boltzmann method. Assumptions included: creeping single-phase, isothermal, unidirectional saturated flow of a Newtonian fluid. The computational model found good agreement with experimental data of Phelan [16]. However, their model was very slow.

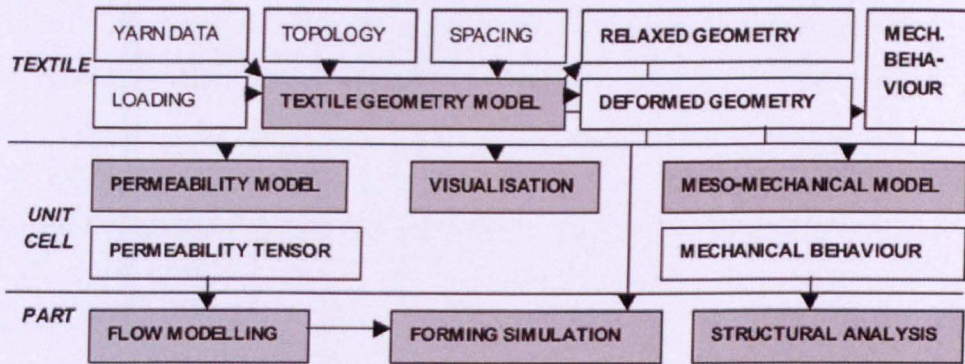


Figure 2.4 Integrated design tool [26]

Sobera et al. [27] used CFD to study NBC (Nuclear-Biological-Chemical) protective clothes on different scales focusing on different aspects of flow, heat and mass transfer. The textile material was modelled as a porous material with particular macroscopic properties. They used the commercial CFD solver Fluent 6 for the simulations. The porous material was treated as a fluid zone, where the pressure drop was imposed as a sink in the momentum equation according to Darcy's law. They assumed laminar steady flow. They showed that the Reynolds Averaged Navier Stokes (RANS) approach used in CFD simulation is sufficiently accurate for engineering purposes, particularly when it is used to predict global heat and mass transfer. From meso-scale Direct Numerical Simulation, it was found that the flow underneath the clothing is laminar and periodic, with a magnitude much smaller than

the free stream velocity. Micro-scale Direct Numerical Simulation revealed a simple relation between textile porosity and permeability [27]. Although predicted results had satisfactory agreement with experimental data, they did not predict through thickness fabric permeability.

Wang et al. [28] modelled a full 3-D geometry of an idealized multifilament woven fabric, wherein the filaments were packed in hexagonal arrangement, to predict permeability using the CFD code from Fluent Inc., and compared it to the homogeneous anisotropic lumped model of Gebart [3]. They assumed that the flow is steady state laminar, incompressible with very low velocity and Reynolds number. The finite volume method implemented in Fluent code was exploited to solve the continuity and the conservation of momentum around the filaments and yarns within a unit cell model. Air flow was assumed normal to the fabric plane. They showed that Gebart's model slightly underestimate the permeability of multifilament fabrics even at high yarn's solid volume fraction.

Lekakou et al. presented a model to predict in-plane permeability in non-crimp stitch bonded fabrics [29]. The model was based on the combined flow through the multi-layer assembly in the non-crimp fabric. The permeability of each layer of the assembly was predicted on the basis of a meso-/micro-flow computer model. In this the meso-flow between fibre tow was considered as Stokes' flow. Darcy's law was employed to mode micro-flow through each fibre tow, taking into consideration injection and capillarity pressures in both types of flow. This model was tested in biaxial non-crimp stitch bonded fabrics with either chain or tricot stitch. The permeability predictions were very sensitive to the dimensions of the meso-channel cross-section and required input data from a detailed microstructural analysis for meso-channels with varying cross-sections. Tows were assumed to be rectangular and elliptical cross-section. Good agreement existed between predictions and experiments, although it is highly likely that this required empirical adjustments of certain fabric parameters. This model did not predict through thickness permeability.

Nordlund et al. proposed a computational model for global permeability and applied it to biaxial non-crimp stitched fabrics (NCF) [30]. This model focused on a detailed

Through thickness air permeability and thermal conductivity analysis for textile materials

meso-scale description of the fabric geometry, which takes into account the local permeability distribution in a fabric due to perturbations of geometry as well as geometrical features which arise from the stitching process. They showed that this significantly affected the global permeability. Steady, incompressible, laminar and Newtonian flow through the unit cell was solved with the commercial CFD code CFX5.6 from ANSYS Inc. The code is based on a finite volume method and uses a non-structured solver. They predicted in-plane permeability, which was very sensitive to the perturbation of the geometry. Permeability of the fabric can be increased by a more precise stitching process, which reduces the amount of crossings. It was shown that the global permeability was also very sensitive to the mean channel width. However, the proposed model did not show good agreement with experimental data.

Wong et al. proposed two efficient numerical approaches to predict permeability based on fabric architecture [31]. The “Stream Surface” method reduces the complexity of the flow domain by representing the 3-D volumes with their 2-D curvilinear mid-surfaces while retaining the 3-D attributes. The second method, “Grid Average”, discretises the 3-D domain into a 2-D regular grid with weighted average permeabilities for the individual elements. Flow equations were solved for the reduced meshes generated from these two approaches to calculate the effective permeability. These approaches were applied firstly to a single tow model, and then to 2x2 twill weave fabric. TexGen software was used to create the unit cell geometry. He compared his two approaches to FLUENT™ CFD package. His simplified models showed the potential to predict permeability accurately and rapidly for practically any type of textiles. He studied the influence of four geometric parameters on in-plane permeability: tow aspect ratio (width/height), the shape of the tow, the cell fibre volume fraction, and, the cell aspect ratio. It was shown that permeability decreased with increase in tow aspect ratio; and permeability increased when the tow shape changed from a rectangular shape to an ellipse. His two approaches agreed well with the CFD results. He showed that his method is much faster than CFD simulations [31]. However, there were no comparison with any experimental data, and these two approaches did not take into account through thickness permeability.

Verleye et al. presented the results of simulations with a Stokes solver, implemented in the permeability predicting software FlowTex [32]. They assumed that the flow is laminar. They were interested only in steady state solutions which lead to the incompressible Stokes equations. They used monofilament fabric Natte 2115 for experiments as it is a stable fabric close to actual textile reinforcements. They compared results to those of a Navier-Stokes solver and validated using theoretical results for model problems and with experimental data for real textiles. Predicted results were reasonably close to the experimental data and the computational time was reduced by using Stokes solver instead of Navier-Stokes. Later, Verleye et al. proposed a fast and accurate simulation method for the permeability of textile reinforcement based on a finite difference discretisation of the Stokes equations [33]. They used single layer, multi-layer and sheared models for the simulations. They took into consideration the influence of intra-yarn flow and different boundary conditions. A finite difference Navier-Stokes solver, NaSt3DGP, was used for simulations. They assumed that the yarns are porous solids. Experiments were carried out using highly automated central injection rig, called the PIERS set-up (permeability identification using electrical resistance sensors). The experimental permeability values were higher than the numerical values. For woven fabrics, a relative difference of 40-50% between the experimental and numerical values was observed. The results were closer for the lower fibre volume fraction textiles. Computations based on a single layer model resulted in a small over-estimation of the experimental values, as nesting is neglected. For textiles with high volume fraction, intra-yarn flow has an important influence on the permeability values [33]. However, they studied in-plane permeability only without taking into consideration through thickness air permeability.

Vakil et al. [34] described a novel method to model forming fabrics. The flow non-uniformity and its probable effect on particles were considered in their research. CFD package FLUENT was used to simulate flow through fabrics. The resistance of multilayer fabric was found to be nearly equal to the sum of the resistances of each layer considered in isolation. In addition, they considered the effect of jet-to-wire speed ratio on the flow. An angled approach flow to the fabric produced very little change in the average flow perpendicular to the fabric (for example, little change in fabric permeability), but it had marked effect on shear stress in the vicinity of the

paper-side filament. However, there was no comparison of their results with any experimental data.

In this thesis a CFD model based on TexGen and CFX 11.0 as the most accurate and up-to-date computational software to predict through thickness air permeability of the unit cell of fabric is developed for plain weave and twill weave fabrics (Chapter 4).

2.5 EXPERIMENTAL STUDIES OF AIR PERMEABILITY AND FORCHHEIMER EQUATION

Several authors have studied permeability experimentally. Among them, Niu and Gu conducted research on an immersion-resistant and moisture-permeable smart fabric [35]. The fabric was formed when cotton fibres in the Polyester/Cotton fabric were grafted with acrylic acid (AAc) or acrylamide (AAm). A moisture permeability test was carried out according to Chinese National Standard GB/T12704-91, and air permeability according to GB/T 5434-1997. Their tests showed the average size of pores was affected by fabric tightness while the interspace was affected by fibres' fineness. The smaller the pores were, the lower the air permeability; the thicker the yarns, the more reliant the air permeability was on the condition that there was no much difference on fibre quantity and fibre fineness in the yarns. They developed a mathematical model for water permeability of fabrics. It was built on Hagen-Poiseuille flow and based on the concept of hydraulic radius. They assumed that yarn diameters, cross sections and porosity were equal for warp and weft yarns, and the flow was laminar. However, their model did not take into account permeability through yarns.

Jia, Wang and Liu studied a chemical method used for decreasing the permeability of polyester fabric [36]. They used thin polyester fabric which was treated with m-cresol-tetrachloroethane to make compact the fabric to decrease its permeability. In the treatment process the different concentration of the m-cresol, processing temperature and processing time were selected. Using the chemical method can reduce the air permeability of the thin polyester fabric. The optimum processing temperature and time were determined to decrease the permeability of fabric

effectively. Their work is purely experimental and did not include any comparison to analytical or computational models.

The use of the Forchheimer equation (see equation (2.13)) to describe through thickness permeability instead of Darcy's law has been discussed by several researchers. The linear term results from viscous effects, which are predominant at low Reynolds number. The quadratic term results from inertial effects. Huang et al. [37] made a literature review on non-Darcy flow in porous media. One of the aspects of the discussion concerned the inertia resistance factor β (Forchheimer equation) and whether its value should be constant over the range of flow rates of practical interest. They suggested models for flow beyond the Forchheimer regime. At higher superficial fluid velocities v_D , an additional quadratic term was proposed by Dupuit and Forchheimer [37]. For non-Darcy flow in porous media such as textiles the velocity becomes large enough so that it is more reasonable to use Forchheimer equation instead of Darcy's law. Forchheimer equation is presented below [37]:

$$-\Delta P = \frac{\mu}{B} v + \beta \rho v^2 \quad (2.13)$$

The Forchheimer coefficient β is generally deduced experimentally from the slope of the plot of the inverse of the apparent permeability $1/k_{app}$ vs. the dimensional pseudo Reynolds number $\rho v/\mu$ (also known as the Forchheimer graph) [37].

A volume average study by Douglas and Huiping [38] indicates that microscopic inertial effects distort the velocity and the pressure fields, which in turn lead to Forchheimer effects. Non-dimensionalization for 1D isotropic case yields:

$$\Pi_{pg} = -c_0 - c_1 Re_d \quad (2.14)$$

where $\Pi_{pg} = \Delta p d^2 / \mu v_D$ is the dimensionless pressure gradient, d is a characteristic length-scale (usually the average or nominal pore diameter), and Re_d is the Reynolds number based on d . Hence, c_0 is the inverse dimensionless permeability and c_1 is the dimensionless Forchheimer coefficient [38],

$$c_0 = \frac{d^2}{K} \quad \text{and} \quad c_1 = dF \quad (2.15)$$

Through thickness air permeability and thermal conductivity analysis for textile materials

Wang and Liu [39] studied the Forchheimer equation and the inertial parameter β based on solving Navier-Stokes equations in two-dimensional percolation porous media. The model of the pore connectivity was based on two-dimensional site percolation. Void spaces occupied an $L \times L$ square lattice with the probability p . They assumed nonslip boundary conditions at the solid-fluid interface. The pressure drop was set to be ΔP . In the horizontal direction periodic conditions were used. SIMPLE method was used to solve the Navier-Stokes equations. They showed that the Forchheimer parameter is a function of the system size L and porosity α , $\beta = \beta(\alpha, L)$. The simulation results showed that the inertial parameter in the Forchheimer equation had larger scaling exponents than the permeability [39]. However, there was no comparison of their results to any other analytical models or experimental data.

Clearman [40] used a CFD approach (Fluent) to study directional permeability and Forchheimer inertial coefficient of micro porous structures used in pulse-tube cryocoolers. He compared the equations which Fluent used to solve the simulation to the Forchheimer equation (Equation 2.13) and found that they are similar. Equation (2.16) is taken from Fluent code, it is general momentum equation:

$$\frac{\partial(\epsilon P)}{\partial x} = \underbrace{-\frac{\partial}{\partial x}(\epsilon \rho v_i v_i)}_{Convective\ Acceleration} + \underbrace{\frac{\partial(\epsilon \tau_i)}{\partial x}}_{Viscous\ Stress} - \left[\underbrace{\frac{D_{ij} v_j}{\partial x}}_{Darcy\ Term} + \underbrace{\frac{C}{2} \rho v_{mag} v}_{Forchheimer\ Term_i} \right] \quad (2.16)$$

By comparing general momentum equation from Fluent with Forchheimer equation, it can be shown that the inertial resistance term is related to the permeability and the Forchheimer coefficient by:

$$C = \frac{2\epsilon^3 c_f}{\sqrt{K}} \quad (2.17)$$

In CFD simulation, boundary conditions were based on an assumed mass flow rate at inlet and the gate pressure at outlet based on experimental values; the flow was assumed as steady-state [40]. The results had reasonable agreement with experimental data. However, additional testing was recommended for each porous structure at varying porosities. Based on the governing momentum equation, it is clear that increased porosity for any given sample will decrease the magnitude of the steady flow

pressure drop, but it is unclear whether varying the porosity for the same porous structure will significantly affect the permeability or Forchheimer coefficient.

Petrasch et al. [41] studied the Forchheimer coefficient for reticulate porous ceramics (RPC) using computer tomography. A 3D digital representation of a 10-ppi RPC sample was generated by X-ray tomographic scans. Structural properties such as porosity, specific interfacial surface area, pore-size distribution, two-point correlation function and local geometry distribution of RPC sample were directly extracted from the tomographic data. A photograph of the scanned 10-ppi RPC sample is presented in Figure 2.5 [41].

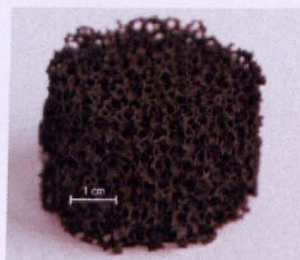


Figure 2.5 Photograph of scanned 10-ppi RPC sample [41]

The permeability and Forchheimer coefficient were determined from direct pore-level numerical simulation (DPLS) and compared to the values predicted by selected porous media flow models, namely: conduit-flow, hydraulic radius theory, drag models, mean survival time bound, s2-bound, fibrous bed correlations, and local porosity theory-based models. A number of models for the prediction of permeability B and Forchheimer coefficient β as functions of the effective porosity and specific surface area were examined. Tables 2.3 and 2.4 present model predictions for the Forchheimer coefficient and the permeability respectively [41].

Table 2.3 Model predictions for the Forchheimer coefficient β [41]

Model	Symbol	Equation
Ergun/MacDonald	β_E	$\beta_E = 1.8 \frac{1-\varepsilon}{\varepsilon^3} \frac{1}{d}$
Ward	β_W	$\beta_W = \frac{0.550}{\sqrt{B}}$
Empirical, cellular foams	β_{Mo}	$\beta_{Mo} = \frac{1.8 \times 10^4 (1-\varepsilon)}{\varepsilon^3 d_c^{-0.24}}$

where ε is the porosity, d is the pore diameter, B is the permeability.

Table 2.4 Model predictions for the permeability B [41]

Model	Symbol	Equation
Conduit flow	B_C	$B_C = \frac{\epsilon d^2}{32}$
Carman-Kozeny	B_{CK}	$B_{CK} = \frac{\epsilon^3}{k_K (1-\epsilon)^2 A_0}$
Fibrous beds, Davis	B_{Da}	$B_{Da} = \frac{d_f^2}{64(1-\epsilon)^{3/2}(1+56(1-\epsilon)^3)}$
Fibrous beds, Chen	B_{Ch}	$B_{Ch} = \frac{\pi d_f^2 \ln(k_5 / (1-\epsilon)^2)}{4k_4} \frac{\epsilon}{1-\epsilon}$
Fibrous beds, Kyan	B_{Ky}	$B_{Ky} = \frac{(62.3N_e^2(1-\epsilon) + 107.4)\epsilon^3}{16\epsilon^6(1-\epsilon)^4}$
Cylinder, parallel flow	B_{cp}	$B_{cp} = \frac{2\epsilon^3}{(1-\epsilon)(2\ln(\frac{1}{1-\epsilon}) - 3 + 4(1-\epsilon) - (1-\epsilon)^2)}$
Empirical, cellular foams	B_{Mo}	$B_{Mo} = \frac{\epsilon^3 d_c^{0.264}}{1.36 \times 10^8 (1-\epsilon)^2}$
Two-point correlation bound	B_{s2}	$B_{s2} \leq \frac{2}{3} \int_0^{\infty} \frac{r(s_2(r) - \epsilon^2)}{(1-\epsilon)^2} dr$
Two-point correlation, approximation	$B_{s2,a}$	$B_{s2,a} \cong \frac{16}{9} \frac{\epsilon^3}{s^2} (1-\epsilon)$
Mean survival time bound	$B_{D\tau}$	$B_{\tau} \leq \epsilon D \tau$
LPT, L_{δ}	B_{LPT} (L_{δ})	$\int_0^1 \int_0^1 \frac{6}{k_K} \frac{\lambda(\epsilon, s, L) \mu(\epsilon, s, L)}{\frac{2}{k_K} \epsilon + 4s^2 B_{LPT}} d\epsilon ds = 1$

where ϵ is the porosity, d is the pore diameter, B is the permeability, A_0 is the specific surface area based on the solid volume, k_K is the Kozeny constant, d_f is the fibre diameter, $k_4 = 6.1$ and $k_5 = 0.64$ are the empirical parameters, $N_e = \sqrt{\frac{2\pi}{1-\epsilon}} - 2.5$, d_c is the cellular diameter, $s_2(r)$ is the two-point correlation function.

Sung-Min Kim investigated laminar pulsating flow through porous media [42]. He described the Forchheimer equation showing that there are three regimes in laminar flow (Figure 2.6). Region I presents low flow rates where surface-interactive force dominates. Regions II and III represent the laminar flow regime which consists of Darcy's flow (Region II) and Forchheimer flow (Region III). After Forchheimer flow, the turbulent regime starts. There is a critical Reynolds number for transition from Darcy's (viscous flow) to Forchheimer (inertia flow). Kim used CFD code FLUENT 6.3 to perform the simulations for pulsating flow. Two-dimensional structured meshes for five different porous geometries were created by using the Gambit 2.2 software. He assumed that flow was in the x-direction, the no-slip boundary condition applied on the wall, the geometric boundaries and physical conditions were symmetric along the x-axis, the pulsating frequency was 40 Hz, the porosity range was 0.64 to 0.84. For pulsating flow, similar to the case of steady flow, when the mean flow velocity is very small, the Forchheimer term can be neglected, and the permeability coefficient can be obtained. When the mean flow velocity is not small, then the permeability and Forchheimer coefficients both need to be considered.

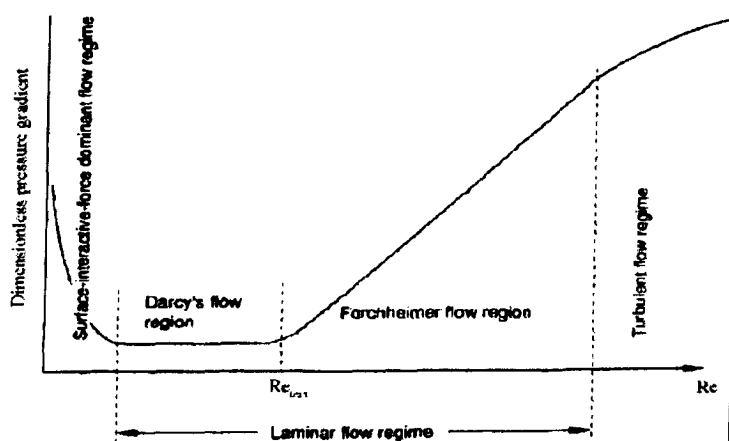


Figure 2.6 Flow regions in a porous medium in terms of Reynolds number [42]

The results confirmed that pulsating flow through porous media leads to phase shifts in velocity and pressure. The magnitudes of the phase shifts depended on the Reynolds number. However, the cycle-averaged Forchheimer coefficients decrease with increasing porosity, and were about two times larger than those for steady flow at the same porosity. Unfortunately, relevant experimental data which would verify the accuracy of the current simulation results for pulsating flow could not be available.

It is clear from the above, that Forchheimer coefficient must be considered in this work. Both experimental and CFD approaches to determine the Forchheimer coefficient will be described in the next chapters.

2.6 PERMEABILITY PREDICTION FOR DEFORMED FABRICS

During the last decades there have been many studies of permeability of deformed fabrics such as sheared or compacted fabric to predict the behaviour of textiles during manufacturing techniques such as resin transfer moulding (RTM), during which resin is injected into a mold cavity filled with a fibrous reinforcing preform [43]. Both experimental and analytical work has been done to predict permeability behaviour of fabrics. It is relevant to this thesis because airbags go through deformation during inflation.

Smith, Rudd and Long [44] investigated a model for simple shear of woven fabrics and its influence on fabric permeability and elastic properties of engineered and woven glass fabrics. In order to measure the effect of shear on fabrics, simple shear deformation was isolated from any other deformation mode. This was achieved by using a four-bar linkage, shown in Figure 2.7, which clamped the reinforcement along two edges [44]. One edge was connected to the laboratory bench and force was applied to the opposite edge. Five commercially available glass-fibre fabrics were tested.

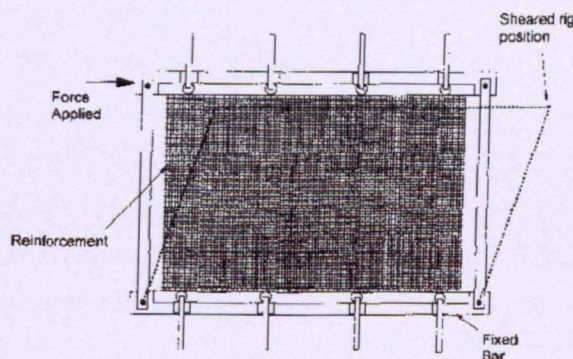


Figure 2.7 Four-bar linkage inter-fibre shear isolation rig [44]

For in-plane permeability experiments they used a radial flow rig which consisted of a thin radial cavity with Newtonian test fluid injected through a central port [44]. They

applied a semi-empirical method to characterise the effect of shear on reinforcement permeability. Predicted results were in reasonable agreement with experimental data, showing the importance of in-plane shear on permeability and hence infusion behaviour.

Bickerton et al. [45] investigated the effect of draping on mould filling processes during manufacturing of compound curved composite parts. An experimental study was designed to show the effect of draping preforms on mould filling. Flow visualization experiments were performed using a conical component. Experimental results showed that draping does significantly change fibre orientation, fibre volume fraction, permeability and injection pressure. Data were compared with numerical predictions for preform deformation and mould filling. They assumed Stokes flow in preform channels and Darcy flow in the preform itself. They considered only in-plane permeability. Mold filling simulations were completed using a code developed at University of Delaware, called LIMS (Liquid Injection Molding Simulation). Preform deformation predictions were found to overpredict in areas of high deformation, due to the assumptions made by the numerical algorithm used. Predictions of injection pressure and flow rate histories were good, while predicted flow front shapes failed to capture some experimental features [45].

Chen and Chou published a series of papers concerned with the study of compaction of woven fabric preforms in liquid composite moulding. Their first paper described a theoretical study of elastic deformation during the compaction of woven fabric preforms in liquid composite moulding for a single layer of fabric [46]. The analysis focused on the unit cell of an orthogonal plain-weave fibrous preform, which was composed of two sets of mutually orthogonal yarns. A 3D model was proposed and was used to predict compressive behaviour of yarns. The assumptions were: the unit cell repeated in the plane of the fabric, which was infinite in extent; the yarn was treated as a transversely isotropic solid (the fibres in the yarns were highly compacted); the external compressive force was applied uniformly on the fabric preform; the elastic deformation of the fabric took place only in its thickness direction, neglecting in-plane deformation; during the compaction process, the yarn shape deformed but the yarn cross-section area remained unchanged. On the basis of

their model based on beam theory, analytical expressions for relations between the fibre volume fraction, the applied compressive force and preform thickness were established. The analyses focused on a unit cell of an orthogonal plain-weave fabric preform. Later, the same authors published a study of compaction of woven fabric preforms for multiple layer fabrics taking nesting into account [47]. They presented the analytical results for the nesting and elastic deformation during compaction of multi-layer woven-fabric preforms. A 3D model of the unit cell for multi-layer fabrics was proposed with the same assumptions as in their previous paper, and was adopted to predict the compressive behaviour of yarns. They proposed an analytical relationship between the applied compressive force and thickness for non-nesting and maximum nesting cases. For the general nesting cases, an empirical relationship between the compressive force and the thickness reduction was proposed.

Later, Chen, Chou and Lang studied fabric compaction behaviour in resin transfer moulding experimentally and theoretically [48]. Compaction experiments were carried out for three types of preforms: continuous strand mats, plain woven fabric, and unidirectional knitted materials. In-situ contact pressure between adjacent fabric layers during compaction was measured using a TekScan (pressure mat) system. The results of pressure measurements motivated the improvement to the compaction model. The theoretical part of their study focused on modelling compaction behaviour of woven-fabric preforms with uniform, linear and sinusoidal inter-layer contact pressure distribution. The improved model was applied to predict the geometry of the resin channels of the preform under compaction. They used the same assumptions as proposed in previous papers. They found from experimental work that, as expected, a longer time was needed to infuse more compacted preforms because of the lower resulting permeability. The infiltration time increased with fibre volume fraction, due to the decrease in preform permeability. The permeability prediction model was based upon approximated two-dimensional lubrication flow in open spaces between yarns, and one-dimensional Darcy's flow within fibre bundles. The basic input data for permeability calculations were the thickness of all fabric layers and all resin channels between fabric layers. The permeability was obtained as a function of fibre volume fraction, as well as thickness reduction, and therefore, the externally applied pressure. This knowledge can be readily used for evaluating the permeability as a function of

applied pressure in the resin transfer moulding process [48]. However, there were no results for through thickness permeability.

Takano et al. [49] used a microstructure-based computational approach to predict the permeability tensor of woven fabrics for resin transfer molding simulation. An asymptotic homogenisation theory was employed to evaluate the permeability from both macro- and microscopic standpoints with the help of the finite element method (FEM). This theory allowed them to study the relationship between mesoscopic woven architecture and macroscopic permeability based on the method of two-scale asymptotic expansions. They presented a typical numerical example to discuss the permeability characteristics of plain weave fabrics undergoing shear deformation in comparison with the undeformed material. They considered a porous medium with periodic microstructures saturated with viscous fluid. They also assumed that all models had the same fibre volume fraction and the cross-sectional area of the yarn, so that only geometrical configurations would be reflected in the values of permeability. Moreover, microscopic flow inside the yarns was not considered as only saturated flow was studied. Comparison to the experimental data was in planed for future works, and the study only considered in-plane flow [49].

Louis and Huber studied the effect of shear on permeability of woven fabrics during resin infusion [50]. They investigated permeability of four- and five-layer carbon fabric. The investigated fabric was increasingly sheared and the corresponding permeability was determined. The experiments were performed using a twill weave fabric. Three different shearing angles were investigated: 10, 20 and 30°. In order to achieve consistent shearing, fabric layers were stacked first and then sheared manually. The experimental set-up is shown in Figure 2.8 [50]. Vacuum was applied at the edges of the tool and the fluid (vegetable oil) was forced by atmosphere pressure to fill the cavity.

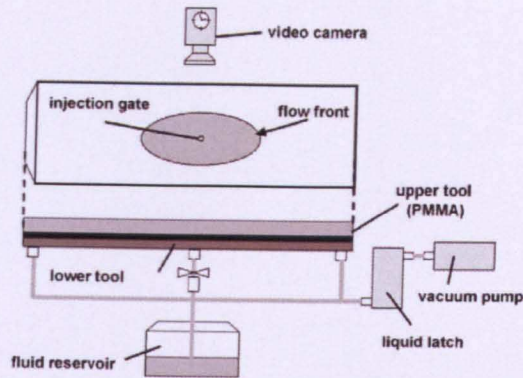


Figure 2.8 Experimental set-up for determination of flow behaviour [50]

The measured material behaviour was imported into commercially available LCM-simulation software which was verified first using a simple plate with sheared fabric, and then using a double curved structure (hemisphere) with draped fabric. Forming simulations were carried out using Pam-Form software from ESI ltd. Two main effects were found. It was found that permeability decreases exponentially depending upon the fibre volume fraction of fabric changed by shearing [50]. This behaviour was expected from the compaction of fibre preforms. Additionally the main axes of the permeability rotated. The rotation angle thereby was dependent on the absolute fibre volume content of the sheared material [50]. However, they did not model through thickness permeability of sheared fabrics.

Endruweit and Ermanni [51] studied in-plane permeability of sheared textiles both experimentally and theoretically. Two-dimensional flow experiments with radial liquid injection were carried out to determine the principal permeability values and the orientation of the permeability principal axes of various glass- fibre fabrics as a function of the fibre angle. Based on experimental results, a basic model to predict the in-plane permeability of sheared initially isotropic fabrics was developed. The principal permeability values were determined based on geometrical considerations, describing initially anisotropic material as a pre-sheared virtual isotropic fabric. The orientation of the principal permeability axes was described by an empirical formula, deduced from experimental observations. Resin flow in both fibre directions was considered as identical. They modelled their fabrics as non-crimp (as shown in Figure 2.9). The deformation modes scissor drape and slide drape were considered (Figure 2.10) [51].

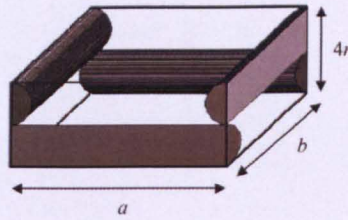


Figure 2.9 Unit cell non-crimp textile with identical fibre material for both fibre directions [51]

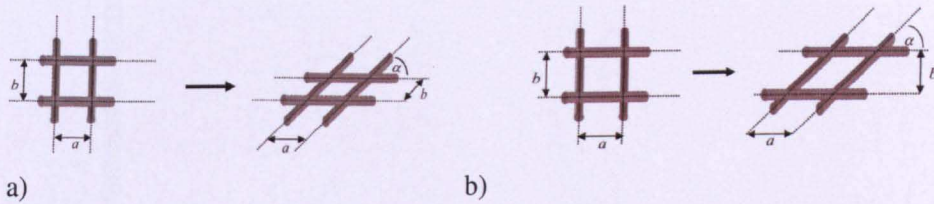


Figure 2.10 Scissor drape (a) and slide drape (b) textile deformation modes [51]

For slide drape, the mobility of the fibres was higher than for scissor drape, causing a higher significance of the fibre reorientation compared to the decrease in porosity than for scissor drape. The normalised permeability values for scissor drape showed qualitatively good agreement with the data of normalised permeability values as a function of the ply angle as published previously. For slide drape, the normalised permeability as function of the angle between the fibre orientations deviated significantly from the one for scissor drape [51].

Loix *et al.* [52] proposed a computational model of the macroscopic flow of non-Newtonian fluids through highly deformed woven fabrics. Their method consisted of two steps. Firstly, the shear deformation of textile reinforcement was studied from meso-scale numerical analysis. Secondly, simulation of meso-scale flow of the polymer through the as-deformed woven fabrics was presented. They considered a periodic balanced glass plain. A schematic of the periodic solid REV (Representative Elementary Volume) of such microstructure is presented in Figure 2.11 [52].

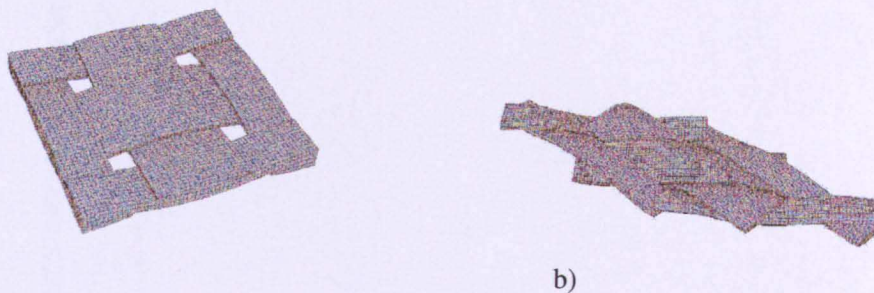


Figure 2.11 Solid REV of the studied plain weave: a) before deformation; b) after a pre-shear angle of 53° [52]

They used the FE code ABAQUS to simulate the shear deformation. The following assumptions were made: very large transformations were taken into account; consistent yarn-yarn contact were assumed; yarns were assumed to behave like transversely isotropic hypoelastic continua; calculations were achieved by subjecting the whole REV to a mean macroscopic displacement gradient corresponding to an in-plane shear. Numerical results emphasised the drastic changes of the permeability when the fabric was sheared. The influence of fluid rheology was also studied in case of generalised Newtonian fluids. A method was proposed to formulate the macroscopic flow law [52]. However, there was no comparison to experimental data.

Based on the literature survey, it is of interest to model permeability through deformed fabrics. Both Darcy and Gebart equations will be used to predict air permeability of deformed fabrics taking into account Chen and Chou's [46, 47, 48] work to calculate thickness reduction and fibre volume fraction after deformation. This is very important for such application as airbags because airbag is going through deformation during inflation.

2.7 THERMAL CONDUCTIVITY PREDICTION USING ANALYTICAL MODELS

The comfort of a garment is dependant on several factors: heat and vapour transfer, lightness, sweat absorption, drying and permeability to moisture and air. Heat transfer continues to be a field of major interest to engineering and scientific researchers as well as designers, developers and manufacturers. Considerable effort has been devoted to research in traditional applications such as chemical processing, general

Through thickness air permeability and thermal conductivity analysis for textile materials

manufacturing, energy devices etc. In addition, a significant number of papers address topics that are at the frontiers of both fundamental research and important emerging applications, such as aerospace, military and sport clothing, insulating textiles materials and so on [53]. Many models are highly specific, whilst others have more general applicability. However, there is still a lack of published studies about through thickness thermal conductivity or heat transfer in textile fabrics.

The earliest model that describes the mechanism of transient diffusion of heat and moisture transfer into an assembly of hygroscopic textile materials was introduced by Henry [54] in 1939. He developed two coupled differential governing equations for the mass and heat transfer in a small flat piece of clothing material. He made several assumptions including that the amount of vapour absorbed by a given quantity of the solid in equilibrium varied in a linear manner with the concentration of vapour and with temperature. It was also assumed that the diffusion constants were independent of the amount of vapour which was absorbed, and of the temperature. Neither of these assumptions will be always true in practice, since the porous solid may swell as it absorbs vapour. Also the rate of diffusion of one gas into another is known to vary as a power of the absolute temperature between 1.5 and 2. The proposed equation for vapour diffusion is the following [54]:

$$\frac{\partial C}{\partial t} = D^* \nabla^2 C - \frac{1-\alpha}{\alpha} \rho_s \frac{\partial M}{\partial t} \quad (2.18)$$

The equation for thermal diffusion is [60]:

$$c\rho_s \frac{\partial T}{\partial t} = k \nabla^2 T + \kappa \rho_s \frac{\partial M}{\partial t} \quad (2.19)$$

However, Henry's work was purely analytical and did not contain any comparison to experimental data.

Brailsford and Major studied thermal conductivity for two-phase media for various types of structure [55]. They showed that for porous media, such as sandstone, the structure plays a vital part in the determination of thermal conductivity. They derived an equation for two-phase media from simple physical models corresponding to various types of structure. For sandstone they assumed that porosity of the solid and fluid region to be the same, and thus equal to the overall porosity. They also assumed that the proportion of the fluid continuous phase was related simply to the true

Through thickness air permeability and thermal conductivity analysis for textile materials

porosity. For natural porous media it had become obvious that the fluid component can play a more important role at low porosities than would be expected for purely random assemblies. Experimental results had reasonable agreement with theoretical work although more experimental work had to be done on the effect of structure on thermal conductivity.

Watt and Darcy [56] performed gravimetric experiments to describe wool-water-vapour adsorption isotherms in the temperature range 20-100°C by using a quartz helical spring mounted in an evacuable apparatus. The wool samples used were pen-grown and degreased by six washes with cold petroleum ether and many changes of distilled water until the pH of the water was unchanged by the contact with the wool. The samples were vacuum-dried in the apparatus. Major factors affecting the measured water content of the wool samples were identified as the previous history of the sample, the amount by which the vapour pressure was changed, and the time allowed for equilibrium to be established; the influence of these factors became more marked at higher temperatures. At higher temperature there were increased water contents at high humidities and decreased water contents at lower humidities. Complete adsorption isotherms were determined over a wider range of temperatures than was previously possible; however, there was no comparison to any analytical model [56].

There are various heat transfer mechanisms for fabrics: conduction by the solid material of the fibres; conduction by the intervening air; thermal radiation and convection [57]. In the absence of radiative heat transfer, the 1-D heat flow at a position x is given by

$$Q(x) = -k \frac{dT}{dx} \quad (2.20)$$

where T is the temperature and k is the thermal conductivity.

Thermal conductivity k can be calculated using a rule of mixtures which combines thermal conductivities of the air (k_A) and of the fibre (k_F) as shown in equation (2.21):

$$k = (1 - V_f) k_A + V_f k_F \quad (2.21)$$

where V_f is the fibre volume fraction.

Through thickness air permeability and thermal conductivity analysis for textile materials

The radiative heat transfer is usually expressed as “radiative conductivity” multiplied by the temperature gradient (see Table 2.5):

$$Q_{RAD} = -k_{RAD} \frac{dT}{dx} \quad (2.22)$$

Table 2.5 Equations for different heat transfer modes and their thermal resistances [57]

Transfer mode	Amount of heat transferred	Thermal resistance
Conduction	$Q = \frac{T_1 - T_2}{L / kA}$	L / kA
Convection	$Q = \frac{T_{surf} - T_{env}}{1 / h_{conv} A_{surf}}$	$1 / h_{conv} A_{surf}$
Radiation	$Q = \frac{T_{surf} - T_{surr}}{1 / h_r A_{surf}}$	$1 / h_r A$

Farnworth studied the mechanisms of heat flow through clothing insulation [68]. His model described combined conductive and radiative heat flow through fibrous insulating materials assuming that there was no convective heat flow. It was compared to experimental values of thermal resistance for several synthetic fibre battings and of a down and feather mixture. It was shown that the difference in resistance per unit thickness among the various materials may be attributed to their different absorption constants. They assumed that a 10-mm thick sample of a 1% fibre batting is held between plates of 90% emissivity at temperatures of 25 and 35°C. The experimental results agreed well with the theory over the region 5 to 8 mm thickness. They explained experimental data by a simple radiative conductivity model. They showed that a high absorption constant will be obtained if the sample has a high fibre volume fraction or small fibre diameter. However, they did not look at the thermal conductivity of very thin fabrics.

Li and Holcombe [59] introduced an extended mathematical model that takes into account the water vapour sorption kinetics of wool fibres to better describe the coupled heat and moisture transport in fabrics. They assumed that the water vapour uptake rate of the fibre consisted of two stages of sorption. The first stage was represented by a Fickian diffusion with constant diffusion coefficient. The second-stage sorption followed an exponential relationship. They used a Crank-Nicholson

implicit finite difference technique to generate the solutions. The predictions from the two-stage model were compared with those from a Nordon-David model and a simple Fickian diffusion model, and with experimental observations on a sorption cell. The two-stage model showed good agreement with the experimental data. However, their model was used for wool fabrics only. There is no evidence that this model would work for other kinds of fabrics.

Yasuda et al. [60] measured the surface temperature of the first-layer of fabric during nonsteady-state transport of water vapour through layered fabrics. The mass of the first layer was changed by tightly stacking the same fabrics, and surface temperature rise was measured as a function of the mass and the kind of polymers. The rise in surface temperature was proportional to the mass of fabrics and the water absorption characteristics of the polymers. They confirmed that the temperature rise that occurs in the space between layered fabrics is due mainly to the heat of absorption of water vapour.

Le and Ly [61] developed a model for the interactive heat and mass transfer that occurs in the forced convection of steam through an absorbing fibrous textile assembly. Application of the model to the steaming of a wool fabric bed revealed a fast front which was associated with condensation and a sharp rise in temperature, and a slow and much broader front which brings equilibrium to the moisture content of the bed. For the initial conditions it was assumed that the textile assembly was uniform in temperature and moisture content and in equilibrium with the moist air surrounding it. The fibres and absorbed moisture were assumed to form a homogenous solid whose properties were specified by the moisture content. The model assumed no movement of liquid water. The pressure difference between the two sides of the bed caused the steam to flow and displace air as it penetrates the bed. The velocity of the steam-flow through the fabric bed was small and the flow was assumed to be Darcian. Experiments carried out on a specially built steaming apparatus gave good agreement on the fabric temperature and regain [64]. However, more work is needed to account for the variation of the diffusivity of a liquid in absorbent material with temperature and concentration.

Ghali, Jones and Tracy [62] developed a numerical model for simulating the heat and mass transfer in fabrics during wicking. The model was applied to two different knitted fabrics: cotton and polypropylene. There were several assumptions: the fibrous system is represented by an ideal continuum divided into volume fractions of liquid, solid and liquid vapour and air mixture at particular locations; the solid phase was considered to be non-deformable which means that mechanical swelling and shrinkage were not included; Darcy's law was used to describe the transient flow through the saturated and unsaturated regions in the fibrous medium; there was no convective flow of the vapour-air mixture; the liquid components were incompressible and the vapour-air mixture was an ideal gas. The model showed that as the water wicked through the fabric specimens, two temperature zones were formed. Within each region the temperature gradient is small, but between the regions it is more significant. The variation of the fractional saturation is continuous along the specimens. Experiments were conducted to obtain the temperature distribution during wicking for the two fabrics. The model had good agreement with the experimental results. However, there were no results for woven fabrics [62].

Fohr, Couton and Treguier [63] developed a model of heat and water transfer through layered fabrics, such as clothing. They considered hydrophilic and hydrophobic treatments, membranes glued onto a layer, and surface modification of the textile (abrading). Physical phenomena taken into account were sorption and desorption; free water condensation or evaporation; liquid, vapour, and adsorbed water diffusion; and heat conduction and contact resistance between layers. Their model was dynamic for one-dimensional transfers. It showed that there was a presence of liquid in certain places in textile layers due to liquid diffusion as well as vapour sorption. In a small average volume, a local thermodynamic equilibrium between solid, liquid and gas phases was assumed. This hypothesis, which seems satisfactory for a thick layer of fibrous insulation such as rockwool, is questionable when dealing with thin textile layers. Fabrics have two scales of pores generated by the manufacturing process – interfibre and interyarn pores, and the diffusion properties of heat and water in liquid and vapour form are determined from this pore network. They assumed that: each layer acts as a homogeneous one with physical parameters which were determined experimentally; contact resistance should occur between the layers; transfer through

Through thickness air permeability and thermal conductivity analysis for textile materials

layers is one-dimensional, from the skin to the outer environment; heat and water transfers were associated with adsorbed (regain) or free water condensation or evaporation. Air filtration through fabric layers was not considered. Radiation was taken into account outside the layers. They compared their model to experimental data presented in the literature [63]. However, more experimental work has to be done to measure the diffusion coefficient for water and contact resistance.

Ghali et al. [64] experimentally investigated the effect of the coupled convection heat and mass exchange within clothing. They also created a model to determine the heat and mass transfer coefficients between the air penetrating the void space and the solid fibre as a function of the velocity of penetrating air. Experiments were conducted inside environmentally controlled chambers to measure the transient moisture uptake of untreated cotton fabric samples as well as the outer fabric temperature using an infrared pyrometer. Moisture uptake was measured at three different volumetric flow rates to represent airflow penetration that could result from slow, medium and vigorous walking. The theoretical analysis was based on a two-node adsorption model of the fibrous medium. An outer node represented the exposed surface of the yarns which was in direct contact with the penetrating air in the void space between the yarns. The inner node represented the inner portion of the solid yarn which was completely surrounded by the outer node. The outer node exchanged the heat and moisture with the flowing air and the inner node, while the inner node exchanged heat and moisture by diffusion only with the outer node. A set of four coupled differential equations were derived describing time-dependent convective heat and mass transfer between the penetrating air and the solid fibre in terms of relevant unknown transport coefficients. The unknown model parameters were adjusted to fit the experimental data. The outer heat and mass transfer coefficients were found to increase with the air penetration flow rate. The physical model of the system as a cross flow of air over a group of cylinders (yarns) had given higher coefficients than the empirical values of the two-node model as expected [64].

The above-mentioned models ignored the effect of the atmospheric pressure on heat and moisture transfer of hygroscopic fabrics. Luo et al. [65] developed a model that takes into account the effect of atmospheric pressure on the heat transfer of fabrics. A

dynamic model of simultaneous heat and mass transfer in hygroscopic porous materials was developed. In the model, evaporation/condensation and movement of water, sorption/desorption of fibre and the effect of atmospheric pressure on mass transfer in porous media were considered. They assumed that the moisture sorption at the fibre surface was instantaneously in equilibrium with the surrounding air. They also assumed that the diffusion coefficient was concentration-dependent and a quadratic function of the water content when sorption was less than 540s. In order to be able to generate a solution they had to specify initial and boundary conditions on the fabric surface in terms of density, saturation, temperature and atmospheric pressure. To derive a numerical solution, they used a finite volume method. They compared the theoretical model to experimental results reported in the literature. It was concluded that atmospheric pressure had a significant impact on heat and mass transport processes in hygroscopic porous materials [65]. Their model can be applied in functional clothing design and other engineering and scientific fields involving heat and mass transfer in porous media.

Sobera et al. [66] studied the performance of protective clothing by coupling various types of numerical simulation of flow, heat and mass transfer. They aimed to develop predictive models for the performance of protective clothing at full body scale. For meso scale Direct Numerical Simulation they used the commercial CFD solver Fluent 6 which is based on an unstructured finite volume formulation. The porous material was treated as a fluid zone where the pressure drop was imposed as a sink in the momentum equation according to Darcy's law. For micro-scale simulations of the flow around the textile fibres they again used Fluent. Due to the low fibre diameter and low velocity; the flow remained laminar and steady. From meso-scale Direct Numerical Simulation it was found that the flow underneath the clothing is laminar and periodic, with the magnitude much smaller than the free stream velocity. It showed that for free flow velocities, the flow underneath the clothing is laminar and periodic. Micro-scale Direct Numerical Simulation revealed a simple relation between textile porosity and permeability. A good agreement was found between flow and heat transfer predictions of Direct Numerical Simulation and Reynolds Average Simulation [66]. However, model did not predict global heat and mass transfer accurately.

Wang et al. [67] proposed a new model of effective thermal conductivity for heterogeneous materials with co-continuous phases. In their approach three methods have been combined to predict thermal conductivity. Their model has significant difference from the conventional five fundamental structural models (Series, Parallel, two forms of Maxwell-Eucken (ME), Effective medium theory (EMT)) which are presented in Table 2.6 [67]. The series and parallel models represent a laminate (layered) structure of phases. The other three models are based on the phases being continuous or dispersed: The ME model represents one continuous phase and one or more dispersed phases and in the EMT model all phases are mutually dispersed. These models are very difficult to implement into fabric thermal conductivity calculations. In his structural model Wang assumed an isotropic material with two continuous phases A and B and one dispersed phase C (Figure 2.12). He used series and parallel models to predict the effective thermal conductivity of material with co-continuous phases [67].

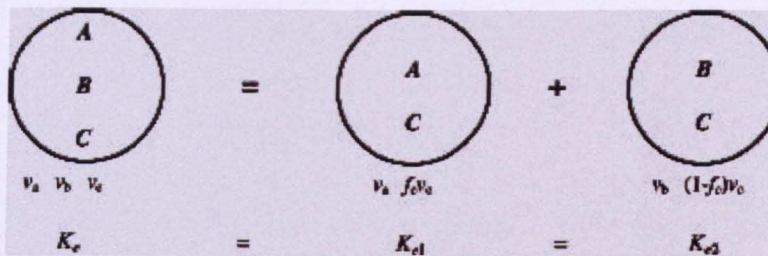


Figure 2.12 A structural model with two continuous (A and B) and one dispersed (C) phase [67]

Using the thermal field model, Wang considered an anisotropic spherical inclusion inserted into an isotropic material with effective thermal conductivity subjected to a uniform temperature gradient as shown in Figure 2.13 [67].

Through thickness air permeability and thermal conductivity analysis for textile materials

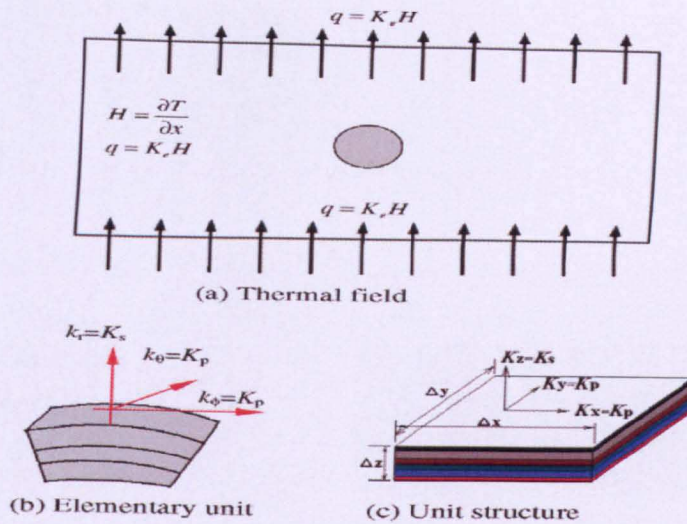

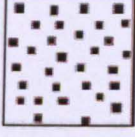



Figure 2.13 A single spherical inclusion dispersed in an infinite medium with heat transfer in one direction: a) thermal field; b) elementary unit; c) unit structure [67]

Wang's model had two applications: to produce composite models using the combinatory rules and to narrow the bounds of the effective thermal conductivity for heterogeneous materials where physical structure can be characterised into general classes. However, there was no comparison with experimental data, only with other theories [67]. It did not take into account textile fabrics' structures.

Table 2.6 The five fundamental structural effective thermal conductivity models for two phase materials [67]

Model	Structure schematic	Effective thermal conductivity equation	Ref.
Parallel model		$K = v_1 k_1 + v_2 k_2$	
Maxwell-Eucken 1 (ME1) (k1 – continuous structure, k2- disperse phase)		$K = \frac{k_1 v_1 + k_2 v_2 \frac{3k_1}{2k_1 + k_2}}{v_1 + v_2 \frac{3k_1}{2k_1 + k_2}}$	[68] [69]

EMT model		$v_1 \frac{k_1 - K}{k_1 + 2K} + v_2 \frac{k_2 - K}{k_2 + 2K} = 0$	[70] [71]
Maxwell-Eucken 2 (ME2) (k1 – disperse phase, k2 – continuous phase)		$K = \frac{k_2 v_2 + k_1 v_1 \frac{3k_2}{2k_2 + k_1}}{v_2 + v_1 \frac{3k_2}{2k_2 + k_1}}$	[68] [69]
Series model		$K = \frac{1}{v_1/k_1 + v_2/k_2}$	

There is a lot of research on thermal conductivity and heat transfer applying to particular clothing applications. Among them, Luo and Xu [72] presented a new algorithm to simulate 2D transient heat and moisture transport behaviour through fabric. They established a 3D geometric fibre model first with anisotropic fibres. The model was deduced by mass and energy conservation. Assumptions included: fibrous porous media volume change was neglected in the simulation process; the inertial force was ignored due to the relatively low velocities for liquid transfer; forced convection such as the effect of wind penetration was neglected; radiation in the process was neglected. They used a finite-difference time-domain approach to solve the partial differential equations. It described the physical mechanisms of heat and moisture transfer in fabric, providing detailed information of the transferring process in fibrous media. The simulation results demonstrated that the new method was relatively accurate and easily implemented. However, the effect of radiation and convection in the 2D transient model needed to be added.

Dias and Delkumburewatte [73] created a theoretical model to predict the thermal conductivity of knitted structures in terms of porosity, thickness and moisture content. The theoretical model consisted of two parts: the porosity model demonstrated the

Through thickness air permeability and thermal conductivity analysis for textile materials

variation of porosity with fabric thickness, width of wales, and width of courses, fibre density and yarn count; the thermal conductivity model showed the variation of the thermal conductivity with thermal conductivity of fibre, the porosity and the moisture content. The pattern of the plain knitted structure and the heat flow model are shown in Figure 2.14 [73]. They considered only thermal conductivity through fabric, assuming that heat entered from one surface and that flow to another surface was normal to the fabric. They assumed that the heat energy losses from the boundaries were negligible. It was assumed that the heat energy passed sections of air, water and fibrous material on its way from the heated surface to the ambient surface. They developed that following equation to connect thermal conductivity with porosity and moisture content:

$$k = \frac{k_m k_a k_w}{(1 - \alpha)k_a k_w + (\alpha - \alpha w)k_m k_w + \alpha w k_m k_a} \quad (2.23)$$

where α is the porosity and w is the moisture content

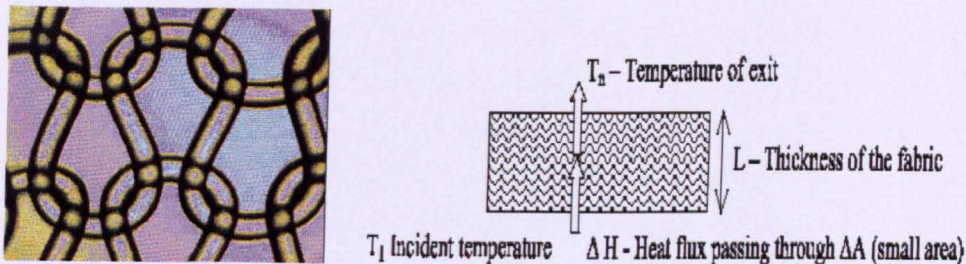
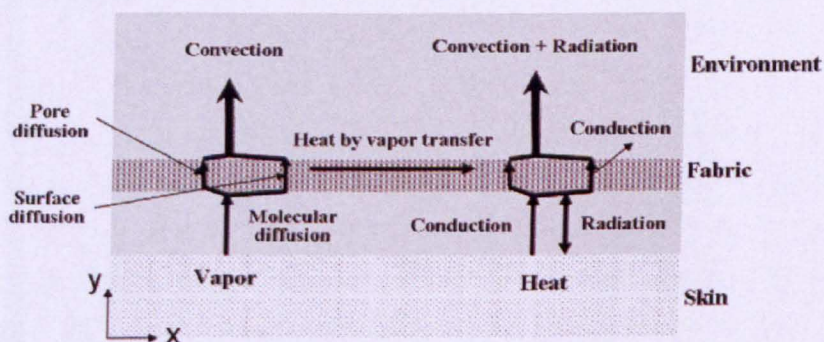


Figure 2.14 Schematic diagram of heat flow through structure and stitch diagram of a plain knitted structure [73]

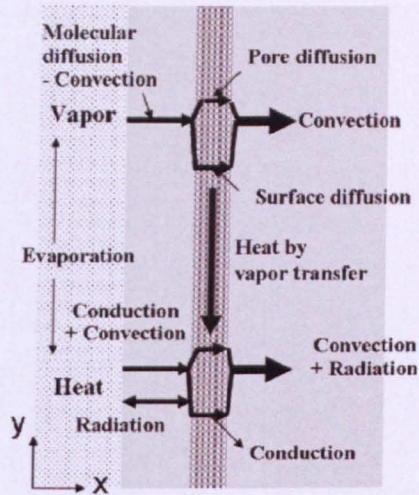
The validity of the model was examined by comparison with results of experiments conducted using different knitted fabrics, in which the porosity, thickness and fibre and water content were different. They showed that the thermal conductivity of a dry plain knitted fabric decreases with increase of porosity, however, with increased water content, an increase in porosity contributes to an increase in thermal conductivity [73]. However, there was no example for woven fabrics in their theoretical model or experimental data. It would be interesting to see whether their model works as well for woven fabrics as for knitted ones.

Min et al. [74] studied the heat and moisture transfer from skin to environment through fabrics. A mathematical model was set up to simulate the heat and moisture transfer from skin to environment through fabrics by including the radiation heat transfer between surfaces and the surface diffusion along fibres. The pathway of the heat and moisture transfer from skin to environment through fabric described in their model is presented in Figure 2.15 [74]. The heat transfer within the fabric was composed of conduction and heat transfer due to the transport of vapour. The conduction is composed of the conduction through solid fibres and through the air filling the interstices between fibres. In the fabric, moisture is transferred by two independent mechanisms of pore diffusion through the interstices between fibres and surface diffusion along the surface of fibres. Temperature and humidity were assumed to be uniform except at the boundary layer adjacent to the fabric. Since it was assumed that the temperature of the fabric surface is higher than the temperature of the environment, there should be a natural convection. In addition, it was assumed that at the skin and in the environment the temperature and relative humidity were constant. For their simulations they had chosen cotton, wool and PET fabrics.

The results showed that the contributions of radiation and conduction through air are approximately 20% each of the total heat flux. Surface diffusion does not play a significant role in the total moisture transport if the surface diffusion is restricted to the chemisorption of water molecules onto fibre surfaces. It was concluded that the microclimate played the most significant role in the heat and moisture transfer from skin to environment [74]. In the case of a vertical system, heat and moisture transfer coefficients are dependent on the length of the channel.



a) Horizontal system



b)

Figure 2.15 Pathway of the heat and moisture transfer from skin to environment through fabric [74]

Total heat flux was 10% larger in the vertical system than in the horizontal system and the fabric surface temperature was 0.2°C lower [74]. However, there was no comparison of predicted results with any experimental data.

Lin and Jou [75] who studied heat transfer and thermal protective properties of clothing materials for firefighters' protective clothing. A firefighter's garment should protect the wearer against the negative effect of either direct flame contact or the radiant and convective heat emitted by fires. On the other hand, the flow of heat and moisture from skin to the environment is impeded by the clothing materials. As a result firefighters may suffer from heat stress when wearing protective clothing in different environmental conditions. The purpose of their study was to investigate the heat transfer capability and the thermal protective property of the clothing materials on firefighter's garment performance. A comprehensive experimental work was conducted on a series of fabric combinations for different layers of firefighter's garments to examine their thermal resistance, evaporative resistance, total heat loss, and thermal protective performance. A sweating torso was also used to simulate physiological behaviour. It was found that the high thermal resistance of a clothing system showed good results in thermal protective performance tests but was problematic in physiological tests. Besides, a water vapour permeable moisture barrier

reduced the amount of moisture in firefighter's protective clothing systems when low to moderate physical activities were undertaken [75].

Comfort of clothing material is one of the most important aspects for sport apparel. Little and Liu evaluated and determined thermal and moisture properties of elastic athletic clothing [76]. Different types of athletic wear with different fibres, fibre content and fabric structures were studied by conducting 3D manikin garment testing under controlled environmental conditions. Their paper showed how a clothing system can affect the performance of the athlete when using form-fitted competition garments. To investigate the thermal and moisture properties of elastic athleticwear, eight sets of commercial male athleticwear products were selected. Each set of sample included one long-sleeved top and long tights. The testing parameter included thermal insulation, moisture vapour resistance and percentage of moisture accumulation within athleticwear. Temperature and moisture sensors were placed on the skin surface at head, chest, waist line, arm, leg and thigh. Their study helped to develop an understanding of the thermal and moisture properties of elastic fabrics used in athletics wear, and built up a basis for further engineered design for optimizing the comfort of competition athletic wear. However, more research is needed to compare the sweating manikin trials with both human subject trials and further physical testing [76].

Havelka and Kus [77] described a theoretical analysis of physiological comfort which is influenced by moisture of air under clothing, skin moisture, and temperature of air under clothing, skin temperature and the content of carbon dioxide under clothing. This contribution deals with the comparison of basic measurable physiological properties of sandwich materials as they were used in real clothing made from smart-barrier textiles, with applications in sports clothing. They focused on the theoretical analysis of transport by diffusion of water vapour through porous semi-permeable-barrier material. The area of comfort for men is quite small and for temperature well-being under clothing must be $32\pm 1^{\circ}\text{C}$, relative humidity $50\pm 10\%$, air stream $25\pm 15\text{cm/s}$, as shown in Figure 2.16 [77].

Through thickness air permeability and thermal conductivity analysis for textile materials

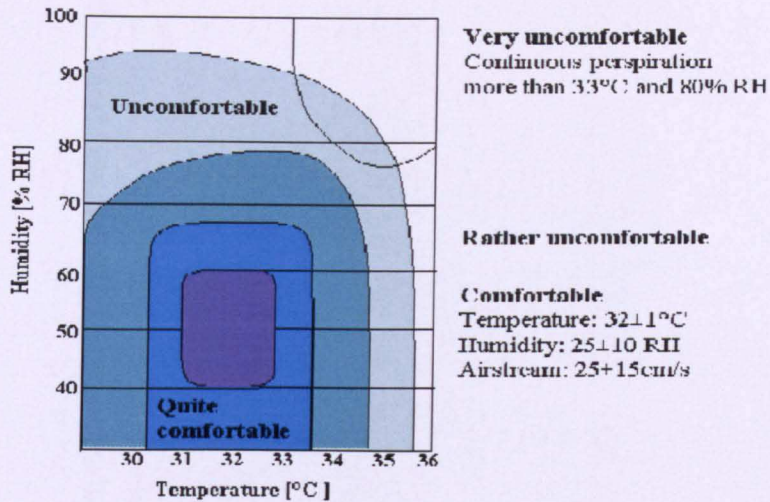


Figure 2.16 Area of clothing comfort [77]

The water transport behaviour of various textile materials has a significant effect on the comfort properties of the wearer. Sarkar, Fan and Chen [78] introduced the novel Transplanar Water Transport Tester (TWTT) for measuring the water transport behaviour in the trans-planar direction for various types of nonwoven fabrics and paper materials. Apart from measuring the initial absorption and surface evaporation, this instrument successfully measured a new parameter named maximum water absorption. In addition, the general trend of the absorption curve was thoroughly investigated and a model was developed using Matlab Software. The instrument comprises two main sections (Figure 2.17) [78]. The first section consists of a horizontal perforated sample podium fitted above a water container, which is placed on a sensitive electronics balance. This water container is connected to a water reservoir, which is fitted on another section of this instrument. The level of water under the perforated plate is kept constant by maintaining a constant height of water in the reservoir. Unlike the existing instruments for water transport behaviour of fabrics or papers, the new instrument has this unique mechanism to control the water level underneath the fabric sample (which is placed on the perforated plate) at a constant level. As a result, the measurements are not affected by the changes in the hydrostatic water pressure during testing. In order to reduce the manual error, a mechanical device is used to place the fabric sample on the sample podium. Automatic data transfer to the computer during testing is another feature of this instrument. Repeated tests on various nonwoven fabric samples and paper materials

showed that the measurements from the instrument are accurate, sensitive and reproducible [78].

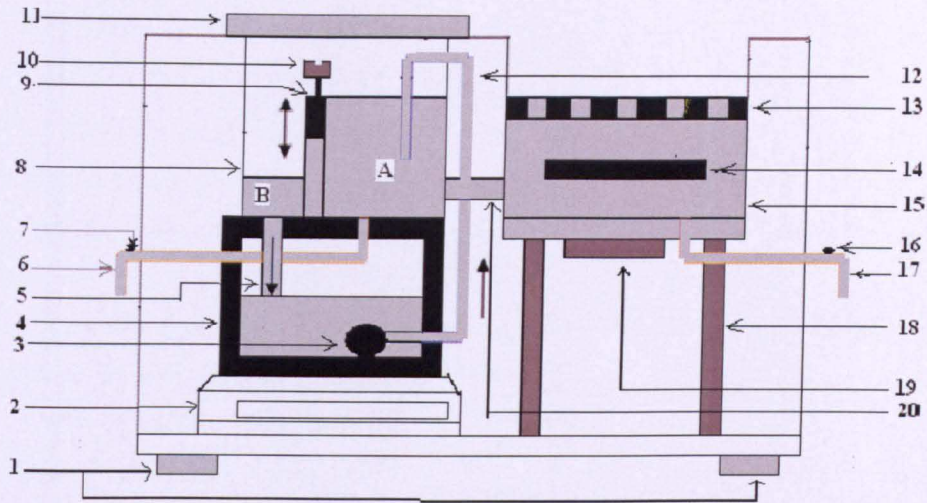


Figure 2.17 Schematic diagram of the Transplanar Water Transport Tester [78]

- 1 - Level Adjusting feet. 2 - Electronic Balance. 3 - Water Pump. 4- Lower water reservoir. 5- Pipe. 6 - Drainage. 7 - Drainage taps. 8 - Upper water reservoir.
- 9 - Height adjustable wall. 10 – Height adjusting screw. 11 - Cover of the upper reservoir. 12 - Pipe. 13 - Perforated plate for placing the sample. 14 - Water Temperature sensor. 15 - Water container under the sample podium. 16 - Tap for Drainage. 17 - Drainage pipe. 18 - Support frame. 19 - Heater. 20 - Soft pipe.

The study showed that the novel Transplanar Water Transport Tester can accurately measure the water transport behaviour of nonwoven fabrics and papers. The main advantage of this instrument is that, it has a unique mechanism to control the water level underneath the absorbing sample at a constant level (i.e. the water level is not reduced with the water transport into or through the fabric sample), as a result the measurements were not affected by the changes of hydrostatic water pressure during testing. Using this instrument it was possible to measure precisely the Maximum Water Absorption (MWA) properties of various materials apart from the initial absorption and surface evaporation, simulating a realistic end use condition [78].

Dasgupta et al. [79] presented effective thermo-mechanical and thermal properties of plain-weave fabric-reinforced composite laminates obtained from micromechanical analyses and a two-scale asymptotic homogenization theory. A unit cell, enclosing the

characteristic periodic repeat pattern in the fabric weave, was isolated and modelled. The orthotropic tensor for effective mechanical stiffness, coefficient of thermal expansion and thermal conductivity were obtained by numerically solving appropriate microscale boundary value problems in the unit cell by the use of three-dimensional finite element analyses. Analytical models consisting of series-parallel thermal resistance networks were developed in order to obtain orthotropic thermal conductivity. The numerical and analytical models are explicitly based on the properties of the constituent materials and three-dimensional features of the weave style. Unit cell model is shown in Figure 2.18 [79]. In the analysis the following was assumed: the laminate is not only orthotropic but also the warp and the fill directions are identical, giving a balanced-ply construction and cubic symmetry; yarn fibre bundles impregnated with resin can be modelled as transversely isotropic unidirectional composites; contact between dissimilar materials is perfect.

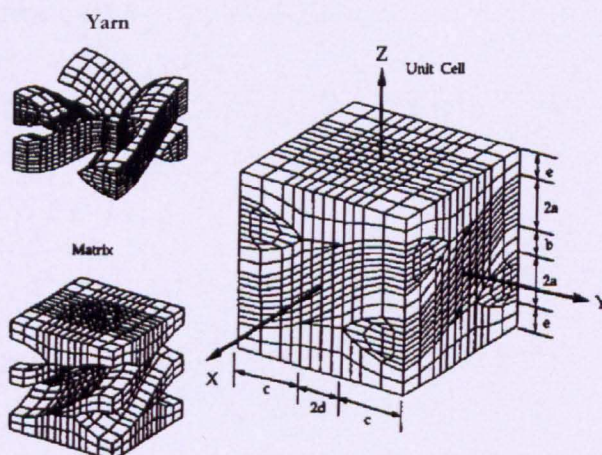


Figure 2.18 Unit cell for plain-weave fabric-reinforced composite showing dimensional parameters [79]

Through thickness air permeability and thermal conductivity analysis for textile materials

They proposed two different thermal models: one for in-plane and another for out-of-plane effective thermal conductivities. In both models, the domain of the mesoscale boundary value problem is a quarter of the unit cell. Equivalent thermal resistances were selectively assembled in series and parallel to form three-dimensional networks in order to simulate the actual heat conduction through the domain. Parametric studies were conducted to examine the effect of varying fibre volume fraction on the effective thermal properties. The thermal conduction properties of low conductivity resin and low fibre volume fraction laminates were dominated by the resin conductivity. Results showed good agreement with experimental data [79]. However, there was no study on transverse thermal conductivity of unbalanced composites or fabrics.

There are many papers containing models for predicting the thermal conductivity of composites or heterogeneous materials based on composition. For instance, Ning and Chou [80] developed a micromechanics model to predict the in-plane effective thermal conductivities of plain-weave fabric composites based on a thermal-electrical analogy. They modelled in-plane thermal conductivity in warp and fill directions for S-glass, E-glass, graphite and Kevlar-49 plain weave fabric-reinforced epoxy composites. Their study focused on non-hybrid plain-weave fabric laminae. The fibre materials of warp and weft yarns were identical, yet their width and thickness were assumed to be different. In addition, it was assumed that thermal contact resistance between the fibre and matrix was negligible; heat flux was along the x direction and the flux lines were straight and parallel to one another; the in-plane effective thermal conductivity of a plain-weave fabric lamina in the warp direction was the same as that of the unit cell in the same direction. Their idealized unit cell is presented in Figure 2.19 [80].

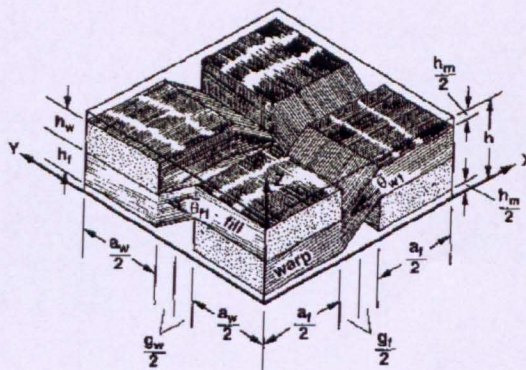


Figure 2.19 The idealized unit cell [80]

Through thickness air permeability and thermal conductivity analysis for textile materials

They described the relationship between the effective thermal resistance, R and the in-plane effective thermal conductivity, k_{ew} , of the half unit cell in the warp direction as presented in Equation (2.24) [80].

$$R = \frac{2(a_f + g_f)}{k_{ew}(a_w + g_w)h} \quad (2.24)$$

where a_f , a_w are yarn width of fill and warp yarns respectively, g_f and g_w are gap width between two neighbouring yarns in fill and warp directions respectively, h is the thickness of lamina.

There was good agreement between their predicted results and published analytical, numerical and experimental models. The model for the plain-weave fabric can be extended to satin-weave composites.

Recently FE modelling became more popular to predict thermal conductivity of composites. Woo and Goo [81] studied thermal conductivity of a carbon-phenolic 8-harness satin woven composite using FE modelling and compared experimental results with predictions. In the analysis, the satin weave unit cell was identified and modelled discretely by 3-dimensional finite elements, considering the interlaced fibre tow architecture. At the unit cell boundary, the corresponding periodic boundary conditions were applied. They investigated the effect of microstructural parameters and boundary conditions on thermal conductivity. The experimental apparatus and the model unit cell are presented in Figure 2.20 [81]. They used a comparative method in which the conductivity is obtained by comparing the temperature difference between a reference specimen with a known thermal conductivity and the test specimen in steady-state conditions [81].

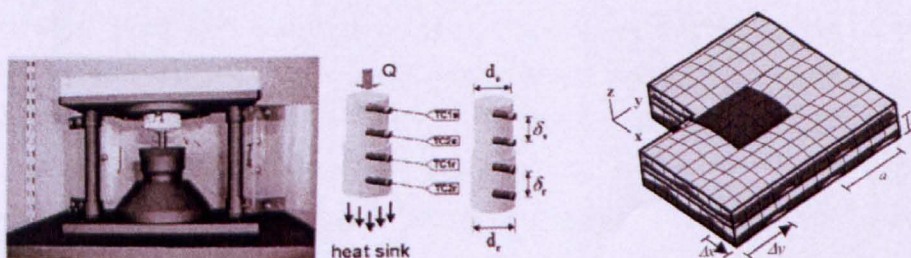


Figure 2.20 Measurement apparatus and Unit cell mesh for a two-layer 8-harness satin weave composite [81]

Through thickness air permeability and thermal conductivity analysis for textile materials

The effective thermal conductivity predicted by finite element analysis agreed reasonably well with the experimental results. The transverse conductivity varied as the phase shift changed, however the amount of variation was not significant. It was found that higher and lower transverse conductivities resulted when temperature and flux boundary conditions were applied. Transverse conductivities converged as the number of layers increased. In relation to fibre volume fraction, conductivity increased almost linearly. It was also found out that conductivity was dependent on the waviness ratio [81].

Hind, Robitaille and Raizenne [82] worked on a model which describes heat transfer through woven composites at the unit cell level. Parameters included yarn section, width, thickness and spacing, fibre volume fraction and thermal conductivities of yarns. The materials modelled were plain woven orthotropic carbon fibre yarns in epoxy. Models and meshes were created using TexGen and Gambit and the solver was Nastran. Boundary conditions were defined by imposing uniform temperature at all nodes of the top and bottom surfaces of the unit cell. Unit cell sidewalls were set as adiabatic. Simulated effective transverse thermal conductivity of the composite material ranged from 0.43 to 1.14 W/m⁰C. This compared with 0.57 W/m⁰C (measured) for 2/2 twill carbon fibre composite. The parametric study showed that in addition to modifying the overall fibre volume fraction, geometric parameters also affect thermal conductivity for the unit cell with constant fibre volume fraction. The simulations showed that crimp geometry had a major effect on thermal conductivity. It showed the influence of the weave pattern on thermal conductivity. It predicted that thermal conductivity decreased as yarn aspect ratio increased, and as yarn section shape power increased. In addition, thermal conductivity increased as the ratio of yarn width to spacing increased for both in-plane and through-thickness directions; and as yarn or resin conductivity increased [82].

Schuster et al. [83] studied the effect of three-dimensional fibre reinforcement on the out-of-plane thermal conductivity of composite materials. Composite performs were based on 3D orthogonally woven carbon yarns and plied copper wires in the thickness direction. After infusion, using a vacuum-assisted resin transfer molding process, the measured out-of-plane thermal conductivities of the resultant composites showed

significant increase compared to a typical laminated uniaxially or biaxially reinforced composites. They showed that although the through thickness thermal conductivity of the sample increased with fibre volume fraction, the values did not match those predicted by the rule of mixtures. Using finite element models to better understand the behaviour of the composite material, improvements to an existing analytical model were implemented to predict the effective thermal conductivity as a function of the composite material properties. Thermal conductivity measurements were conducted according to ASTM E 1225-04 allowing measurements of circular samples with a diameter of 50.8mm at thickness from 2 to 50 mm. For finite element analyses COSMOSWorks software was chosen. Although the development of a purely analytical thermal conduction model for a complex system is unlikely due to the three-dimensional nature of heat flux, the introduction of two factors to the simple rule of mixtures estimation led to reasonably accurate model predictions for the sample tested. Experimental data showed that with a copper fibre volume content of about 6% the maximum possible out-of-plane thermal conductivity can be increased by a factor of eight over that of a traditional uniaxial or biaxial laminated composite [83].

Summarising all research described above, the rule of mixtures and Ning and Chou [80] analytical model were chosen for our study for one-layered fabrics as reasonably simple approaches which include known parameters. For multiple-layered fabrics a unique method will be developed as there was no approach which was reasonable to apply for textile fabrics. For the influence of moisture content on thermal conductivity, the Dias and Delkumburewatte [73] approach was used due to its accuracy and simplicity.

2.8 CURRENT DEVELOPMENTS

There is much research work on permeability and thermal conductivity which has been published during the last century. There is a better understanding now about factors which influence fabric permeability and thermal conductivity and how these factors can be adjusted to the benefit of a manufacturer. Fabric permeability is influenced by fabric structure, number of gaps and their orientation within the fabric. Yarn permeability can have a significant influence on fabric permeability, especially

Through thickness air permeability and thermal conductivity analysis for textile materials

for very tight fabrics when almost all flow goes through the yarns. Fibre orientation and fibre volume fraction are two of the main factors influencing fabric permeability. Deformation such as shear or compaction can change fabric permeability dramatically. Thermal conductivity is influenced by fabric structure, fibre conductivity and moisture content.

While research interest has continued to grow in numerical simulation and analytical description of flow through fabrics, its application in industry is still limited. There is still a large dependence on experimental data. The reason for this is that simulations for fabric permeability require accurate data on the fabric structure. Another problem is the simulation time. For complicated structures simulation time can be between several hours to several days. Cost considerations dictate that for a successful industrial simulation, the software must be easy to use, cover a large variety of fabric structures, and be reliable and fast. So far, no model fits all these criteria.

A significant observation is that permeability through gaps in textiles and permeability through yarns have been developed separately by many researchers. Only a few authors tried to connect these two mechanisms together. In addition, there is a lack of information regarding permeability through deformed fabrics. Thermal conductivity was studied by many authors, however, there is only limited work describing thermal conductivity of textile fabrics, taking into consideration moisture content.

The focus of this work is to develop a generic model which can describe various types of fabrics and account for the effects on permeability of factors such as fabric structure (yarn width and yarn spacing, gaps between yarns and inside yarns, thickness, and interlacing pattern), fabric finishing, nesting in multi-layer fabrics, fabric shear and compression. It also aims at predicting thermal conductivity of fabrics taking into consideration the influence of moisture. A suite of models with these capabilities would be able to predict both permeability and thermal conductivity for arbitrary fabrics. These approaches are described in the next chapters.

CHAPTER 3

PERMEABILITY PREDICTION OF TEXTILES USING ANALYTICAL METHODS

3.1 INTRODUCTION

One of the core aims of developing a textile permeability model is to predict permeability taking into account different factors such as fabric structure, porosity, fibre properties etc. This would complement experimental data by allowing the prediction of fabric permeability before doing experiments and could help manufacturers to produce fabrics with improved properties. Engineers will be able to predict how fabric will behave under different conditions and modify the configuration to suit the specific application. This chapter describes the development of a predictive through thickness air permeability model for different types of fabrics. An accurate description of the fabric structure is critical to a successful prediction. The issues regarding creating an accurate geometrical model are discussed.

The analytical model described in this chapter is a combination of Darcy's [2] analytical model and Kulichenko model [7] which predicts the permeability through gaps between yarns, with Gebart's model [3] to predict permeability within yarns. These models were chosen based on the literature review described in Chapter 2.

Experimental measurements of through thickness permeability are briefly described in the second part of this chapter. Ten fabrics with different weave styles and materials were investigated. Fabric specification and experimental results are provided.

In the third part, predicted results are compared to the experimental data and analysed. The conclusions are presented at the end of this chapter.

3.2 DEVELOPMENT OF ANALYTICAL MODEL FOR THROUGH THICKNESS PERMEABILITY OF FABRICS

A fluid passes through a fabric according to two different mechanisms: flow through the gaps between yarns and flow through yarns. The nature of these two mechanisms is different. The two mechanisms are illustrated in Figure 3.1: the velocity of air flow through gaps is denoted v_g , through yarns as v_y and average velocity through the whole fabric as v_f .

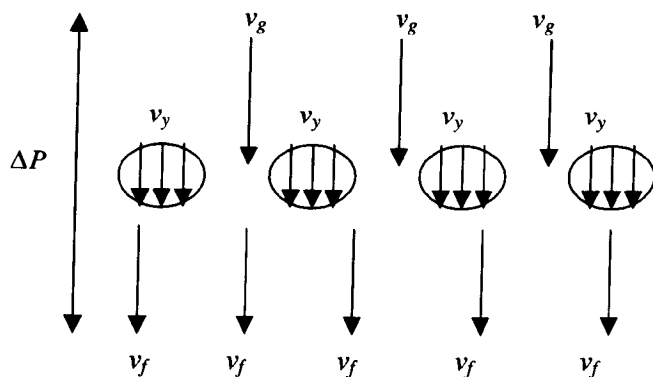


Figure 3.1 Mechanism of air flow v_f through fabric thickness

3.2.1 Analytical model of air flow through gaps

For many practical approaches, most of the fluid will travel through the gaps rather than through the yarns, particularly for loose textiles (those with relatively large gaps). Hence, as a first approximation, the secondary flow through yarns is ignored and yarns are assumed impervious to flow. The approach is to replace the irregular gaps between yarns with narrow hollow cylinders with equivalent hydraulic pore diameter. By assuming laminar flow (pressure drop is small), the velocity of fluid in the gaps can be calculated and hence textile permeability can be estimated.

According to Darcy's law [2] air permeability through gaps between yarns can be described as follows:

$$B_g = \frac{\mu t v_g}{\Delta P} \quad (3.1)$$

where B_g is the permeability through gaps, μ is the gas/liquid viscosity, t is fabric thickness, v_g is the velocity through gaps and ΔP is the pressure drop.

Through thickness air permeability and thermal conductivity analysis for textile materials

Kulichenko's analytical model [7] can be used to calculate the velocity of the flow through gaps. Kulichenko developed a model of the "ideal soil" pore system, a system of parallel capillaries. It was assumed that the flow is laminar. The pore cross-section size and shape is constant over the entire length as was described in Chapter 2.

$$v_g = \frac{v_f}{R} \quad (3.2)$$

$$v_f = \frac{\Delta P}{80\mu} \frac{d_h^2 L}{t} \quad (3.3)$$

where v_g is the velocity through gaps, v_f is the velocity through entire system, d_h is the hydraulic pore diameter and L is the looseness factor.

It was assumed that the pore is of rectangular shape. The following equation is used to calculate the hydraulic pore diameter [93]:

$$d_h = \frac{2(s_e - d_e)(s_p - d_p)}{(s_e - d_e) + (s_p - d_p)} \quad (3.4)$$

where s_e is the warp spacing and s_p is the weft spacing in mm.

Combining equations (3.1) and (3.3) gives the following equation to calculate textile permeability assuming that all the flow is through the gaps:

$$B_g = \frac{d_h^2}{80} \quad (3.5)$$

The looseness factor is used to calculate the porosity of the fabric. It represents the ratio of the width of the pores in the fabric to the yarn width. Hence $s = 0 \dots 1$, where low values of s represent tight fabrics, and high values of s represent loose fabrics.

Looseness factor can be calculated as follows [10]:

$$L = \frac{s - d}{d} \quad (3.6)$$

where s is the spacing of the yarns, mm; d is the yarn width, mm.

For an unbalanced fabric where $s_e \neq s_p$ and $d_e \neq d_p$, the looseness factor is calculated as follows:

$$L = \frac{L_e + L_p}{2} \quad (3.7)$$

where L_e and L_p are looseness factors in warp and weft direction respectively.

For loose fabrics, ignoring the flow through yarns might be a reasonable assumption, but for tight fabrics and for composites applications where yarns are impregnated by resin flow, it is necessary to consider the flow of fluid through yarns.

3.2.2 Analytical model of air flow through yarns

Gebart's [3] analytical model is used to calculate yarn permeability according to the literature review made in Chapter 2. It has two expressions as shown in Equations 3.8 and 3.9 for in-plane and transverse permeabilities respectively. It was assumed that flow goes perpendicular to the fibres, taking into account only transverse permeability (equation 3.9).

$$B_x = \frac{8r^2 (1 - V_f)^3}{57 V_f^2} \quad (3.8)$$

$$B_y = \frac{16}{9\pi\sqrt{6}} \left(\sqrt{\frac{V_f^{\max}}{V_f}} - 1 \right)^{5/2} r^2 \quad (3.9)$$

where V_f is fibre volume fraction and $V_f^{\max} = \pi/(2\sqrt{3})$.

A hexagonal arrangement of fibres is chosen because the results are closer to the experimental results than for a cubic arrangement as shown in the literature review in Chapter 2. In order to calculate yarn permeability, microscopic images are used similar to the one in Figure 3.2. Fibre volume fraction V_f and fibre radius r are calculated using Image J software [94]. Fibre volume fraction and fibre radius for each fabric was taken as an average of 3 measurements (see Appendix B). Image J calculates the area of the yarn region and also the area of each fibre and number of fibres within the region. For each fabric three measurements in different places of images were made to obtain more accurate results. Then fibre volume fraction is calculated using Equation (3.10). Both fibre and yarn areas were calculated as the average of five yarns.

$$V_f = \frac{\text{Fibre area}}{\text{Yarn area}} \times \text{Number of fibres} \quad (3.10)$$

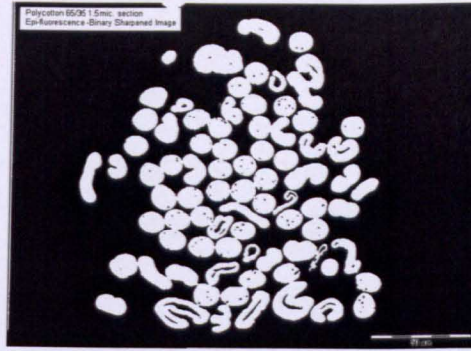


Figure 3.2 Microscopic image of fibres for plain weave U2 fabric with 65%w/v PET fibres and 35%w/v Cotton fibres which have irregular shape.

3.2.3 Analytical model of air flow through whole fabric

To calculate permeability through a whole fabric, the following method is used:

Suppose that air flows through gaps between yarns and through yarns. Let B_g , v_g and A_g be permeability, velocity through gaps and area of gaps respectively and B_y , v_y and A_y be permeability, velocity through yarns and area of yarns respectively. Then B_f , V_f and A_f are fabric permeability, average velocity through the fabric and the area of fabric respectively. Suppose that the thickness of the fabric is equal to the thickness of gaps, which is also equal to the thickness of yarns, $t_f = t_g = t_y$.

Also: $A_f = A_g + A_y$. Then flow rate can be found as: $Q = v_f A_f = v_g A_g + v_y A_y$

According to Darcy's law: $B_g = \frac{\mu v_g}{\Delta P}$ then $v_g = \frac{B_g \Delta P}{\mu}$ and $v_y = \frac{B_y \Delta P}{\mu}$

$$\text{Then } v_f = \frac{v_g A_g + v_y A_y}{A_f} = \frac{B_g \Delta P A_g}{\mu A_f} + \frac{B_y \Delta P A_y}{\mu A_f}$$

After simple rearrangement of the previous equation the following is obtained:

$$\frac{B_f \Delta P}{\mu} = \frac{\Delta P}{\mu A_f} [B_g A_g + B_y A_y] \text{ and } B_f = \frac{B_g A_g + B_y A_y}{A_f}$$

where $\frac{A_y}{A_f}$ is the cover factor and $\frac{A_g}{A_f}$ is the looseness factor.

Air permeability through the fabric can then be calculated as:

$$B_f = B_g L + B_y (1 - L) \quad (3.11)$$

3.3 EXPERIMENTAL MEASUREMENT OF THROUGH THICKNESS PERMEABILITY

3.3.1 Air permeability

Through thickness air permeability was measured according to British Standard BS EN ISO 9237:1995 [85]. According to this standard, air permeability is obtained by measuring the velocity of air passing perpendicularly through a test specimen under specified conditions of test area, pressure drop and time. Apparatus for testing is shown in Figure 3.3 [86]. The equipment which was used for these experiments is an air permeability tester FX 3300. The rate of the air flow passing perpendicularly through a given area of fabric is measured at a given pressure difference across the fabric test area over a given time period. Pressure drop across the specimen test area was set in a range from 100 to 2500Pa, with an accuracy of at least 2%. A suction fan forced the air through the test specimen and adjusted the flow of air gradually until a certain pressure drop was achieved across the test area of the fabric. Test surface area was set as 10cm². Leakage near the edges of the fabric was taken into account by measuring it separately and subtracting from the test results.

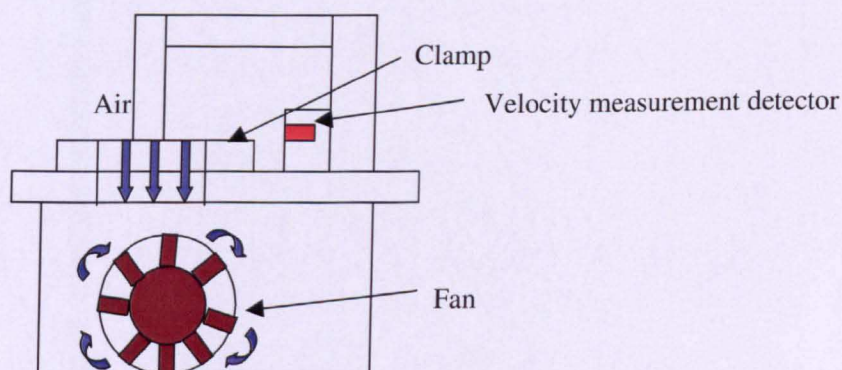


Figure 3.3 Air permeability tester FX3300 [86]

Ten fabrics with different weave styles and materials were investigated. The details of the fabrics are given in Table 3.1. The fabrics were analyzed and measured carefully before modelling. The yarn cross-sections were cut using a laser beam razor blade and the cross-section images were obtained using a TM – 1000 Tabletop microscope. The images were used to measure the yarn spacing and yarn widths. The fabric thickness was measured using the Kawabata Evaluation System for Fabrics (KES-F) (Kawabata, 1982) at a pressure of 0.05KPa [87] (for more details see Appendix C). For each fabric the experiment was repeated three times with a fresh sample.

Table 3.1 Fabrics specification

Fabric code	Description and composition	Structure	Looseness factor L	Fibre radius r μm	Yarn fibre volume fraction V_f	Thickness (mm)	Yarn spacing (mm)		Yarn width (mm)	
							Warp	Weft	Warp	Weft
U1	100% Cotton	Plain	0.32	4.3	0.56	0.323	0.470	0.410	0.405	0.279
U2	65/35 PET/Cotton	Plain	0.32	5.4	0.58	0.229	0.235	0.365	0.195	0.255
U3	100% mercerised, bleached cotton poplin	Plain	0.14	5.3	0.64	0.228	0.195	0.362	0.23	0.25
A1	100% Nylon, Airbag fabric	Plain	0.10	19.9	0.68	0.200	0.450	0.516	0.460	0.423
A3	100% Nylon, Airbag fabric	Plain	0.12	10.3	0.70	0.200	0.356	0.370	0.350	0.30
C1	67PET/33Cotton Desized, scoured, bleached and mercerised	2/1twill	0.32	5.9	0.56	0.419	0.340	0.480	0.310	0.310
C2	67PET/33Cotton Dyed but not finished	2/1twill	0.17	5.9	0.63	0.425	0.33	0.532	0.300	0.430
C3	67PET/33Cotton Finished	2/1twill	0.33	5.5	0.57	0.427	0.300	0.510	0.270	0.330
C7	67PET/ 33Cotton Desized, scoured, bleached and mercerised	2/1twill	0.13	5.7	0.60	0.452	0.340	0.450	0.300	0.400
C8	67PET/ 33Cotton Finished	2/1twill	0.18	5.7	0.61	0.455	0.340	0.430	0.300	0.350
C9	60Cotton/ 40PET Desized, scoured, bleached and mercerised	2/2twill	0.11	5.6	0.67	0.560	0.356	0.520	0.332	0.450
C10	60Cotton/ 40PET Finished	2/2twill	0.13	5.7	0.56	0.610	0.342	0.446	0.313	0.380

Through thickness air permeability and thermal conductivity analysis for textile materials

As seen from Table 3.1 fabrics C1, C2 and C3 have similar 2/1 twill weave structure and geometric parameters. However, these fabrics are interesting due to different finishing. They are used to see the effect of finishing on fabric permeability.

3.3.2 Oil permeability

Oil permeability experiments were conducted to evaluate the effect of liquid viscosity on fabric permeability. In the following, experiments for permeability determination are discussed for a constant volume flow Q of the injected liquid. This can easily be adjusted accurately by using a piston pump and setting the piston velocity v_p for a given diameter d_p of the piston. For each location i in the injection system with cross-sectional area A_i , the actual fluid velocity v_i can be determined from the equation of continuity

$$A_p v_p = A_i v_i \quad (3.11)$$

with

$$A_p = \left(\frac{d_p}{2} \right)^2 \pi \quad (3.12)$$

While setting the volume flow, the maximum applied injection pressure must not exceed 10 bar, since the allowable pressure is limited by the equipment (pressure transducers, tubes). A piston pump for the injection experiments is realised using an Instron testing machine for controlling the piston velocity.

The viscosity μ of the test fluid, which needs to be given for determination of the permeability, can either be measured simultaneously with the injection experiments or can be determined from viscosity data as a function of fluid temperature. In the latter case, the temperature of the fluid in the piston pump is relevant, since the retention period of the fluid in all other parts of the system is relatively short. The thickness h of the uncompressed textile specimens is to be determined prior to the experiments.

The measurement cell for determination of the through-thickness permeability B_3 is shown in Figure 3.4. The tool consists of a stiff cylindrical flow channel with liquid

Through thickness air permeability and thermal conductivity analysis for textile materials

inlet at bottom and liquid outlet on top. The inner diameter d of the flow channel is 80 mm. The textile specimens are arranged horizontally. They are held in position by a perforated plate, which also allows a parallel flow perpendicular to the fabric plane. The influence of the perforated plate on the permeability measurements can be neglected [95]. Pressure transducers are mounted on both sides of the fabric specimen.

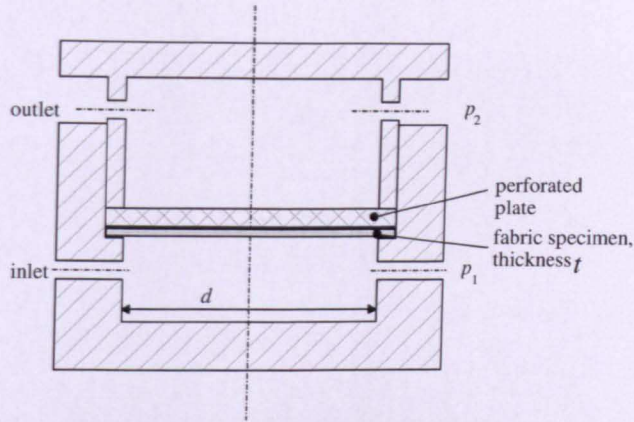


Figure 3.4 Schematic configuration of the B_3 measurement cell and oil rig

With the set-up described above, the pressure values measured by the transducers, which are mounted on both sides of the textile specimen, are determined for given volume flow rate Q , and the pressure drop ΔP is calculated. The saturated permeability

$$B_3 = -\frac{Q\mu t}{\Delta P A} \quad (3.13)$$

Through thickness air permeability and thermal conductivity analysis for textile materials

is determined from the ratio $Q/\Delta p$, which should be constant. From the set of values for Δp , the average value and the standard deviation are calculated. The cross-sectional area

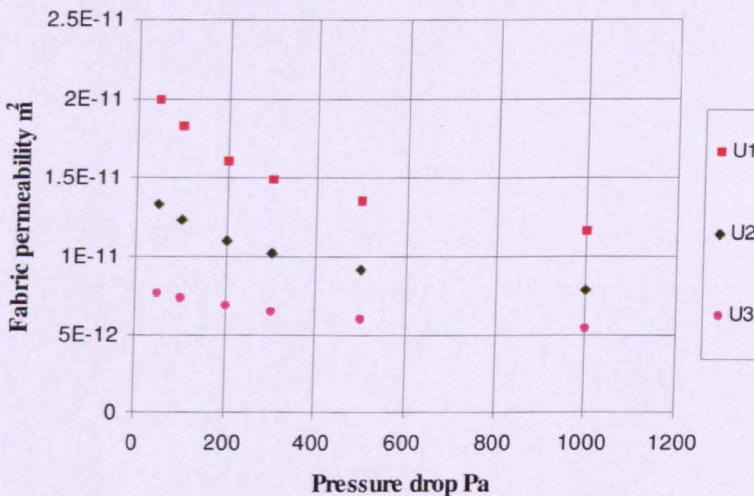
$$A = \left(\frac{d}{2}\right)^2 \pi \quad (3.14)$$

is given by the diameter d of the flow channel.

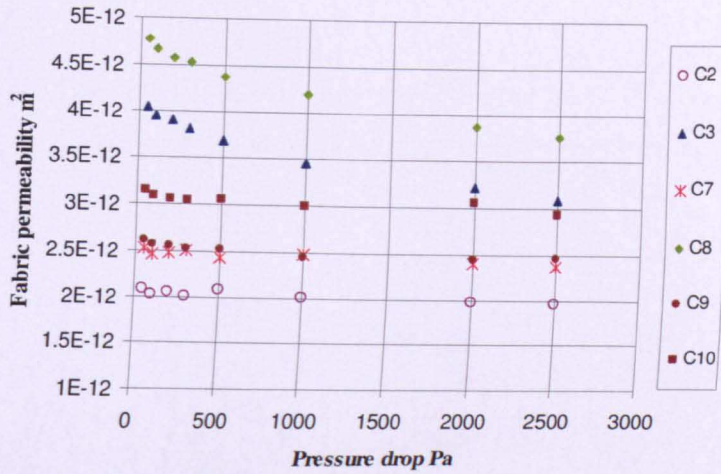
The acquisition and evaluation of experimental data is controlled via a LabVIEW Virtual Instrument (VI). The VI plots the acquired pressure values in real-time and, when the measurement is stopped, calculates the permeability value and generates a protocol file. Before the measurement can be started, it is to be made sure that the textile is completely wetted and no more air is entrapped in the cavity. To achieve this, a pre-experiment is run, until the indicated pressure values become stable.

3.4 RESULTS AND ANALYSIS

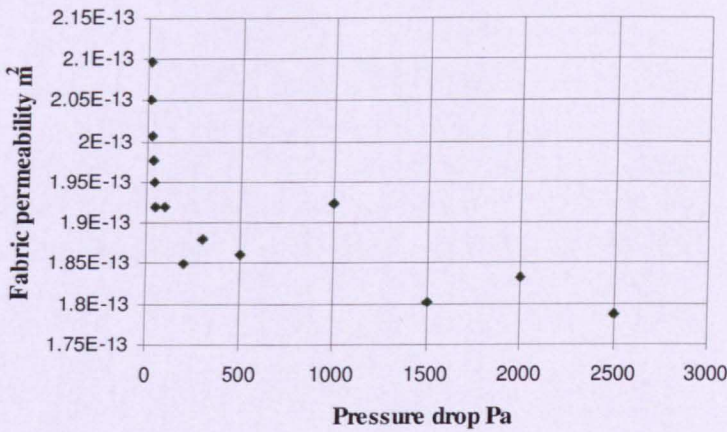
Experimental results for air permeability showed non-linear behaviour in fabric permeability under different pressure (see Figure 3.5). This can be explained by the Forchheimer effect (for more details see Chapter 2 [38], [39]).



a) Cotton fabrics



b) PET/Cotton fabrics



c) Nylon fabric

Figure 3.5 Experimental results of non-linear behaviour of fabric permeability

For the analytical method, to match the experimental set up, a pressure drop of 500 Pa was assumed as it was shown above that flow velocity and fabric permeability vary with pressure drop. Since the fluid used was air at 23°C, air viscosity $\mu = 1.831 \cdot 10^{-5}$ Pa·s [28]. The velocity and permeability calculated using analytical method (equations 3.1-3.4, 3.6, 3.9, 3.11) was compared with experimental results for the fabrics (Table 3.2). In Table 3.2 velocity and permeability through gaps and through yarns as well as overall velocity and permeability through fabrics is presented.

Table 3.2 Comparison between predicted and measured velocity and permeability through gaps yarns and whole fabrics

Fabric code	Predicted permeability through fabric B_f^{pred} pm^2	Measured permeability B_f^{exp} pm^2 (\pm SD)	Predicted/Measured permeability ratio
U1	30.209	12.135(\pm 0.047)	2.5
U2	13.807	8.031(\pm 0.020)	1.7
U3	0.1370	5.789(\pm 0.016)	0.02
A1	0.3027	0.182(\pm 0.0024)	0.13
A3	1.4228	0.240(\pm 0.0047)	1.85
C1	10.5966	3.988(\pm 0.0047)	2.6
C2	4.6131	2.018(\pm 0.0060)	2.3
C3	10.9087	3.609(\pm 0.0055)	3.0
C7	3.1465	2.331(\pm 0.0033)	1.3
C8	4.8347	4.191(\pm 0.0075)	1.6
C9	2.6112	2.485(\pm 0.0008)	1.05
C10	3.7936	2.904(\pm 0.0026)	1.3

Comparison between through thickness air and oil permeabilities for two fabrics is presented in Figure 3.6. There is a good agreement between the two experimental techniques.

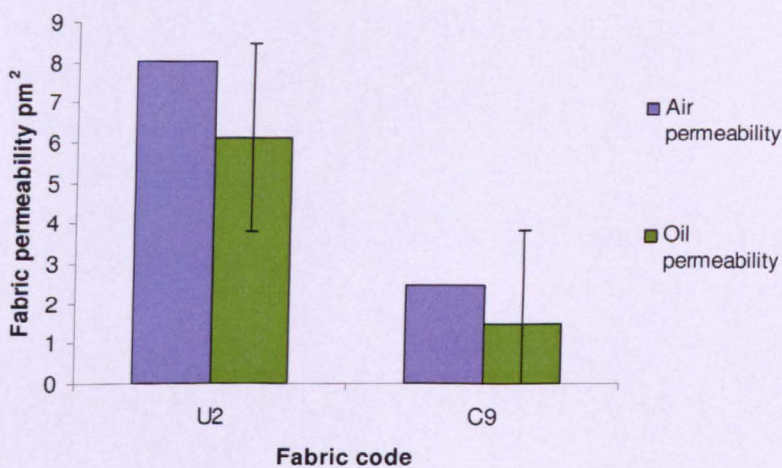


Figure 3.6 Comparison between experimental results for through thickness air and oil fabric permeabilities

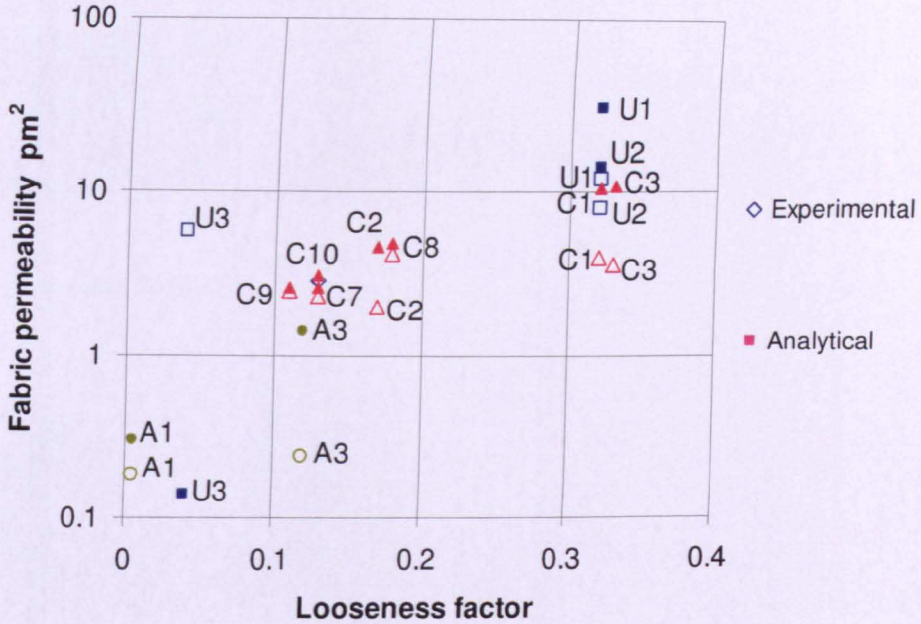
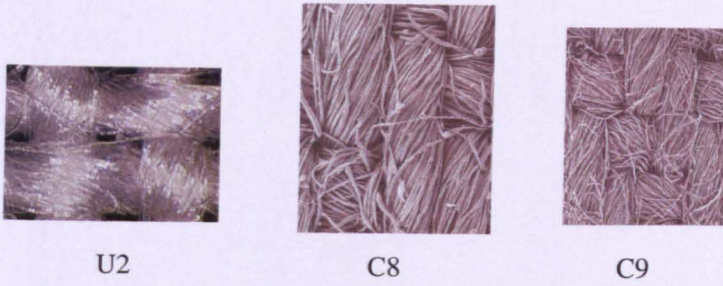


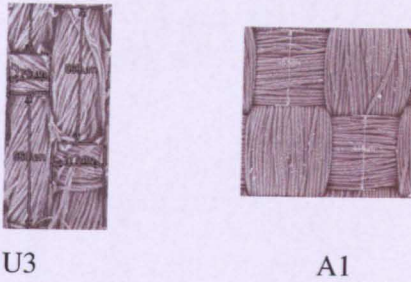
Figure 3.7 Comparison between measured and predicted through thickness air permeability

As seen from Figure 3.7 and Table 3.2 fabric permeability increases with increase of looseness factor which is expected as fabrics becomes looser and more permeable. All predicted results can be divided into four main groups according to the agreement with experimental results: 1) in very good agreement - C7, C9 and C10 fabrics; 2) in good agreement - U2, C8 and A3; 3) in average agreement - U1, C1, C2 and C3; 4) in poor agreement - U3 and A1. This might be due to the simplifying assumptions made in the analytical model. For example, fabrics with rectangular pore shape (C9, U2, C8) has very good and good agreement with experimental data, whereas very tight fabrics with overlapping yarns (U3, A1), where it is not clear what is the shape of the pore, have poor agreement (Figure 3.8).

Through thickness air permeability and thermal conductivity analysis for textile materials



a) rectangular pore shape



b) tight fabrics

Figure 3.8 Microscopic images of fabrics: a) rectangular pore shape; b) tight fabrics

Figure 3.9 shows a comparison between fabric permeability of C1, C2 and C3 fabrics which have the same structure but different finishing. As seen from the figure, finishing has significant influence on fabric permeability and on yarn permeability particularly. Yarn permeability decreases as fibres become close to each other during the finishing process as seen from Figure 3.10. C1 is a desized, scoured, bleached and mercerised woven fabric. Fibres inside its yarns are loose with large gaps between each other. C3 fabric is a finished woven fabric (including mechanical shrinkage). Fibres in C3 are very close to each other with almost no gap between them. Fabric permeability of these three fabrics becomes first lower than again increases as seen in Figure 3.9. That happens because first porosity decreases (C2 fabric) and then again increases (C3 fabric) as seen from Table 3.2. Figure 3.9 shows the same trend between predicted and experimental results.

Through thickness air permeability and thermal conductivity analysis for textile materials

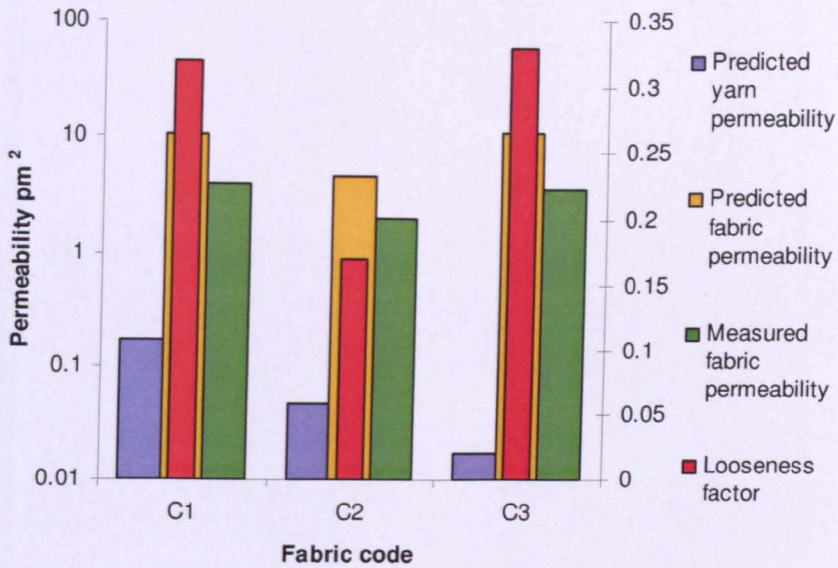


Figure 3.9 Comparison between yarn and fabric permeabilities for C1, C2 and C3 fabrics

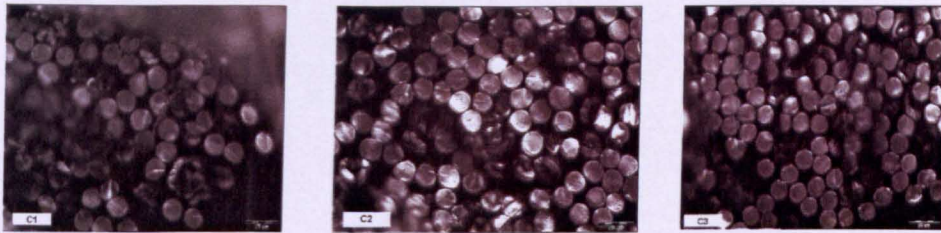


Figure 3.10 Microscopic images of fibres within yarns for C1, C2 and C3 fabrics.

Influence of finishing has also been studied using 100%PET plain woven U4 fabric. Three types of finishing have been applied to it: U4A – Synperonic A7, U4B – Glycerol, U4C – Cirrasol PE 113. These fabrics contain both untwisted and twisted yarns and overlapping regions which makes it more difficult to create and analyse their geometries. Figure 3.11 shows microscopic images of fibres within yarns for U4A, U4B and U4C fabrics. Figure 3.12 shows the influence of finishing on looseness factor L and fabric permeability B_f . As seen from Figure 3.12 finishing has significant influence on looseness factor as the gaps between yarns become larger. It also has an influence on yarn permeability. In U4A fibres are quite loose with significant gaps between each other. Fibres in U4B fabric become closer to each other making gaps smaller and yarn permeability decreases. U4C fabric contains fibres

Through thickness air permeability and thermal conductivity analysis for textile materials

which have significant gaps between each other. This results in an increase in yarn permeability. Predicted and measured fabric permeabilities have similar trend. Predicted results do not have good agreement with experimental data due to the complex geometry of these fabrics. However, the analytical model again shows the same trend as experimental data.

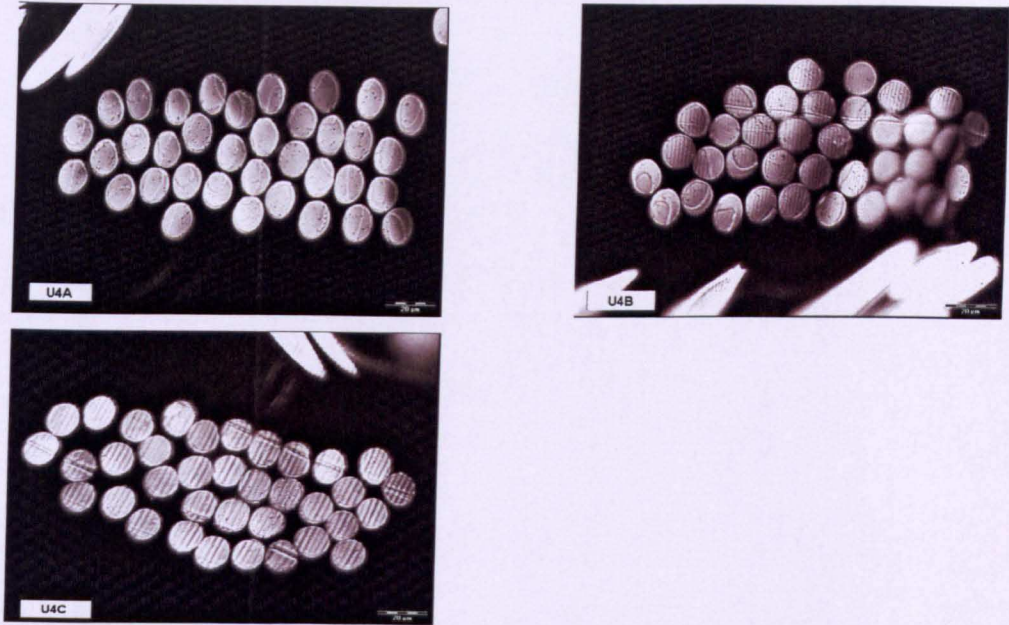
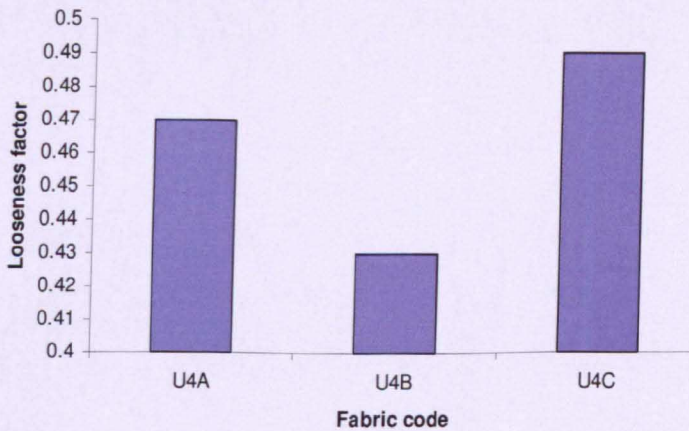
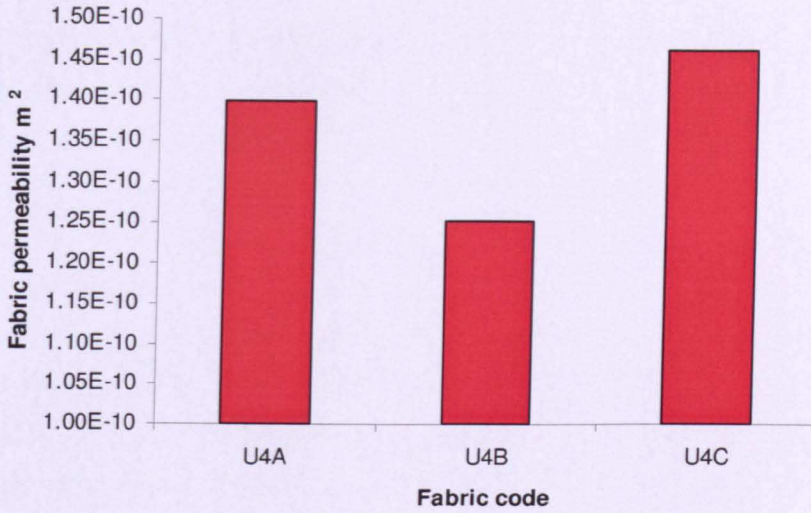


Figure 3.11 Microscopic images of fibres within yarns for U4A, U4B and U4C fabrics

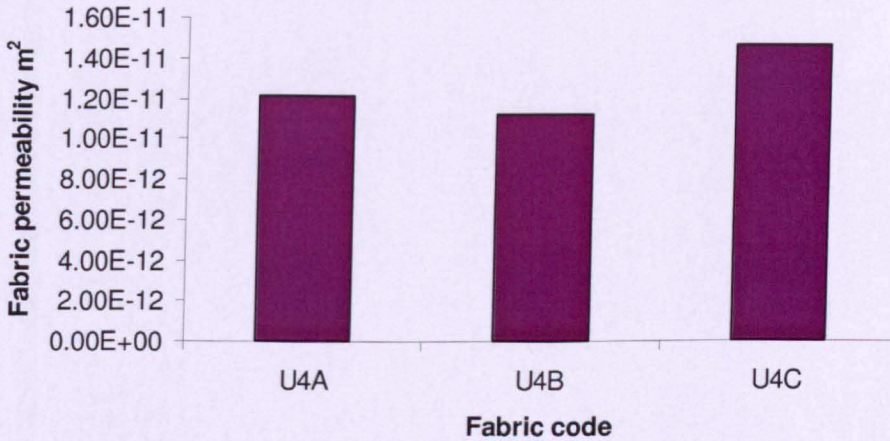


a)

Through thickness air permeability and thermal conductivity analysis for textile materials



Analytical predictions



Experimental results

b)

Figure 3.10 Influence of finishing on: a) Looseness factor L , b) Fabric permeability B_f

3.5 CONCLUSION

Ten fabric permeabilities have been predicted by combining two existing analytical models. Air flow through gaps between yarns is the dominant mechanism for loose fabrics such as U1 and U2. Three fabrics with the same geometry have been

compared to show the influence of finishing on fabric permeability. Predicted results have the same trend as experimental data. Both air and oil through thickness air permeability were measured. There is a good agreement between the two experimental techniques which shows that there is only a slight influence of liquid viscosity on permeability. However, the analytical model has some assumptions which influence the predicted results of the fabric permeability dramatically. Among them is that the pore is rectangular in shape whereas in the reality pore has a more complicated shape (see Appendix C). Another problem in the analytical model is that it cannot model overlapped and very tight fabrics, such as U3 or A3 where predicted results are not in good agreement with experimental data. For almost all twill-weave fabrics the predictions are in good agreement with experiments except for C1 and C3 which may be because weft yarns are twisted and the current analytical model does not take this into account. To avoid these assumptions CFD modelling was used to predict through thickness air permeability of these fabrics, as described in the next chapter.

CHAPTER 4

COMPUTATIONAL MODELLING OF THROUGH THICKNESS AIR PERMEABILITY USING TEXGEN AND CFX 11.0

4.1 INTRODUCTION

One of the main aims of developing a permeability model is to be able to predict permeability accurately and quickly. It was shown in Chapter 3 that the analytical model cannot always predict fabric permeability accurately particularly for very tight geometries such as U3 fabric. For this reason, it is useful to model fabric permeability computationally. With the development of computational systems, many software packages have been created which use fluid dynamics analysis to help engineers to flow through of different types of materials under various conditions. Among such software packages is CFX from ANSYS Inc.

The development of a computational model using the TexGen software [23] to create fabric geometries and CFX 11.0 Computational Fluid Dynamics software [22] to simulate through thickness steady state air permeability of fabrics is described in this chapter. In the first part of this chapter, a modelling approach is described which includes geometric modelling of the unit cells using measured geometric parameters and simulation of through thickness permeability.

The second part of this chapter includes a sensitivity study using the computational model. Dependence of number of nodes and elements on fabric permeability is presented and the influence of meshing on simulation results is discussed.

The third part of this chapter contains a comparison between CFD results and experimental data for through thickness fabric permeability for several fabrics as well as analytically predicted results. Analysis of the results for permeability prediction using CFX 11.0 is presented. Finally, advantages and disadvantages of using CFX and TexGen for permeability prediction in comparison with the analytical approach are discussed.

4.2 MODELLING APPROACH

To simulate through thickness air permeability the following modelling approach has been chosen (Figure 4.1). A unit cell geometry of the fabric was created and meshed in TexGen. CFX 11.0 was chosen for permeability modelling and included three steps: create boundary conditions in CFX-Pre processor, run the simulation in CFX-Solver and view and analyse modelling results in CFX-Post processor.

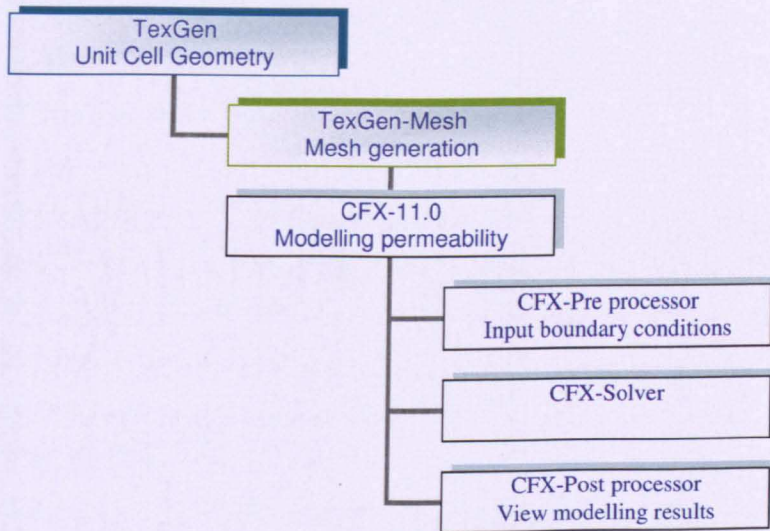


Figure 4.1 CFD modelling approach

4.2.1 Geometric modelling of textile unit cell using TexGen

The Polymer Composites Research Group in the University of Nottingham has created a textile schema, named TexGen [27]. The requirements of this software were to be able to model various types of textile structures as well as export the model for use in a general CAE software package. More information about the workings of TexGen can be found in papers written by Sherburn et al. (2004) and Robitaille et al. (1999, 2003). It is necessary to give a brief description of TexGen as it has been used in this project for geometrical modelling of the unit cell.

TexGen begins with vectors describing the path taken by the yarns within a unit cell. These are then connected to create smoothed path lines, for which user-defined cross sections can be assigned individually to each path line to form yarn volumes. Finally, an analysis domain can be defined around the unit cell. Predefined types of cross-sections available in TexGen are circles, ellipses, shapes produced using a generalised

Through thickness air permeability and thermal conductivity analysis for textile materials

ellipse equation and lenticular shapes. It also allows the user to import self-defined yarn shapes. It is possible to change such properties as yarn width, yarn spacing, fabric thickness, yarn shape etc.

Some of the built-in functions include yarn interference detection and correction algorithms, volume calculation and slice extraction. It is possible to create multiple-layered fabrics using TexGen. One of the recent features of TexGen is the ability to create yarns individually which is useful for very tight and overlapping fabric geometries (see Appendix C).

There are a variety of output options including IGES, STEP files and more recently, Surface Mesh and Volume Mesh files which allows the created geometry to be exported after meshing it in TexGen. The unit cell was meshed in TexGen and saved as .vtu file. Microscopic images were used to measure textile thickness, width and length of weft and warp yarns to create the geometry of the unit cell in TexGen (for geometric parameters see Chapter 3). An example of geometry created in TexGen is represented in Figure 4.2 (more fabrics are presented in Appendix C).

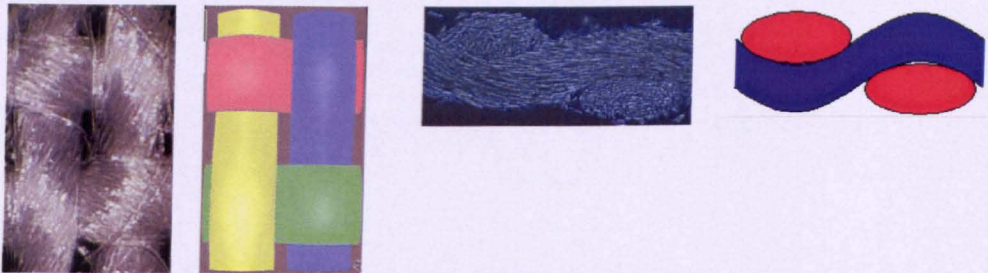


Figure 4.2 Microscopic image of plain weave PET/Cotton U2 fabric and its model in TexGen

Figure 4.3 shows meshed unit cell geometry for U2 fabric. In this case, the number of elements (tetrahedral) is 34600; the number of nodes is 8637.

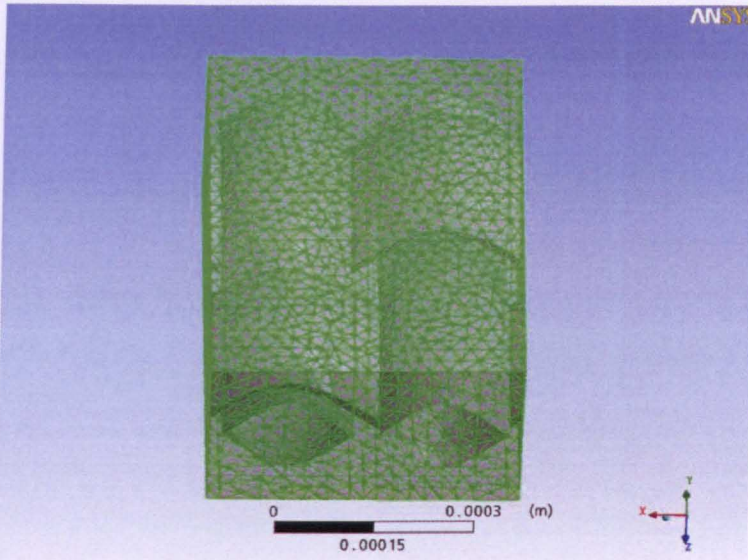


Figure 4.3 Meshed unit cell geometry for U2 fabric

4.2.2 Computational modelling of unit cell using CFX 11.0

A commercial CFD software package, CFX 11.0, marketed by ANSYS Inc. was used in this project [26]. It includes CFX Pre-processor, CFX Solver and CFX Post-processor. The porous model is at once both a generalization of the Navier-Stokes equations and of Darcy's law commonly used for flow in porous regions. It has an extensive range of physical modelling and multiphysics capabilities, including permeability models, heat transfer, and multiphase models.

In deriving the continuum equations, it is assumed that 'infinitesimal' control volumes and surfaces are large relative to the interstitial spacing of the porous medium, though small relative to the scales that one wishes to resolve. Thus, given control cells and control surfaces are assumed to contain both solid and fluid regions. The general scalar advection-diffusion equation in a porous medium becomes [22]:

$$\frac{\partial}{\partial t}(\alpha\rho\Phi) + \nabla \cdot (\rho B \cdot \nu \Phi) - \nabla \cdot (\Gamma B \cdot \nabla \Phi) = \alpha S \quad (4.1)$$

Hence, in the limit of large resistance, an anisotropic version of Darcy's law is obtained, with permeability proportional to the inverse of the resistance tensor. However, unlike Darcy's law, the software works with the actual fluid velocity components U , which are discontinuous at discontinuity in porosity [22].

From the general momentum equation for a fluid domain:

$$\frac{\partial(\rho v_i)}{\partial t} + \frac{\partial(\rho v_j v_i)}{\partial x_j} = \frac{\partial p}{\partial x_i} + \rho g_i + \frac{\partial \tau_{ji}}{\partial x_j} + S_i^M \quad (4.2)$$

the momentum source, S_i^M can be represented by:

$$S_i^M = -C^{R1}v_i - C^{R2}|v|v_i + S_i^{spec} \quad (4.3)$$

where C^{R1} is a linear resistance coefficient; C^{R2} is a quadratic resistance coefficient; S_i^{spec} contains other momentum sources (which may be directional); v is superficial velocity.

A generalized form of Darcy's law is given by:

$$-\frac{\partial p}{\partial x_i} = \frac{\mu}{B}v_i + B_{loss}\rho|v|v_i \quad (4.4)$$

where μ is the dynamic viscosity; B is the permeability; B_{loss} is the empirical loss coefficient.

Implementation in ANSYS CFX [22]:

Comparing equations (4.3) and (4.4), the following coefficients are set:

$$C^{R1} = \frac{\mu}{B}, \quad C^{R2} = B_{loss}\rho \quad (4.5)$$

Data may sometimes be expressed in terms of the true velocity, whereas ANSYS CFX uses superficial velocity. If so, the coefficients are represented by:

$$C^{R1} = \frac{\mu}{\alpha B}, \quad C^{R2} = \frac{B_{loss}\rho}{\alpha^2} \quad (4.6)$$

where α is the porosity.

To download meshed geometries in to the CFX Pre-processor a bespoke interface was created which allows CFX to identify .vtu files from TexGen correctly and download them without errors. In the CFX-Pre processor, the General Mode was chosen to define all types of CFX simulations because this is the main mode for all kinds of simulations and suited this type of simulation most. Steady state simulation type was chosen because it reflected experimental conditions. One domain was created as an air domain. Air at 25⁰C was used as a liquid material. Opening boundary conditions were chosen. An opening boundary condition allows the fluid to cross the boundary surface

in either direction. For example, all of the fluid might flow into the domain at the opening, or all of the fluid might flow out of the domain, or a mixture of the two might occur. Pressure difference for entrainment is 500 Pa according to the experimental test method. In addition, different pressure drops were used for simulation to show the influence of pressure drop on fabric permeability. Symmetric boundary conditions were input for the four side surfaces of the air domain. The yarn domain was created as porous with isotropic volume porosity and permeability calculated for each fabric using Gebart's equation (see equation (3.9) in Chapter 3). An interface boundary condition was created to connect the air domain with the yarn domains. Output control default values were chosen: iteration interval of 10; maximum number of iterations 500; timescale factor 1; residual type RMS; and residual target of 0.000001. An example of boundary conditions for the unit cell of U2 fabric is represented in Figure 4.4. Here blue arrows represent opening boundary conditions for the upper and lower parts of the unit cell and red arrows represent symmetry boundary conditions for the sides of the unit cell.

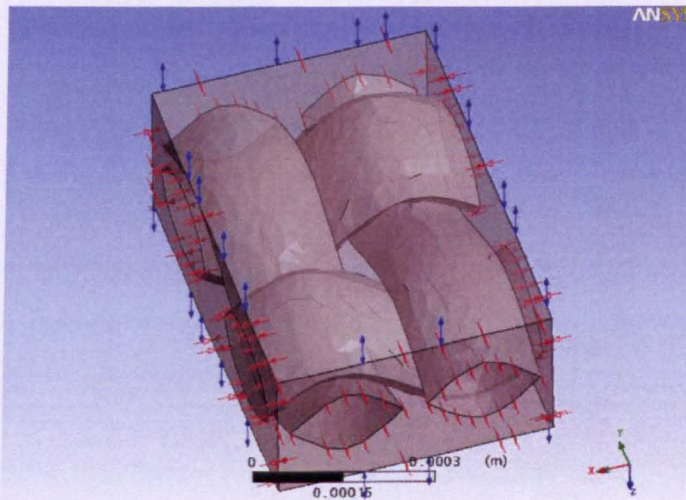


Figure 4.4 Boundary conditions for the unit cell of U2 fabric

After all main parameters for simulation were defined, CFX-Solver started the simulation saving the results automatically in .res files which can be viewed and analysed in CFX-Post processor (Figure 4.5). In the Post-processor average output velocity through the unit cell was calculated (see Appendix D).

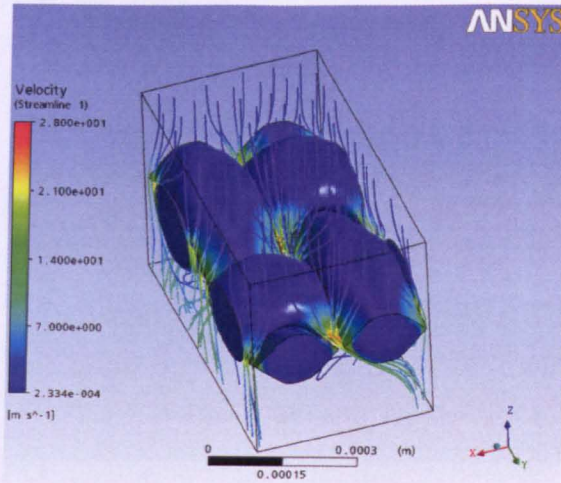


Figure 4.6 Streamline average velocity for the unit cell of U2 fabric

4.3 SENSITIVITY STUDY

Sensitivity of simulation results to the mesh density were studied. Figure 4.7 represents dependence of average outlet velocity on global number of elements for one fabric. It is seen that velocity is dependent on the global number of nodes. However, the run time increased dramatically with number of nodes or elements. If the mesh is very fine (900000 elements) it can take approximately 10 hours to run the simulation in comparison with a simulation of the unit cell with 34600 elements which takes approximately 1 to 2 hours to run. CFX 11.0 terminate the simulation with an error, if the number of elements was more than one million. Number of elements was chosen as approximately 34600 for the simulations described in this chapter as this gives accurate results and does not require too much time to run the simulation.

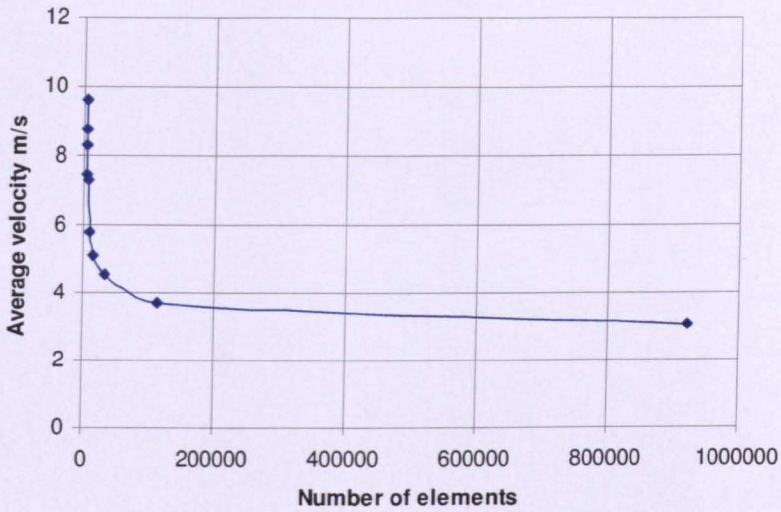


Figure 4.7 Dependence of average output velocity on global number of elements for U2 fabric

Figure 4.8 presents influence of yarn spacing on fabric permeability for U2 fabric. Warp spacing was changed between 0.235mm and 0.535mm. It is noticeable that even small changes of yarn spacing lead to an increase in fabric permeability. This means that geometric accuracy is very important and can be one of the main reasons for differences between measured and predicted results for fabric permeability.

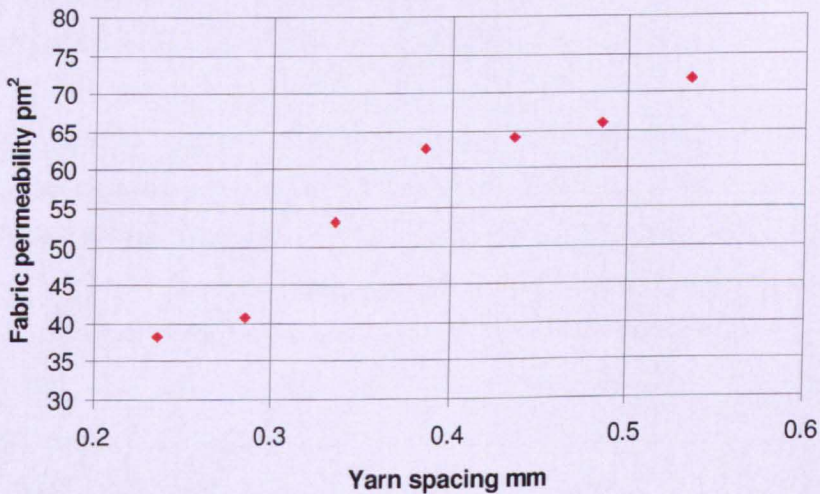


Figure 4.8 Influence of change in yarn spacing on fabric permeability for U2 fabric

The permeabilities of A1 fabric obtained using CFD are presented in Figure 4.9 with various yarn porosities. It can be seen that in the case of textile A1 the estimated permeability is highly sensitive to the yarn porosity and, therefore, yarn permeability which was calculated using Gebart's equation (3.9) from Chapter 3. This is to be expected as the textile geometry in Figure 4.9 clearly shows that the yarns are tightly packed with only small gaps between them. As a consequence, the resistance to flow through these small gaps is sufficient to force a significant proportion of the air flow through the yarns.

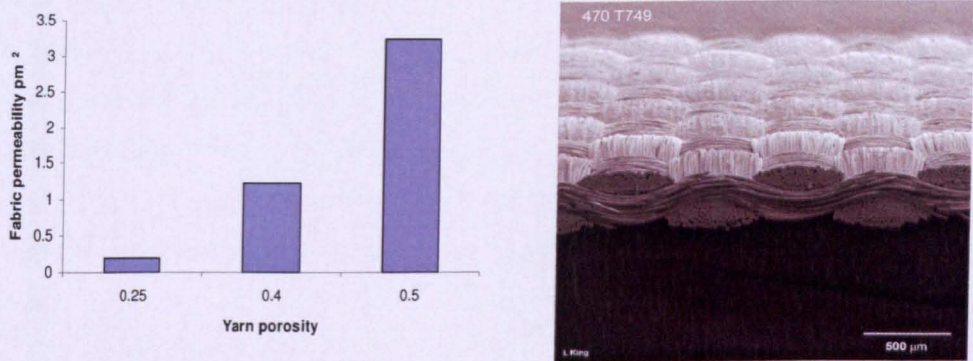


Figure 4.9 Textile permeability estimates obtained using Computational Fluid Dynamics (left) for A1 fabric (right)

In the case of textile A1 it may be seen that the CFD model predicts a permeability of 0.21pm² when the yarn porosity was calculated using Image J (Appendix B) as 0.25. This compares with a measured value of 0.18pm². The sensitivity of permeability of textile A1 to the yarn porosity and permeability underline the importance of accurately determining these parameters in trying to develop a predictive model. A doubling of the yarn porosity results in an order of magnitude increase in the estimated textile permeability.

4.4 RESULTS AND ANALYSIS

The velocity was taken from the CFX post-processor and the permeability was calculated using Darcy's law. Table 4.1 presents comparison between predicted results using both analytical and CFD methods and experimental data for through thickness air permeability. As seen from Table 4.1 both analytical and CFD methods did not give accurate predictions for U3 fabric due to its tighter structure with

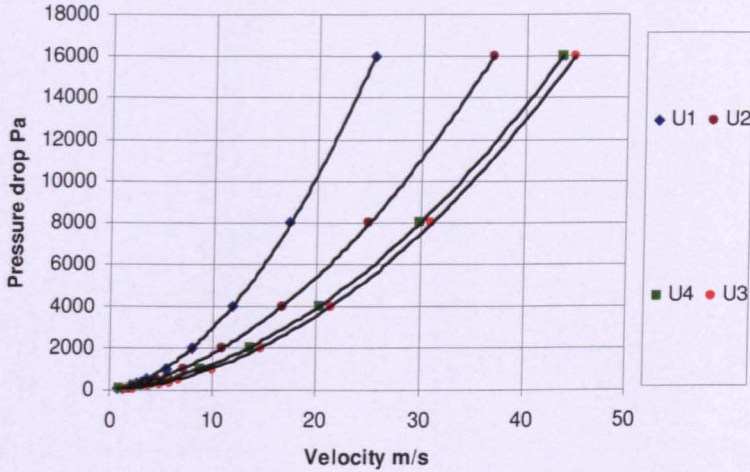
overlapping yarns. For A1 fabric both methods gave close predictions for fabric permeability but the CFD method is closer to the experimental data. For U1 and U2 fabrics the analytical prediction gives results closer to the experimental data. However, for twill-weave fabrics C2, C3 and C8 there is no good agreement between predicted and measured results. For these fabrics there is much better agreement between analytical results and measured data. This is mostly because of difficulties in creating geometry close to the real fabrics. As seen from Appendix C, geometric models of the unit cell for these three fabrics are not very close to the real fabrics. This is due to limitations in the use of TexGen. More work should be done on air permeability prediction for fabrics using the CFD approach such as improving geometry model by writing a Python script rather than using TexGen interface. It is time consuming process and needs thorough study.

Table 4.1 Comparison between fabric permeabilities at 500 Pa pressure using the different approaches

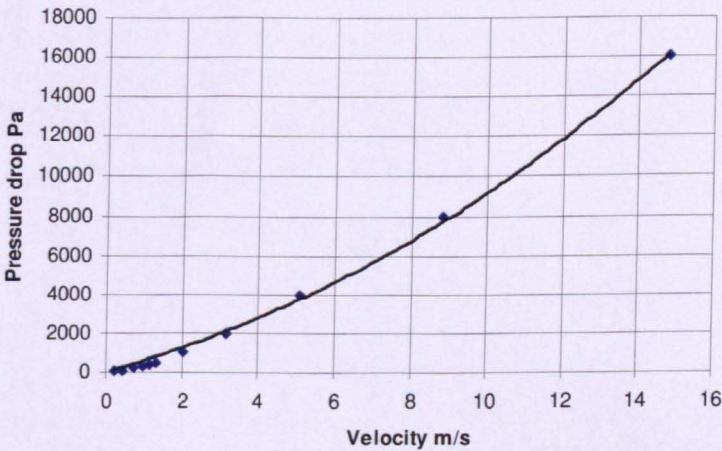
Fabric code	Measured permeability B_f^{exp} pm^2	Predicted permeability using analytical approach B_f^{analyt} pm^2	Predicted permeability using CFD approach B_f^{CFD} pm^2
U1	12.14(± 0.047)	30.30	42.92
U2	8.03(± 0.020)	13.80	25.51
U3	5.78(± 0.016)	0.13	22.01
C2	2.08(± 0.006)	4.61	136.42
C3	3.60(± 0.0055)	10.90	101.08
C8	4.19(± 0.0075)	4.83	109.44
A1	0.18(± 0.0024)	0.27	0.21

Figure 4.10 presents a study showing the influence of pressure drop on through thickness air permeability for several fabrics using the CFD approach. During simulations pressure drop was changed in the range 50Pa to 16000Pa. Figure 4.10 shows that fabric behaviour is non-linear when the pressure drop changes. This shows that it is reasonable to use an extended form of Darcy's law which includes the

Forchheimer coefficient (Equation (2.13) in Chapters 2). As seen from Figure 4.10 CFD predicts non-linear behaviour of fabrics according to Equation (4.2). It is not possible to model this non-linear relationship using the analytical model from Chapter 3.



a) U1, U2, U3, U4 fabrics



b) A3

Figure 4.10 Velocity versus pressure drop for several fabrics (CFD modelling). Data is plotted as discrete data points. A quadratic polynomial is fitted to each data set (solid lines).

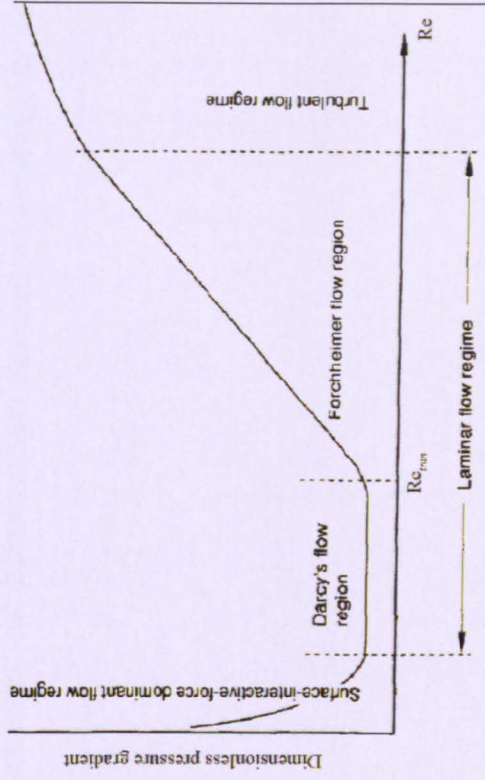
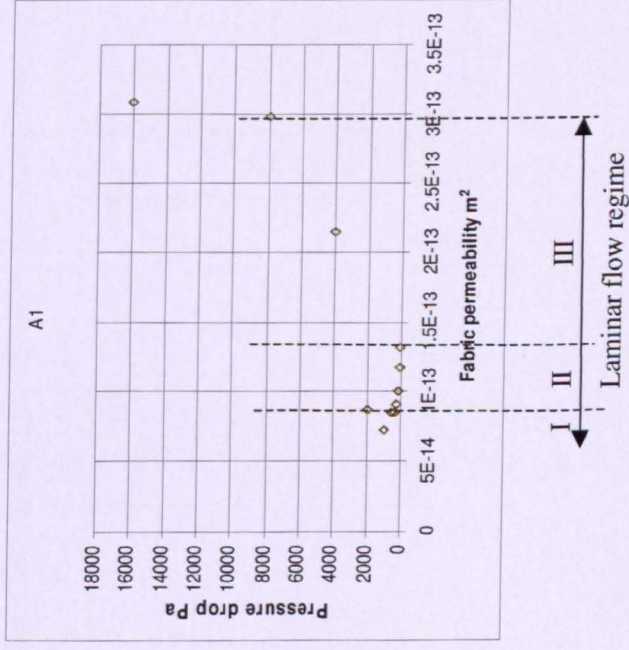
From Figure 4.10 it is possible to predict fabric permeability and Forchheimer coefficient for each fabric using the equations for the solid lines using a least squares approach (Table 4.2).

Table 4.2 Predicted fabric permeability and Forchheimer coefficient for variety of fabrics plotted in Figure 4.9

Fabric code	$B \text{ nm}^2$	β
U1	25.46	18.43
U2	24.28	8.13
U3	62.99	6.11
U4	36.97	6.06
A3	3.31	30.19

Figure 4.11 shows the influence of changing the pressure drop on fabric permeability for A1 fabric predicted using CFX 11.0. There are two regimes in laminar flow. Region I presents the low flow rate region where surface-interactive force dominates. Regions II and III present a laminar flow regime which consists of Darcy flow (Region II) and Forchheimer flow (Region III). After the Forchheimer flow regime, the turbulent regime starts [40]. There is a critical Reynolds number for the transition from Darcy's (viscous flow) to Forchheimer (inertia flow). It may vary depending on material. In this study the pressure drop for the transition regime is 1000Pa (as seen from Figure 4.11) which is relatively small compared to the real pressure drop of 100000Pa which an airbag fabric might experience during car collision [96].

As seen from Figures 4.10 and 4.11 the CFD analysis suggests that fabrics behave according to the Forchheimer equation. In tighter fabrics like A1 it is possible to see all three regions of laminar flow. Looser fabrics like U1, U2, U3, U4, and A3 demonstrate behaviour in the Forchheimer flow region (Figure 4.10).



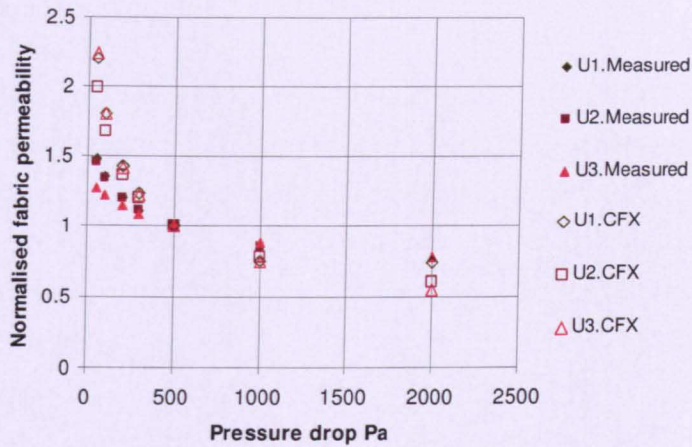
a)

b)

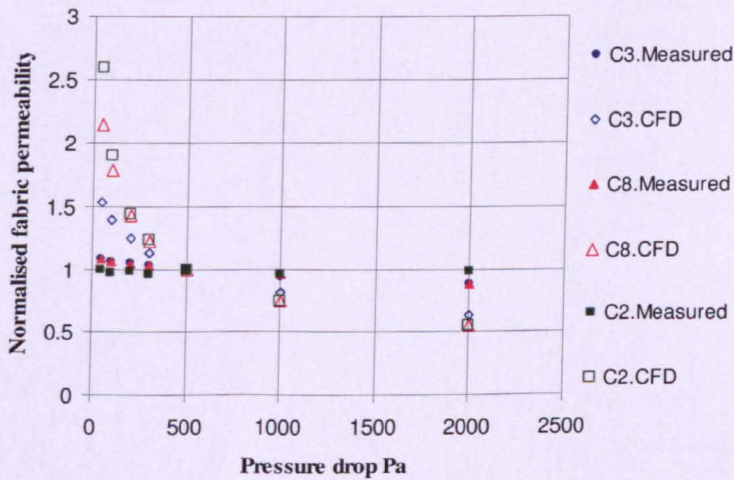
Figure 4.11 Influence of pressure drop on: a) predicted fabric permeability for A1 fabric; b) example from [45]

- I – Surface-interactive-force dominant flow region;
- II – Darcy’s flow region;
- III – Forchheimer flow region

Figure 4.12 presents a comparison between experimental data and CFD simulation results at different pressures. The experimental results for permeability are generally much lower than predicted CFD results. This may be due to some imperfections in geometrical modelling of fabrics as discovered above. In this figure both experimental and predicted fabric permeability normalised by dividing by the corresponding value at a pressure drop of 500Pa.



a) Cotton fabrics



b) PET/Cotton fabrics

Figure 4.12 Comparison between experimental data and CFD predictions for permeability versus pressure drop

4.5 ADVANTAGES AND DISADVANTAGES OF TEXGEN AND CFX 11.0

Advantages:

- TexGen can model a large range of geometries including plain-weave, twill-weave, and satin-weave;
- TexGen can model key physical parameters such as warp/weft width, warp/weft spacing, yarn height and cross-section which helps to create accurate models for unbalanced fabrics;
- TexGen can automatically generate meshes, saving time in analysis;
- There is an existing support network for CFX (e.g. tutorial examples, research studies, website forum etc) to help to correct errors which may occur during simulations.
- CFX is able to predict the non-linear dependence of flow rate on pressure, which is similar to experimental observations.

Disadvantages:

- In TexGen it is difficult to model very tight fabrics and fabrics with overlapping yarns, for example U4 fabric (see Appendix C);
- In CFX the solution can take a long time for a large model. For example for a plain woven unit cell consisting of 900000 elements it takes approximately 10 hours to run the simulation;

4.6 CONCLUSIONS

The results presented in this chapter showed that the CFD simulations are very sensitive to the yarn porosity and yarn permeability as well as the geometric parameters of fabrics. A small change in yarn porosity can lead to a dramatic change in the predicted through thickness air permeability. A sensitivity study has been presented showing the influence of number of nodes and elements on fabric

permeability. Using A1 fabric, with a tight structure, the significant influence of yarn porosity on fabric permeability was shown. CFD results showed good agreement with measured data for A1 fabric, as it was easy to model its unit cell. There was not good agreement for other fabrics, especially for twill-weaves as it was difficult to model the unit cell geometry close to the real fabric. The limitations of the TexGen/CFD approach are also presented, most notably is the difficulty in modelling very tight fabrics in TexGen. Current models assume an idealised shape of the yarn and use idealised yarn paths. In reality, there is a lot of mixing of fibres between the yarns within the fabric structure (see Appendix C) and often there are no distinct boundaries. The current fabric model cannot take this into consideration.

Nevertheless the studies here have highlighted the strengths of using CFD simulations in comparison with the analytical approach presented in Chapter 3. It showed that TexGen can model a large range of geometries including plain-weave and twill-weave. TexGen is good at meshing the unit cell geometry. It showed that it is possible to provide a permeability prediction using CFD simulations for real fabrics in the same order of magnitude as experimental data with an accurate geometric model. While in theory CFX 11.0 should provide the most accurate solutions, it can be very difficult and time consuming to generate an accurate geometry in TexGen due to specific features such as overlapping yarns. However, CFD modelling can represent the Forchheimer effect whereas the analytical model from Chapter 3 cannot do this.

CHAPTER 5

PERMEABILITY OF DEFORMED FABRICS

5.1 INTRODUCTION

The ability to accurately predict the permeability of deformed fabrics is very important in order to manufacture with techniques such as resin transfer molding (RTM) and liquid composite molding (LCM) as was shown in Chapter 2. However, it is also important for clothing and airbag fabrics because fabrics deform while wearing them or in the case of airbag fabrics, when they emerge during collision. During the past two decades experimental and analytical work was carried out to attempt to predict and measure the permeability of fabrics used in various manufacturing processes (for more details see Chapter 2). The aim of this chapter is to predict analytically the through thickness air permeability for various deformed fabrics using a similar analytical approach as for undeformed fabrics. In addition, experimental work was carried out to verify the predicted results. Three deformation mechanisms as the most common for the fabrics were chosen: shear, compaction and tension.

The approach developed in Chapter 3 for undeformed fabrics is applied here to predict the permeability of deformed fabrics. The analytical model described in this chapter is a combination of the Kulichenko model [7] which predicts the permeability through gaps between yarns, with Gebart's model [3] to predict permeability within yarns. The method to calculate fibre volume fraction and porosity for fabrics after shear deformation is described in the first part of this chapter.

Experimental set-up and measurements of through thickness permeability for sheared fabric are presented in the second part of this chapter. Experimental results of through thickness permeability are compared between undeformed and deformed fabrics.

In the third part of this chapter, predicted results for deformed fabrics are compared with experimental data. The results are analysed and discussed. Finally, some conclusions are made.

5.2 DEVELOPMENT OF AN ANALYTICAL MODEL FOR THROUGH THICKNESS PERMEABILITY OF DEFORMED FABRICS

Three main fabric deformation mechanisms identified as the most common are described in this chapter: pure shear, compaction and tension. Pure shear is an occurrence of a shear strain, which is a deformation of a material substance in which parallel internal surfaces slide past one another. The permeability of the fabrics will change after shear as seen from the literature review in Chapter 2. It is very important to know how the permeability of the fabric will change after the shear for clothing fabrics, for example, to support the optimal comfort level for the person who is wearing it even after shear. Compaction is another important deformation mechanism for fabrics causing them to lose pore space, which leads to a decrease in fabric permeability. Later in this chapter, an analytical model to predict the permeability of compacted fabrics is presented. One more deformation mechanism which influences fabric permeability is tension. Both airbags and clothing fabrics could be under a certain amount of tension during their application. It is necessary to know how much tension a fabric can withstand successfully and how tension will influence permeability.

5.2.1. Pure shear

Pure shear is presented in Figure 5.1 [54].

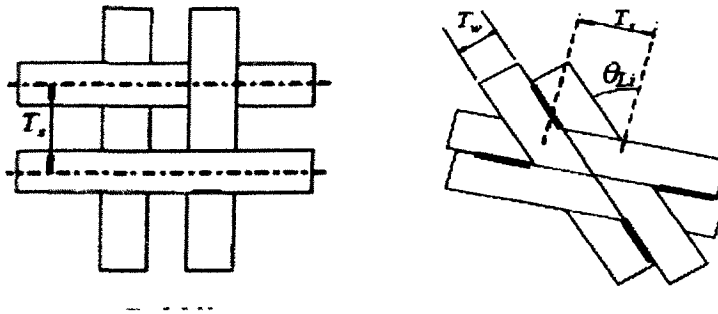


Figure 5.1 Pure shear for bi-directional fabrics [54]

Shear deformation is a complicated mechanism. In this thesis, a model for sheared fabric is presented taking into account two stages of shear deformation as seen from the literature review in Chapter 2: shear before yarns in the fabric reach the locking angle (the angle at which adjacent yarns come into contact) and shear after the locking angle. They are two completely different mechanisms. To calculate locking angle for each fabric the following method is used [97]:

$$\Theta_L = \cos^{-1}\left(\frac{d}{s}\right) \quad (5.1)$$

where d is yarn width, s is yarn spacing after shear in mm.

Firstly, the gaps between yarns reduce whilst yarns remains undeformed which means that fibre volume fraction within the yarns does not change at the beginning of the shear. Gap width and length start decreasing [46]. It is assumed that thickness stays constant during shear. Permeability through gaps can be calculated according to the modified equation of Darcy's law [2] described in more detail in Chapter 3:

$$B_g^{def} = \frac{\mu t v_g^{def}}{\Delta P} \quad (5.2)$$

where B_g^{def} is permeability through deformed gaps, μ is the gas/liquid viscosity, t is fabric thickness, v_g^{def} is velocity through gaps and ΔP is the pressure drop.

$$v_g^{def} = \frac{\Delta P}{80\mu} \frac{d_h^{def^2}}{t} \quad (5.3)$$

where v_g^{def} is velocity through deformed gaps, d_h^{def} is the hydraulic diameter of a deformed pore.

The following equation is used to calculate the hydraulic diameter of deformed pore:

$$d_h^{def} = \frac{2(s_e^{def} - d_e^{def})(s_p^{def} - d_p^{def})}{(s_e^{def} - d_e^{def}) + (s_p^{def} - d_p^{def})} \quad (5.4)$$

where s_e^{def} is deformed warp spacing and s_p^{def} is deformed weft spacing, d_e^{def} is deformed warp width in mm; d_p^{def} is deformed weft width in mm.

Permeability through the whole fabric in this case can be calculated using the following equation:

$$B_f^{def} = B_g^{def} L^{def} + B_y^0 (1 - L^{def}) \quad (5.5)$$

where looseness factor L^{def} is calculated as $L^{def} = \frac{s^{def} - d^{def}}{d^{def}}$, and B_y^0 is the initial permeability through the yarns.

Secondly, when fabric is sheared until there is no gap remaining between yarns, yarns start to experience shear and compaction. Permeability through gaps becomes equal to zero and all flow goes through yarns. In this case, yarn fibre volume fraction V_f

increases during shear. Yarns are compressed by neighbouring yarn and their width decreases, however, it was assumed that yarns thickness does not change. Permeability through yarns can be calculated using Gebart's equation [3]:

$$B_y^{def} = \frac{16}{9\pi\sqrt{6}} \left(\sqrt{\frac{V_f^{max}}{V_f^{def}}} - 1 \right)^{5/2} r^2 \quad (5.6)$$

where B_y^{def} is the permeability of deformed yarns, V_f^{max} is the maximum fibre volume fraction which is $V_f^{max} = 0.9065$ (for hexagonal packing), V_f^{def} is the fibre volume fraction of deformed yarns, and r is the fibre radius.

Fibre volume fraction for deformed fabrics in warp direction V_f^{def} can be calculated as follows [64]:

$$V_f^{def} = \frac{2}{\pi[1 - d^{max}/d^0]} V_a \quad (5.7)$$

where V_a is yarn packing fraction, d^{max} is maximum width reduction of warp yarn, and d^0 is warp width before deformation.

$$d^{max} = (1 - 2/\pi)d^0 \quad (5.8)$$

d^{max} is about 36% of the original width d^0 .

$$V_a = \frac{\pi V_f^0}{2}$$

Reduction after shear for any shear angle can be calculated as follows:

$$\begin{aligned} d^{red} &= d^0 - d^{def} \quad (5.9) \\ d^{def} &= s^0 \cos\theta_s \end{aligned}$$

where s^0 is yarn spacing before shear; θ_s is the shear angle.

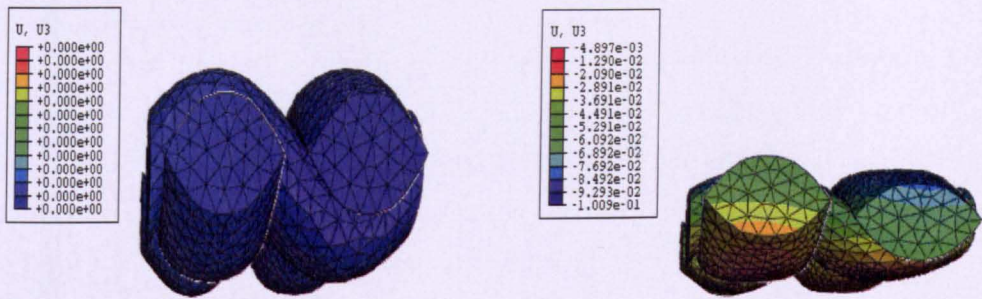
Permeability through sheared fabric is equal to the permeability through deformed yarns:

$$B_f^{def} = B_y^{def} \quad (5.10)$$

5.2.2 Compaction

Another mechanism of deformation which is important for fabrics or airbags is compaction. During compaction the pore size reduces which leads to a reduction in

fabric permeability which, for clothing, may cause discomfort for the wearer. In this thesis, compaction was simulated with the use of software package Abaqus [24]. Abaqus software was chosen for this model as it was widely used in the Composites Research Group at Nottingham University and was known as the most convenient software to model fabric deformation accurately. The unit cell of the fabric was created and meshed using TexGen as described in Chapter 4 and then transferred to Abaqus for the simulations. The results of the simulations were used to calculate the deformed gap width and length as well as deformed yarn width and thickness. These parameters were used to calculate velocity and fabric permeability. Compaction of U2 fabric modelled in Abaqus software package presented in Figure 5.2 [20], [98].



a) before deformation

b) maximum compaction

Figure 5.2 Compaction of U2 fabric modelled in Abaqus FE software [20]

Firstly, changes in permeability through gaps during compaction are described. Permeability can be calculated using:

$$B_g^{def} = \frac{\mu t^{def} V_g^{def}}{\Delta P} \quad (5.11)$$

where thickness during compaction can be calculated as $t^{def} = t^0 - t^{red}$, where t^0 is original thickness, t^{red} is thickness reduction.

Velocity of fluid through gaps can be calculated using equation (5.12) [7]:

$$v_g^{def} = \frac{\Delta P}{80\mu} \frac{d_h^{def 2}}{t^{def}} \quad (5.12)$$

where $d_h^{def} = \frac{2L^{def}W^{def}}{L^{def} + W^{def}}$ is hydraulic diameter of deformed pore, L^{def} is the length of deformed gap, W^{def} is the width of deformed gap in mm.

Secondly, permeability through yarns for deformed fabrics can be calculated using deformed fibre volume fraction V_f^{def} as in Gebart's work [3] (equation (5.6)).

Thirdly, fabric permeability during compaction can be calculated as follows:

$$B_f^{def} = B_g^{def} L^{def} + B_y^{def} (1 - L^{def}) \quad (5.15)$$

where looseness factor L^{def} can be calculated as $L^{def} = \frac{s^{def} - d^{def}}{d^{def}}$

5.2.3 Tension

All fabrics may experience tension during wearing, whilst airbags are under tension during inflation. That is why it is important to be able to predict how much tension each fabric can stand before losing its properties such as permeability. Tension can be in the warp or weft direction or in both directions at the same time. During tension yarn are stretched which decreases their width and increases yarn volume fraction. In addition, it increases the gap size which leads to an increase in fabric permeability. The effect of tension was simulated with the use of FE software package Abaqus [20]. The results of the simulations were used to calculate the deformed gap and yarn width and length, and fibre volume fraction after tension. These parameters were used to calculate velocity and fabric permeability. In this model, the same approach as for sheared fabric was used. Equations (5.2-5.5) were applied to the tension mechanism. Tension for U2 fabric in warp and weft directions modelled in Abaqus software package is presented in Figure 5.3 [20], [99].

Before tension

Maximum tension

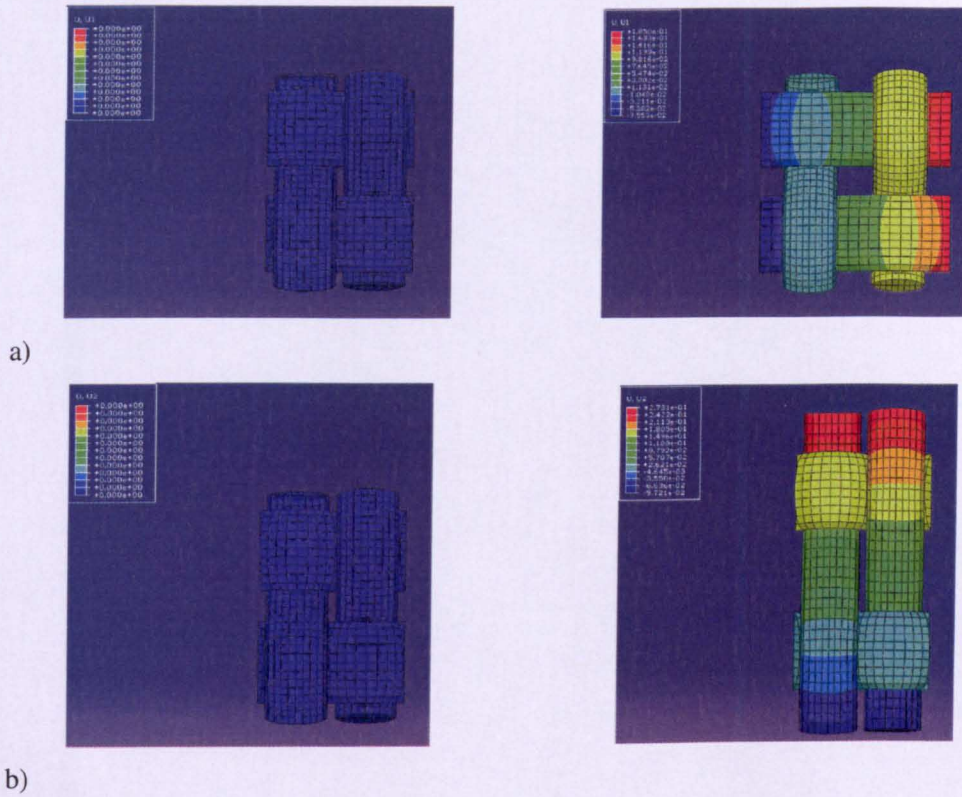
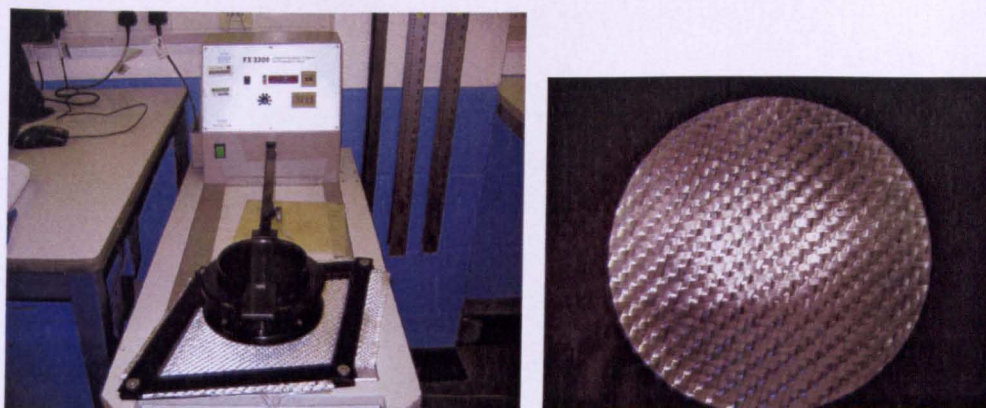


Figure 5.3 Tension for U2 fabric in: a) weft direction; b) warp direction [24]

5.3 EXPERIMENTAL MEASUREMENT OF THROUGH THICKNESS PERMEABILITY OF DEFORMED FABRICS

Through thickness air permeability of sheared fabric was measured according to British Standard BS EN ISO 9237:1995 [85]. A picture frame shear rig was created according to the geometrical parameters of the permeability tester. The equipment which was used to these experiments was the air permeability tester FX 3300 (Figure 5.4 (a)) [86] as described in Chapter 3. Glass-fibre fabric Chomarar 800S4-F1, with a specification as presented in Table 5.1, is shown in Figure 5.4 (b) after shear. This is the only fabric available for this work which was possible to shear without buckling due to the nature of glass fibres and the fact that the fibres in yarns were very loose, which means yarn fibre volume fraction was low although the whole fabric structure was very stable.



a) b)
Figure 5.4 Experimental set-up for through thickness air permeability of sheared Chomarat 800S4-F1 fabric (a) and after share to an angle of 40° (b)

Table 5.1 Fabric specification

Fabric code	Description and composition	Structure	Thickness (mm)	Yarn spacing (mm)		Yarn width (mm)	
				Warp	Weft	Warp	Weft
Chomarat 800S4-F1	Glass fibre	Satin	1.16	3.16	3.16	3.16	3.16

5.4 RESULTS AND ANALYSIS

5.4.1 Experimental results

Experimental results for through thickness air permeability of sheared fabric is presented in Figure 5.5. During the experiment, fabric was parallel to the warp and weft directions by the same shear angle. Then fabric was placed on the permeability tester without taking it out of the shear rig to measure the fabric permeability. Fabric was sheared manually to 29° , 41° and 49° . Fabric permeability was measured once for each sample as scatter was shown to be small from previous experimental work (see Chapter 3). Although Chomarat fabric is very tight as seen from Table 5.1, it was possible to achieve a shear angle of 49° due to the fact that fibres inside yarns were loose. The theoretical locking angle for this fabric is 0° as there is no gap between the yarns (see Table 5.1).

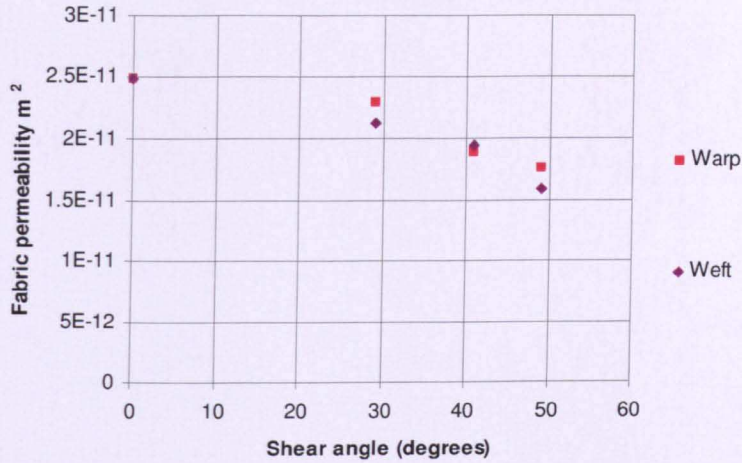


Figure 5.5 Experimental results of fabric permeability versus shear angle for Chomarar 800S4-F1 fabric sheared in warp and weft directions

5.4.2 Predicted results using analytical model

Locking angle for each fabric studied in Chapter 3 and 4 was calculated using equation (5.1) (Table 5.2). It is seen from Table 5.2 that for very tight fabrics like U3, A1 or Chomarar 800S4-F1 locking angle is 0° because there is no any gap between yarns, so shear deformation occurs within yarns from the beginning of deformation.

Table 5.2 Locking angle

fabric code	warp width d (mm)	warp spacing s (mm)	locking angle θ_L (degrees)
Chomarar	3.16	3.16	0
U1	0.405	0.47	30
U2	0.195	0.235	34
U3	0.195	0.195	0
A1	0.513	0.45	0
A3	0.35	0.356	11
C1	0.34	0.38	26
C2	0.3	0.33	25
C3	0.27	0.3	26
C7	0.3	0.34	28
C8	0.3	0.34	28
C9	0.332	0.356	21
C10	0.313	0.342	24

Figure 5.6 represents changes in predicted fabric permeability for the range of fabrics during shear. As seen from Figure 5.6 permeability through fabrics decreases quickly before the locking angle, however, after locking angle fabric permeability continue to decrease but at a slower rate as the shear and compaction within the yarns occurs.

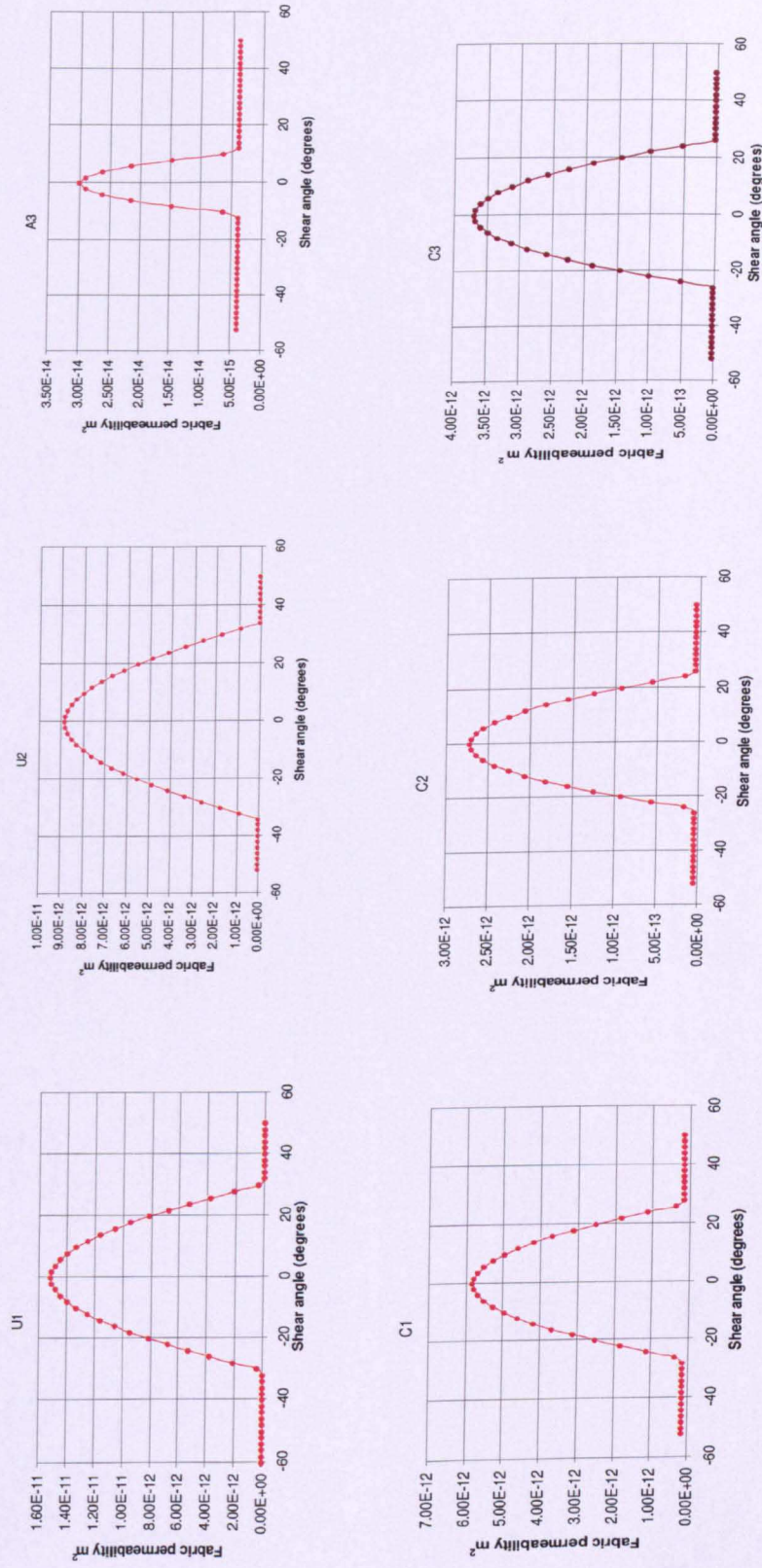


Figure 5.6 Predicted fabric permeability of sheared fabrics B_f^{def}

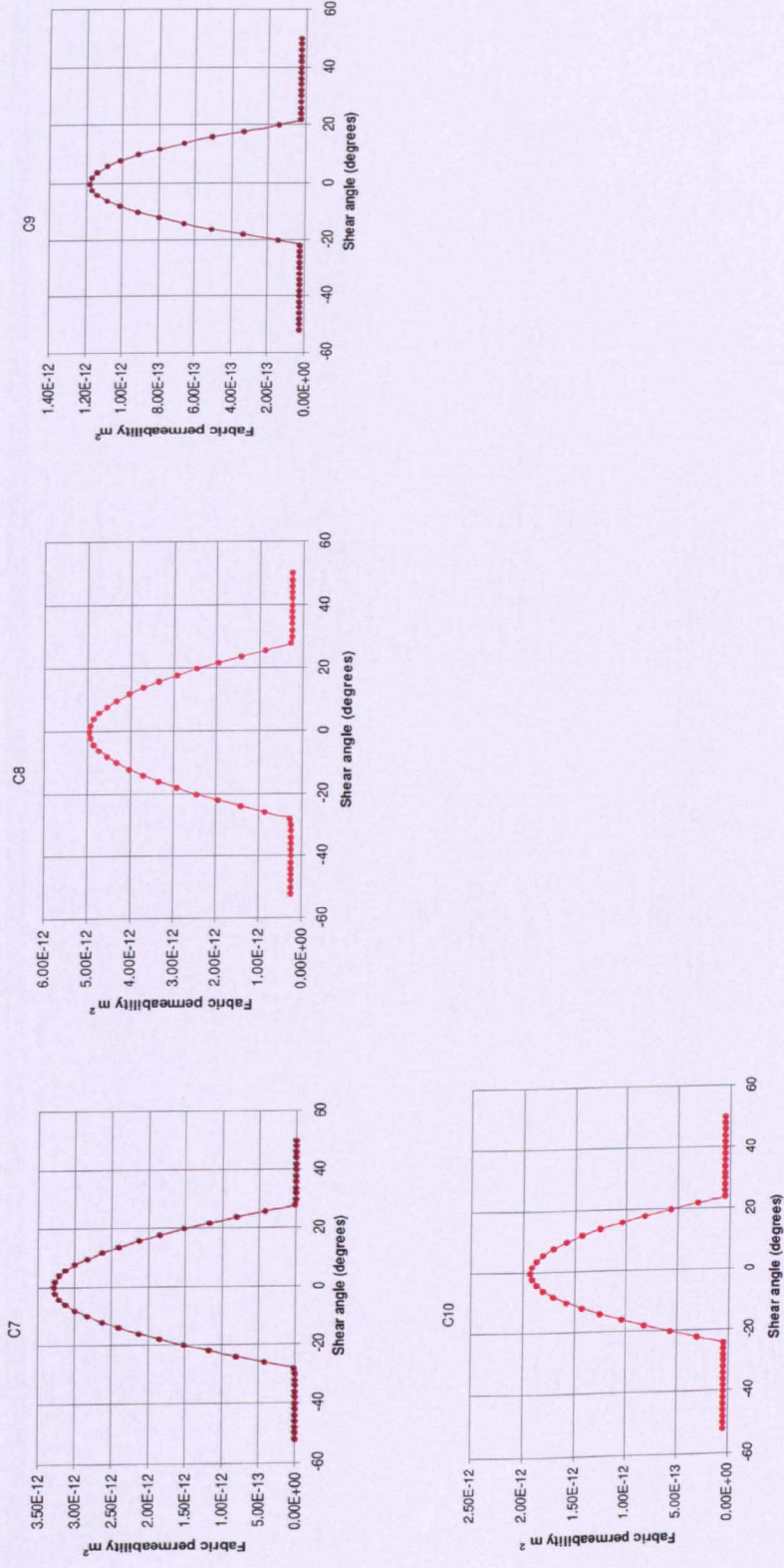
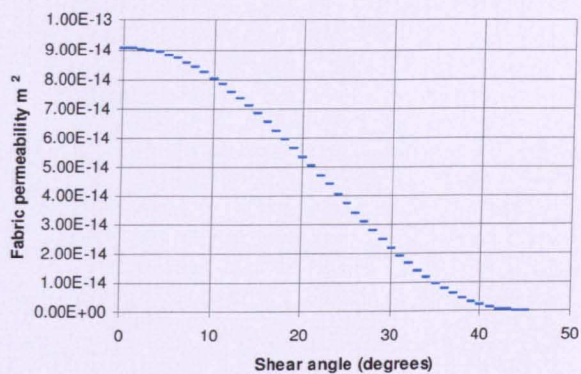


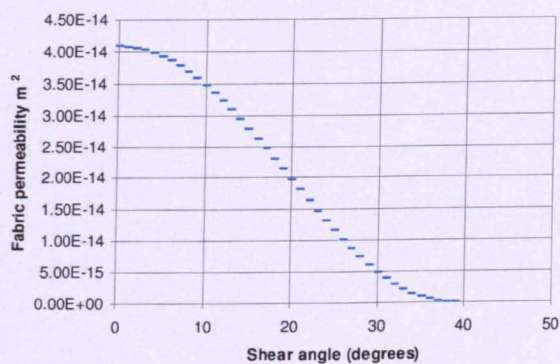
Figure 5.6 Predicted fabric permeability of sheared fabrics B_f^{def} (continued)

Through thickness air permeability and thermal conductivity analysis for textile materials

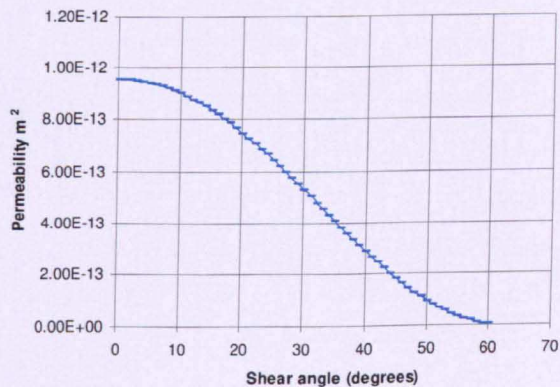
As seen from Table 5.2, U3, A1 and Chomarat 800S4-F1 are very tight fabrics, their locking angle is 0° . Figure 5.7 presents predicted fabric permeability for sheared U3, A1 and Chomarat fabric.



a) U3



b) A1



c) Chomarat 800S4-F1

Figure 5.7 Predicted results for fabric permeability of sheared fabrics

Through thickness air permeability and thermal conductivity analysis for textile materials

Analytical work with the help of Abaqus software to model the compaction of the fabric was carried out for U2 fabric as this fabric has simple plain woven structure which is easy to model in TexGen (Appendix C). Figure 5.8 presents predicted fabric permeability of U2 fabric during compaction calculated using equations (5.11-5.15). It is seen from Figure 5.8 that the maximum compaction achieved was 44% due to the Abaqus limitations. It is shown that there is some influence of compaction on fabric permeability for U2 fabric. It may be due to the fabric structure as U2 fabric has quite large gaps between the yarns (Appendix C) and even though the fabric was compacted by 44%, gap size did not decrease dramatically, leaving room for the flow to pass through. Due to tighter unit cell geometries of other fabrics (Appendix C) Abaqus software was not able to simulate their compaction to any significant degree before error occurred.

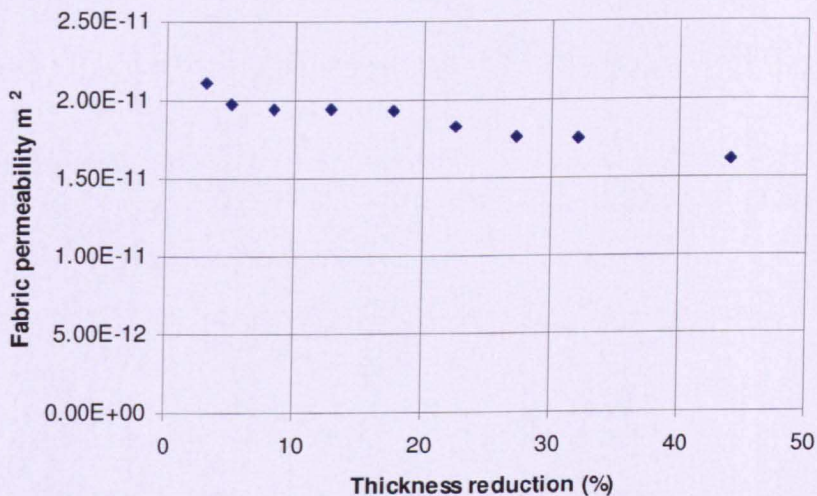
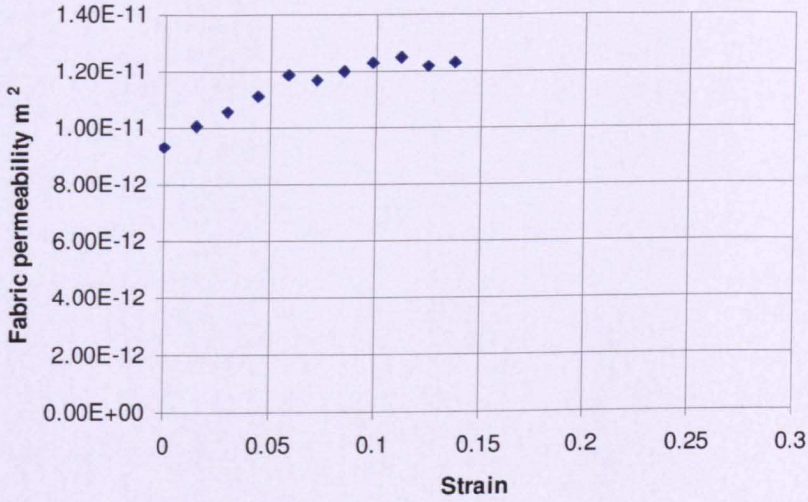


Figure 5.8 Predicted results for influence of compaction on fabric permeability of U2 fabric

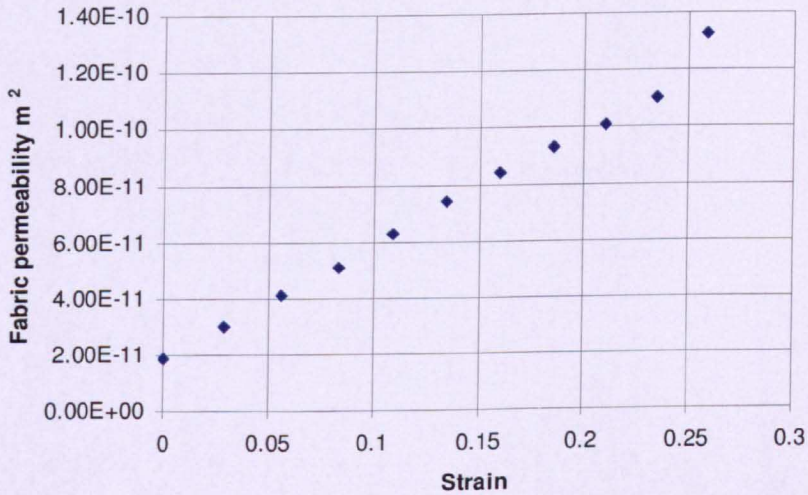
The effect of in-plane tension was studied using the approach described earlier in this chapter. Tension in warp and weft directions firstly was modelled separately and then together. The predicted influence of in-plane tension on fabric permeability for U2 fabric in warp and weft directions is presented in Figure 5.9. As seen from Figure 5.9 tension in weft direction has much more influence on fabric permeability than tension in warp direction for U2 fabric. This can be explained as the gap size increases more

Through thickness air permeability and thermal conductivity analysis for textile materials

during tension in weft direction than in warp direction (as seen from Figure 5.3). In addition, weft yarns have more curvature and more spacing than warp yarns due to the weaving process that makes them stretch more easily, leading to a more significant increase in pore diameter and fabric permeability.



a) Warp direction



b) Weft direction

Figure 5.9 Influence of tension on fabric permeability for U2 fabric

Figure 5.10 shows the influence of biaxial tension (warp and weft simultaneously). It is noticeable that the graph is “random”, which needs more study.

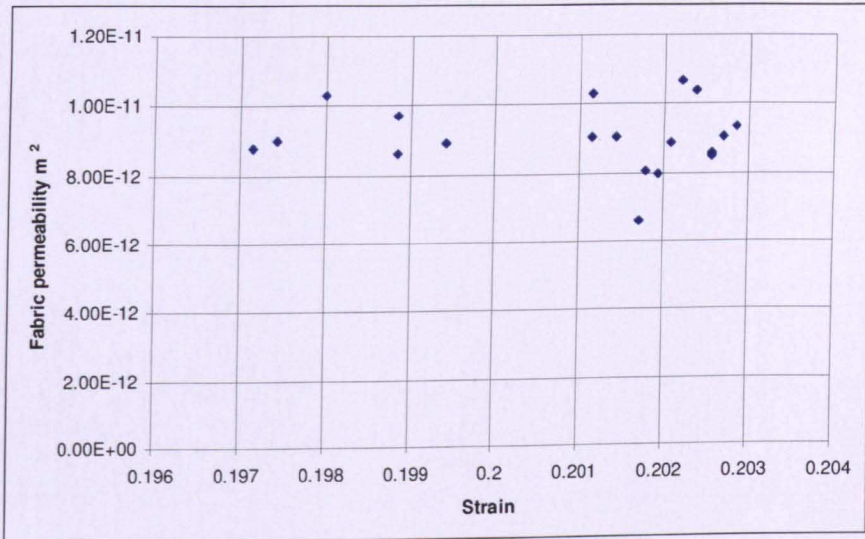


Figure 5.10 Analytical prediction of influence of biaxial tension for U2 fabric

5.4.3 Comparison between predicted results and experimental data

Figure 5.11 presents a comparison between measured data and predicted results for Chomarat 800S4-F1 fabric during shear. It was only possible to shear this fabric in a controlled manner as others tended to buckle during shear which did not give an accurate result. As seen from Figure 5.11 predicted results have poor agreement with the measured data for all shear angles. The analytical model under-predicts the reduction in permeability in comparison to experimental data. However, more experimental work should be done for permeability through sheared fabrics as there is not enough data to draw any firm conclusions.

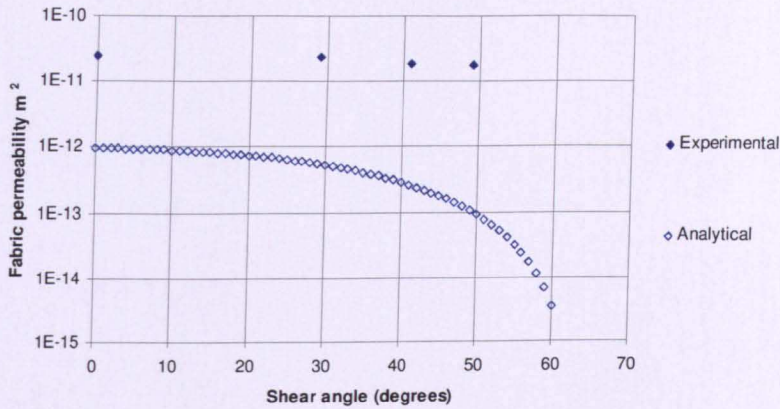


Figure 5.11 Comparison between experimental and analytical results for fabric permeability during shear for Chromarat 800S4-F1 fabric

5.5 CONCLUSIONS

Three common types of deformation of textile fabrics were analysed: shear, compaction and tension. An analytical model for fabric shear has been developed and coupled with the analytical model for permeability s described in Chapter 3. Locking angle for each fabric was calculated. Two mechanisms of shear have been described: shear before and after locking. If fabric has loose fibres inside the yarns, than shear changes the permeability significantly even after locking as seen from Chomarat 800S4-F1 fabric. An experimental set up was designed to fit a shear rig around the air permeability tester to measure the through thickness air permeability of the fabric after shear. Unfortunately, only one glass-fibre fabric Chromarat 800S4-F1 was tested using the shear rig as others buckled when sheared. A more complicated rig could be developed which will include some pre-tension to prevent fabrics from buckling. Predicted results have poor agreement with measured data for all shear angles. An analytical model for compacted fabrics was demonstrated using U2 fabric as the easiest fabric to model both analytically and computationally. Abaqus software package was used to perform compaction simulations with results used later in the analytical model to calculate fabric permeability after compaction. There was no experimental work done for the permeability of compacted fabrics due to time limitations. Tension in warp and weft directions were also studied using U2 fabric. The analytical model included results from computational simulation of tension for U2 fabric performed in Abaqus. Tension was applied in three ways: in warp direction; in weft direction; and in both warp and weft directions. The analytical results showed

**PAGE
NUMBERING
AS
ORIGINAL**

Through thickness air permeability and thermal conductivity analysis for textile materials

more significant influence of tension in weft direction than in warp direction on fabric permeability as there was more spacing between weft yarns than between warp yarns and the increase in gap under tension in weft direction was much larger as seen from Figure 5.3. More computational and experimental work should be done on all three mechanisms of deformations before firm conclusions can be drawn.

CHAPTER 6

THERMAL CONDUCTIVITY OF FABRICS

6.1 INTRODUCTION

The comfort of a garment depends on many factors: heat and vapour transfer, lightness, sweat absorption, drying and permeability to moisture and air. Heat transfer continues to be a field of major interest to engineering and scientific research as well as designers, developers and manufacturers. Some models can take into account the moisture content in fabrics, which significantly affects thermal conductivity (Chapter 2). In this chapter, an analytical model is developed to predict thermal conductivity of fabrics taking into consideration moisture content as it is important for textile fabrics during their application.

The first part of this chapter describes experimental measurements of thermal conductivity. Fabric specific parameters such as specific heat capacity, thickness and fabric density are taken into account during experiments.

The second part shows the development of an analytical model to predict thermal conductivity of fabrics. Two existing approaches for single-layer fabrics are described and compared: rule of mixtures and thermal resistance approach (Chapter 2). A method for thermal conductivity prediction for multi-layer fabrics is also presented. The results are analysed and compared to the experimental data.

In the third part, moisture content experiments are described and experimental results are presented. A simple analytical model to predict thermal conductivity taking into consideration moisture content is developed, and predicted results are compared to experimental data. The influence of relative humidity on thermal conductivity is analysed.

6.2 EXPERIMENTAL MEASUREMENTS OF FABRIC THERMAL CONDUCTIVITY

6.2.1 Experimental set-up

Fabric thermal conductivity was measured according to ISO 8301 [88]. This standard determines mean thermal conductivity of a specimen under steady-state conditions in a body bounded by two parallel, flat isothermal faces and by adiabatic (when no heat is transferred to or from the working fluid) edges perpendicular to the faces. These are made for a thermally homogeneous, isotropic, and stable material [88]. Apparatus for testing is shown in Figure 6.1. A schematic of a thermal conductivity test is shown in Figure 6.2.

The base section of the enclosure contains the heat flow meter and cold plate assembly. This is cooled using water at a stable temperature such that the plate is isothermal. The integral heat flow meter gives a millivolt output proportional to the heat flux into the cold plate. The hot plate is heated electrically. The hot plate is raised and lowered by a screw handle mechanism on top of the enclosure. A dial indicator within the hand wheel enables the thickness of the specimen under test to be determined in situ (as shown in Figure 6.2).

The testing procedure was as follows. Fabrics were prepared (cut and kept in the environmental chamber) in advance. From each fabric three square samples 200x200mm each were cut and labelled with the fabric code. According to the apparatus manual [89] very thin samples should be kept between two layers of rubber (thickness is smaller than 3 mm) to obtain an accurate results. Fabric parameters including the specimen dimensions, thickness (measured during the test using a dial gauge on the loading handwheel) and mass were measured each time before testing. Fabric thickness, density and specific heat capacity (taken from fabric specification) were used as input parameters for testing. Temperature difference for all samples was chosen at 20⁰C. 300 seconds was chosen as sample interval according to [89]. The steady state conditions were reached when five consecutive readings at this interval gave values of thermal resistance to within 3% without changing monotonically in one direction. The calibration constants with silicone rubber mats were the following:

Through thickness air permeability and thermal conductivity analysis for textile materials

$k_1 = -31.7383$, $k_2 = 0.4792$, $k_3 = 6.6346$, $k_4 = 0.0558$, $k_5 = 0.0279$ and $k_6 = -0.0005$ (see Equation (6.1)). These constants were used as default.



Figure 6.1 Thermal conductivity of building and insulation materials unit B480

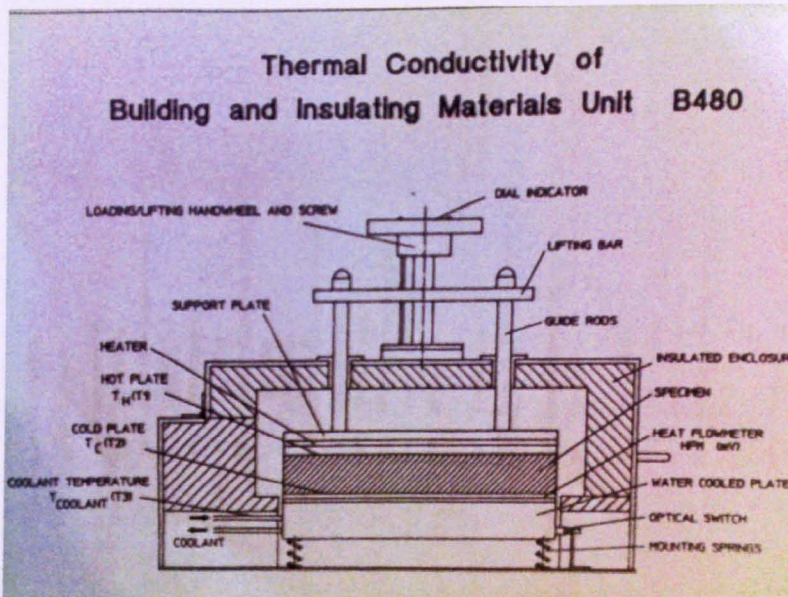


Figure 6.2 Schematic design of thermal conductivity tester unit B480 [89]

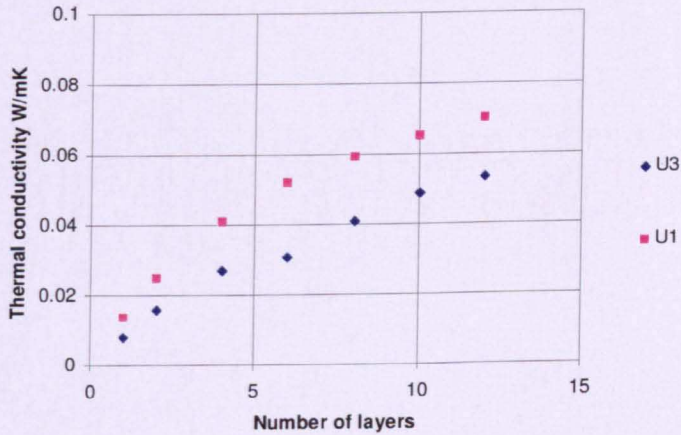
Six fabrics were tested: U1 and U3, A3 and A4; C3 and C9 which have similar composition and structure but different porosity. The details of fabrics are given in Chapter 3. Each fabric was tested with number of layers in a range between 1 to 12 to investigate how thermal conductivity changes due to nesting. All fabrics were held in an environmental chamber at 20°C and 50 % humidity before testing to exclude any influence of environment.

6.2.2 Experimental results and analysis

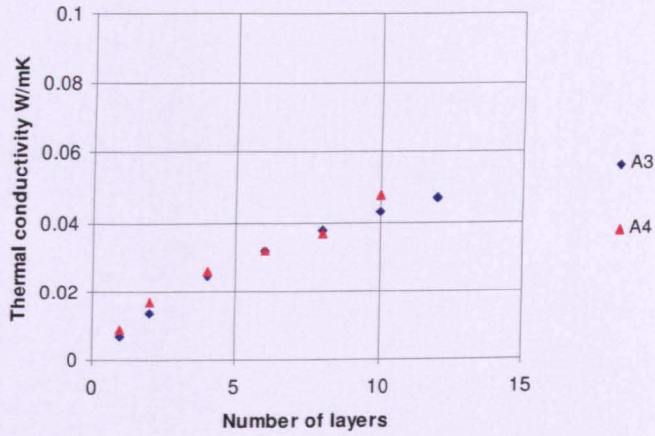
Thermal conductivity results are compared between three pairs of fabrics and presented in Figure 6.3. Each pair of fabrics has similar composition but different porosity (see Chapter 3 for fabric details). Tighter fabrics like C9 and A4 had higher thermal conductivity in comparison to looser fabrics made of the same material like C3 and A3. However, fabric U3 is tighter than U1 but thermal conductivity for U3 is lower than for U1. This can be explained by the different finishing of the two fabrics. U1 is 100% cotton fabric but U3 is 100% mercerised, bleached cotton poplin fabric. For each pair of fabrics results for thermal conductivities are presented in Figure 6.3. Thermal conductivity was defined using the following equation [98]:

$$\lambda = \frac{t_s \left[(k_1 + (k_2 \bar{T})) + (k_3 + (k_4 \bar{T}))HFM + (k_5 + (k_6 \bar{T}))HFM^2 \right]}{dT} \quad (6.1)$$

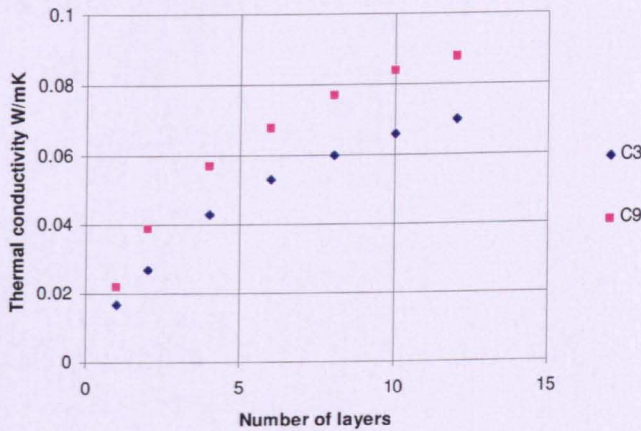
where t_s is the specimen thickness, \bar{T} is mean temperature, dT is the temperature difference, HFM is heat flow meter reading.



a)



b)



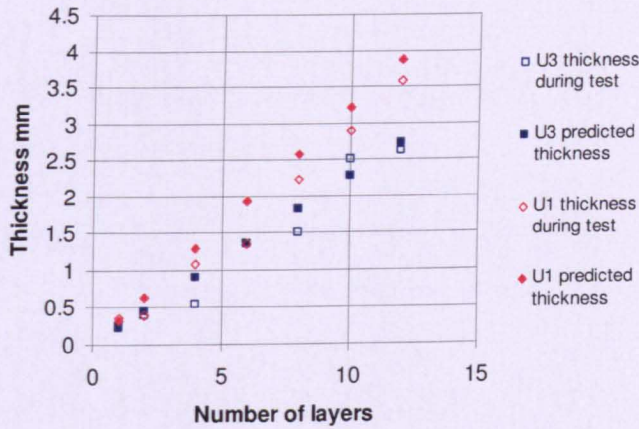
c)

Figure 6.3 Comparison between thermal conductivity values for: a) U1 and U3 plain weave 100% cotton fabrics, b) A3 and A4 plain weave 100% nylon fabrics, c) C3 and C9 twill weave PET/Cotton fabrics

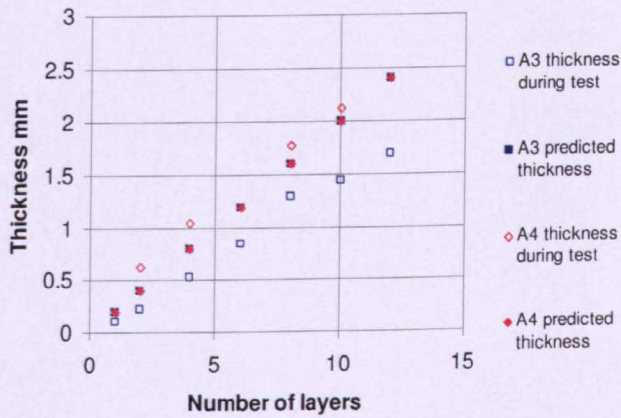
In Figure 6.3 thermal conductivity increases with the number of layers as expected [81]. All graphs have a similar non-linear shape as expected from the literature review (Chapter 2).

For all fabrics thickness during test was measured and compared to the number of layers (Figure 6.4). This is important for example for airbags fabrics because thermal conductivity changes with the number of layers or specimen thickness and if these parameters are chosen incorrectly, it may lead to very high thermal conductivity

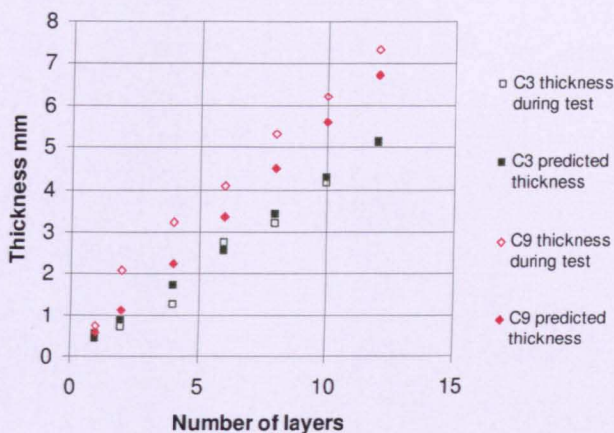
which in its turn influences the fabrics during application. As seen from Figure 6.4 fabrics experienced some compression during the test after they were mounted between hot and cold plates as they were pressed by the loading handwheel. A constant clamping force of 2.5kPa is applied during testing. Predicted thickness was calculated for the ideal case when thickness increases linearly with increased number of layers.



a) U1 and U3



b) A3 and A4



c) C3 and C9

Figure 6.4 Comparison between predicted and measured thickness during test.

6.3 DEVELOPMENT OF AN ANALYTICAL MODEL FOR THERMAL CONDUCTIVITY OF FABRICS

Two simple methods to calculate thermal conductivity are introduced in this section. Predicted results are compared to the experimental results. The first method to calculate thermal conductivity is a rule of mixtures presented in the following equation [64]:

$$k = (1 - V_f)k_A + V_f k_F \quad (6.2)$$

where k , k_A and k_F are fabric, air and fibre thermal conductivity respectively, V_f is the fibre volume fraction.

Fibre thermal conductivity was found in the literature for cotton, nylon and PET fibres [64] - [66], [73] - [77]. It is stated for all samples later in this chapter. Fibre thermal conductivity for a mixture of PET/Cotton was calculated as follows:

For example, C3 (67PET/33Cotton):

$$0.67 * k_F^{PET} + 0.33 * k_F^{Cotton} = 0.67 * 0.24 + 0.33 * 0.243 = 0.1608 + 0.08019 = 0.24 \text{ W/mK}$$

Fibre volume fraction V_f can be calculated using equation (6.3):

$$V_f = \frac{M_f}{\rho t} \quad (6.3)$$

where M_f is fabric areal density, ρ is fibre density and t is thickness of fabric (presented later in this chapter for all samples).

Another method to predict thermal conductivity is based on thermal resistance as described by Ning and Chou [68]. Thermal resistance R_i can be calculated using the following equation:

$$R_i = \frac{L_i}{k_i S_i} \quad (6.4)$$

where L_i and k_i are, respectively, the length and effective thermal conductivity of the i th conductive element in the direction of heat transfer, and S_i is the area of the conduction element cross-section perpendicular to the direction of heat transfer.

The thermal resistance R is related to the thermal conductivity k using the following equation:

$$R = \frac{t}{k} \quad (6.5)$$

In this method the unit cell is divided into small sections, thermal resistance is calculated for each section and then the thermal resistance for the whole unit cell is computed. Example of unit cells for plain weave fabrics is presented in Figure 6.5. It is assumed that thermal resistance for equal sections of unit cells are also equal. Based on this for a plain weave fabric: there is one section of air gap with thermal resistance, $R_{gap} = R_1$. There are four sections with thickness equal to one yarn height which means that the thermal resistance for these sections is also equal, $R_{1yarn} = R_2 = R_3 = R_4 = R_5$. There are four sections with thickness equal to two-yarns which means that $R_{2yarns} = R_6 = R_7 = R_8 = R_9$. Using a similar method, thermal resistance can be calculated for twill weave fabrics.

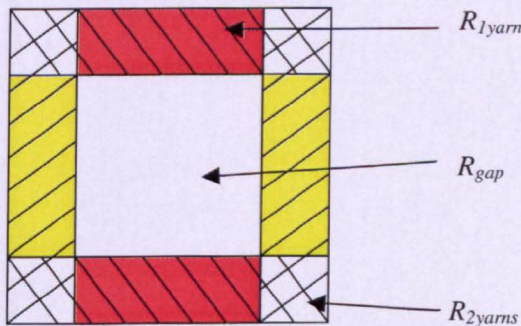


Figure 6.5 Thermal resistances in unit cell of a plain weave fabric

Thermal resistance through unit cell R_{UC} for plain or twill weave fabric can be calculated using equation (6.6):

$$R_{UC} = \frac{1}{4R_{1yarn}} + \frac{1}{4R_{2yarns}} + \frac{1}{R_{gap}} \quad (6.6)$$

Where $R_{1yarn} = \frac{t_y}{k_F((s_e - d_e)(s_p - d_p))}$;

$$R_{2yarns} = \frac{t_f}{k_F d_e d_p}$$
 ;

$$R_{gap} = \frac{t_f}{k_A((s_e - d_e)(s_p - d_p))}$$
 ;

t_y is yarn height (calculated as half of fabric thickness), t_f is fabric thickness, s_e and s_p are warp and weft spacing respectively, d_e and d_p are warp and weft width respectively, k_F and k_A are thermal conductivity of fibre and air respectively.

The above method predicts thermal conductivity through one layer of fabric. Theoretical prediction of thermal conductivity for several layers is difficult because it is impossible to find out the thickness of air gap between fabric layers. An X-ray CT scan for multiple-layered plain weave fabric is shown in Figure 6.6. [90] The air gap can be anything between zero thickness for no nesting to the thickness of two yarns. In Figure 6.6 it is noticeable that in some parts there is no air gap, whereas in other areas there is a large gap between two neighbouring layers.

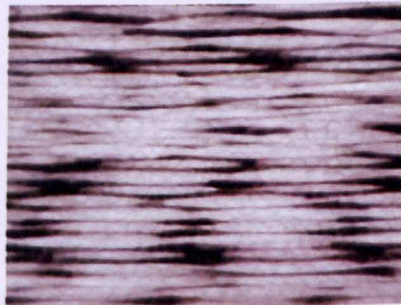


Figure 6.6 X-ray CT scan for multiple-layered plain weave fabric [90]

Taking this into consideration the following method was used to calculate thermal resistance through several layers, taking into account thermal resistance of the air gap between layers, partially based on experimental results. From experiments the thermal resistance was measured for one layer and for ten layer samples. The following equation was then used to calculate thermal resistance of the air gap between layers:

$$R_{gap} = \frac{R_{10layers} - 10R_{1layer}}{9} \quad (6.7)$$

Equation (6.7) can be used to calculate thermal resistance for two, four, six etc. layers:

$$R_{2layers} = 2R_{1layer} + R_{gap} \quad (6.8)$$

6.4 COMPARISON BETWEEN MEASURED AND PREDICTED RESULTS

A comparison between measured and predicted thermal conductivities using the rule of mixtures approach (equations (6.2) and (6.3)) for single layer fabrics is presented in Table 6.1. Thermal conductivity for air k_A is taken as 0.025 W/mK [100].

Table 6.1 Comparison between measured and predicted (Equations 6.2-6.3) thermal conductivity for single layer fabric

Fabric code	Fabric area density M_f kg/m ²	Fibre density ρ kg/m ³	Fibre volume fraction V_f	Fibre conductivity k_F W/mK	Predicted thermal conductivity k W/mK	Measured thermal conductivity k W/mK
U1	0.1428	1540	0.56	0.243	0.147	0.014
U3	0.1215	1540	0.64	0.243	0.165	0.008
A4	0.2137	1150	0.70	0.171	0.127	0.009
A3	0.1448	1150	0.70	0.171	0.127	0.007
C3	0.2542	918	0.57	0.250	0.153	0.026
C9	0.3008	1478	0.67	0.250	0.175	0.022

As seen from Table 6.1 the rule of mixtures approach does not give good agreement with experimental results. This might be because

Predicted thermal conductivity based on thermal resistance (equations (6.4) - (6.6)) is compared to experimental results in Table 6.2. It shows that predicted results are in reasonable agreement with measured ones for A3, A4, C3 and C9 fabrics. However, there is poor agreement with experimental data for U1 and U3 plain woven fabrics. The results of calculation for thermal resistance for air gap using equation (6.7) are shown in Table 6.3.

Table 6.2 Comparison between measured and predicted (using thermal resistance approach) thermal conductivity for single layer fabrics

Fabric code	Predicted thermal resistance of unit cell R_{uc} m^2K/W	Measured thermal resistance of fabric R_f m^2K/W	Predicted using eqs. (6.4 - 6.6) thermal conductivity of unit cell k_{uc} W/mK	Measured thermal conductivity of fabric k_f W/mK
U1	0.0036	0.023	0.087	0.014
U3	0.0013	0.028	0.17	0.008
A3	0.036	0.029	0.005	0.007
A4	0.074	0.022	0.002	0.009
C3	0.016	0.026	0.026	0.017
C9	0.013	0.026	0.042	0.022

Table 6.3 Thermal resistance for air gap based on experimental results (m^2K/W)

Fabric code	$R_{10layers}$	R_{1layer}	R_{gap}
U1	0.050	0.023	-0.02
U3	0.047	0.028	-0.026
A3	0.046	0.029	-0.027
A4	0.048	0.022	-0.019
C3	0.065	0.026	-0.022
C9	0.066	0.026	-0.022

As seen from Table 6.3 thermal resistance for the air gap between layers for all fabrics is negative as fabrics were under pressure during experiments (see Figure 6.2), so there were no significant gaps between fabric layers. This means that there should be no influence of thermal resistance of gap between layers on the results.

6.5 EXPERIMENTAL MEASUREMENT OF MOISTURE CONTENT OF FABRICS

6.5.1 Experimental set-up

Moisture content in fabrics was measured according to British Standard BS EN ISO 12571:2000 “Hygrothermal performance of building materials and products – Determination of hygroscopic sorption properties” [92]. According to the above standard, hygroscopic sorption is exchange of water vapour between ambient air and porous material until the point of equilibrium is reached. Experimental set-up is presented in Figure 6.7.

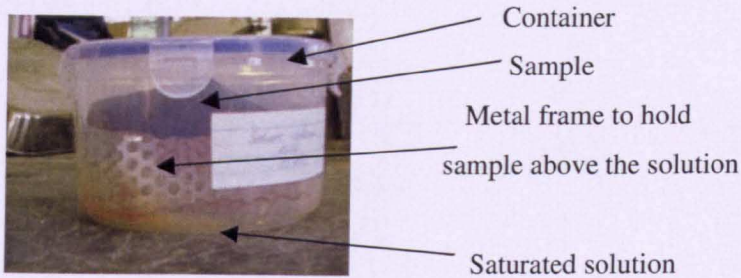
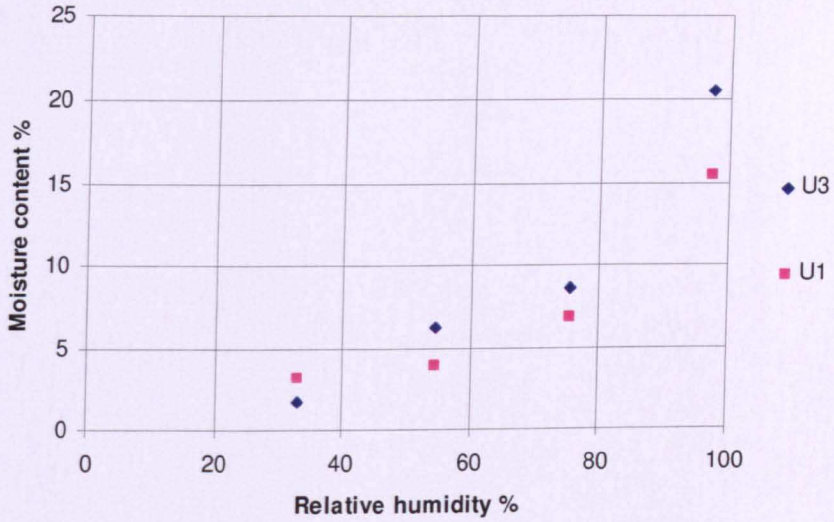


Figure 6.7 Experimental set-up for moisture content measurement

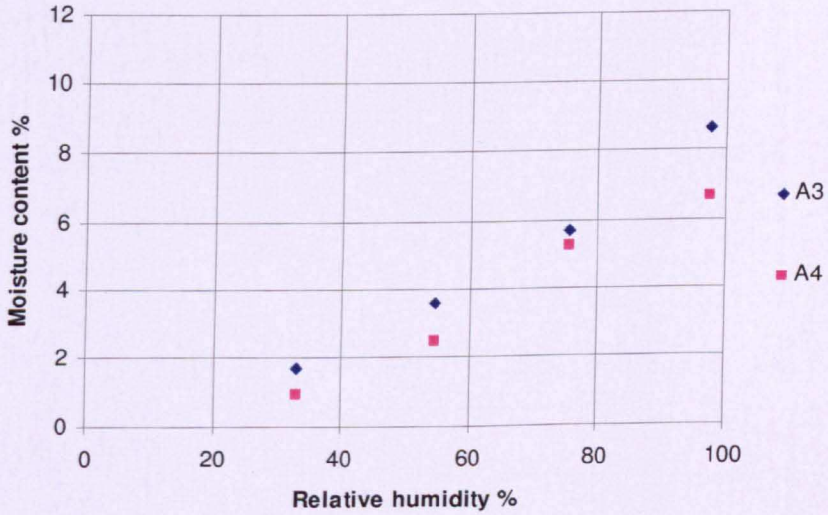
For each fabric four specimens were placed in four different environments with a certain fixed relative humidity. The four environments were as follows: magnesium chloride $MgCl_2$ with relative humidity of 33.07%, magnesium nitrate $Mg(NO_3)_2$ with relative humidity of 54.38%, sodium chloride $NaCl$ with relative humidity of 75.47% and potassium sulphate K_2SO_4 with relative humidity of 97.59%. Each of these salts is dissolved in 50ml of distilled water. All four containers with specimens were put inside an environmental chamber at $20^{\circ}C$ and 50% humidity. The moisture content was determined when equilibrium with the environment was reached. Equilibrium with environment was established by weighing the specimen until constant mass was reached and the wet mass was found. After that specimens were dried at $105^{\circ}C$ for 24 hours and weighed again to obtain dry mass. The same six fabrics as for thermal conductivity experiments were chosen (see Chapter 3 for fabric details).

6.5.2 Experimental results and analysis

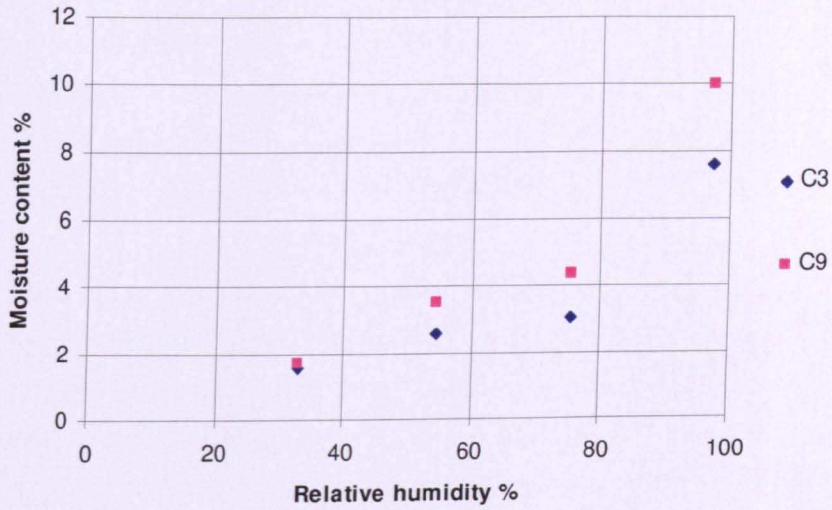
Results of moisture content experiments are presented in Figure 6.8.



a) U1 and U3



b) A3 and A4



c) C3 and C9

Figure 6.8 Experimental results of moisture content for: a) U1 and U3, b) A3 and A4, c) C3 and C9

As seen from Figure 6.8, for pure cotton fabrics (U1 and U3) moisture content is approximately twice of Nylon fabrics (A3 and A4), which in turn are similar to PET/Cotton fabrics (C3 and C9). The shape of the curves for different fabrics is also different. For pure cotton U1 and U3 fabrics and PET/Cotton fabrics C3 and C9, the shape is exponential whereas the curves for Nylon fabrics A3 and A4 are close to linear because cotton fabrics are hygroscopic (able to attract water molecules from the surrounding environment) and fibres tend to swell with increase of relative humidity absorbing more moisture. C9 fabric contains 60% of cotton fibres and 40% of PET fibres in comparison with C3, which has 33% cotton and 67%PET fibres, which makes moisture content in C9 higher than in C3 as seen from Figure 6.8 because cotton fibres absorb moisture more than PET fibres.

6.5.3 Study of influence of moisture content on thermal conductivity of fabrics

Moisture content influences the thermal conductivity of fabrics as seen from several studies described in the literature [60], [63], [73] [74], [76], and [78]. Thermal conductivity increases when porosity decreases. When the water content in pores is

Through thickness air permeability and thermal conductivity analysis for textile materials

increased, there is an increase in thermal conductivity, due to the higher thermal conductivity of water. Dias and Delkumburewatte [73] analysed influence of moisture content on thermal conductivity of knitted fabrics. Predicted results from their model found good agreement with experimental data. To calculate thermal conductivity taking into consideration moisture content, they used the following equation:

$$k = \frac{k_m k_A k_w}{(1 - \alpha)k_A k_w + (\alpha - \alpha w)k_m k_w + \alpha w k_m k_A} \quad (6.9)$$

where k_m , k_A and k_w are thermal conductivities of material, air and water respectively, α is porosity of fabric, w is water content.

Table 6.4 shows the influence of moisture content on thermal conductivity. Thermal conductivity of air and water were taken as $k_A = 0.025\text{W/mK}$ and $k_w = 0.60\text{W/mK}$ respectively [100]. Thermal conductivity and moisture content of fabrics were taken from experimental data. Moisture content for fabrics was chosen at 54.38% humidity as closest to the moisture content during thermal conductivity experiments. Five fabrics presented in Table 6.4 were chosen because they had the full data to predict thermal conductivity with influence of moisture. As seen from Table 6.4 there is a good agreement between measured and predicted results for U3 and A3 fabrics, however, there is a poor agreement for U1, C3 and C9 fabrics.

Table 6.4 Influence of moisture content on thermal conductivity of fabrics at 55% relative humidity

Fabric code	Porosity α	Moisture content w	Measured thermal conductivity k_f W/mmK	Predicted thermal conductivity k_f W/mmK
U1	0.32	0.0404	14.0	5.91
U3	0.14	0.0623	8.0	9.53
A3	0.12	0.0363	7.0	8.66
C3	0.33	0.0258	17.0	5.79
C9	0.11	0.0351	22.0	10.73

Figure 6.9 shows the predicted influence of relative humidity on thermal conductivity k_f for selected fabrics. It is noticeable that there is no significant influence of moisture content on thermal conductivity for very some fabrics such as A3, C3; whereas for U1, U3 and C9 fabrics there is a dramatic influence of relative humidity on thermal conductivity. This can be explained by the nature of fabrics: hygroscopic fabrics like cotton (U1, U3 and C9) show change in thermal conductivity to convective flow at higher humidities, due to fibre swelling and decrease in free air volume in the fabric, and possibly, some increase in fabric thickness. The fabrics which are much less hygroscopic, such as nylon (A3), showed much less variation with relative humidity. Other authors have described similar results (see Chapter 2).

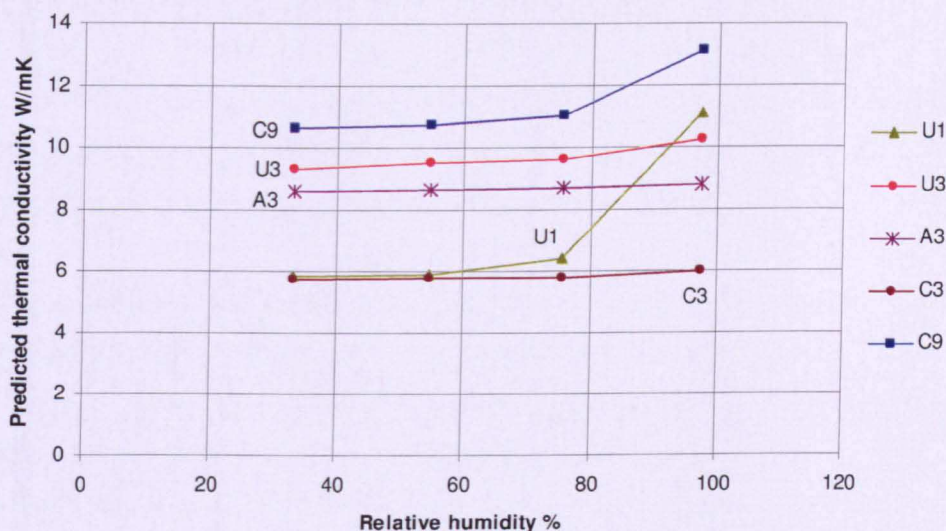


Figure 6.9 Influence of relative humidity on thermal conductivity

6.6 CONCLUSIONS

An analytical model for thermal conductivity prediction has been developed using two different approaches: a rule of mixtures and a thermal resistance approach. Rule of mixtures approach did not give good agreement with experimental results. The thermal resistance approach showed that predicted results are in good agreement with measured ones for A3, A4, C3 and C9 fabrics. However, there was not good agreement with experimental data for U1 and U3 plain woven fabrics. Comparison between these two analytical methods and experimental results are presented in Figure 6.10.

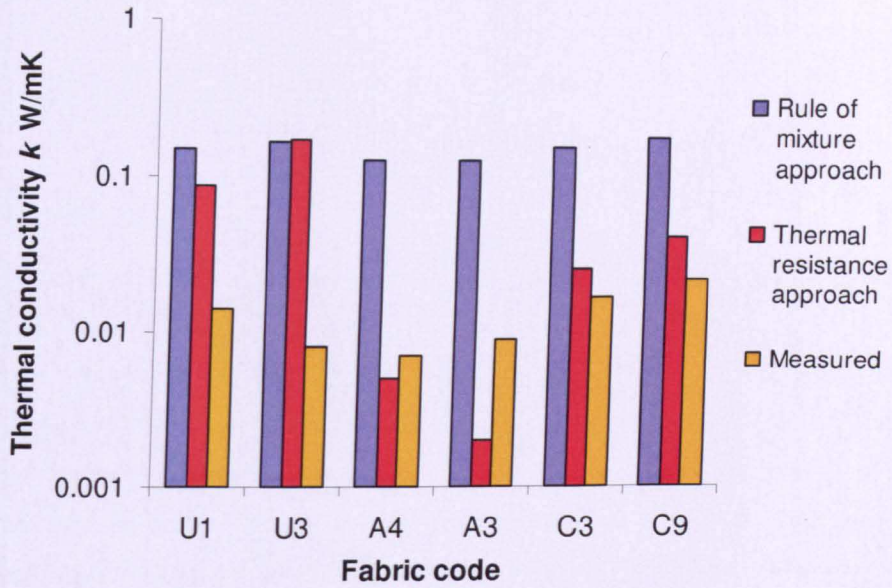


Figure 6.10 Comparison between two analytical approaches and experimental data for thermal conductivity for single layer fabrics

It is noticeable that there is no significant influence of moisture content on thermal conductivity for very tight fabrics. This study showed that it is quite difficult to accurately predict the thermal conductivity of fabrics using existing models as they have many simplifying assumptions which influence the predicted results significantly. Fabric thermal conductivity needs more study to improve upon existing models. A CFD approach might improve predictions and avoid many of the assumptions.

CHAPTER 7

DISCUSSION AND CONCLUSIONS

7.1 INTRODUCTION

The work described in this thesis was performed within the Technology Strategy Board project “Materials modelling: Multi-Scale Integrated Modeling for High Performance Flexible Materials”, which was supported by several partners: Unilever UK Central Resources, OCF PLC, Croda Chemicals Europe Ltd, ScotCad Textiles Ltd, Carrington Career and Workwear Ltd, Moxon Ltd, Airbags International, Technitex Faraday Ltd. It also included three research groups from different universities: University of Nottingham, University of Manchester and Heriot-Watt University. The main objectives of the project related to this thesis were: model yarn-fabric scale; develop ‘unit cells’ for a variety of weaves; generate FE models automatically using the Nottingham TexGen schema; develop CFD model to predict through thickness air permeability; model thermal conductivity of fabrics; air and/or oil through thickness permeability, thermal conductivity and moisture content measurement; develop a model to predict permeability of deformed fabrics in yarn-fabric scale.

According to the main objectives of the project, the aim of this thesis was to create a general model for through thickness air permeability and thermal conductivity including moisture content using analytical and computational methods for different types of textile fabrics. An analytical model for deformed (shear, compaction and tension) fabrics was developed. Experimental work was performed for fabric permeability (air and oil) and thermal conductivity to verify predicted results. The findings and achievements of the work are discussed in this final chapter. The recommendations for further work are made based on the limitations of the proposed approaches. Significant conclusions arising from this work are summarised at the end.

7.2 GENERAL DISCUSSION

The main part of the thesis was dedicated to through thickness air permeability of fabrics. Both undeformed and deformed fabrics were of interest. For undeformed fabrics the following key points are highlighted based on the results from Chapters 3 and 4:

- Ten fabrics permeabilities were predicted by a combination of two existing analytical models. Air flow through gaps between yarns is the dominant mechanism for loose fabrics such as U1 and U2. For tight fabrics, air flow through gaps between yarns and within yarns both govern the fabric permeability.
- Three fabrics with the same geometry have been compared to show the influence of finishing on fabric permeability. Predicted results have the same trend as experimental data.
- Both air and oil through thickness permeability experiments were performed. There is a good agreement between the two experimental techniques which shows that there is little or no influence of liquid viscosity on permeability.
- The analytical model has some assumptions which dramatically affect the predicted results of fabric permeability. Among them is that the pore is rectangular in shape whereas in reality pore has a more complicated shape.
- Another problem with the analytical model is that it cannot model overlapping and very tight fabrics, such as U3 or A3 where predicted results are not in good agreement with experimental data. For almost all twill-weave fabrics the predictions are in good agreement with experiments except for C1 and C3 which might be because of the shape of the gaps between yarns. Fabrics with rectangular pore shape have good agreement with experimental data, whereas fabrics with the non-clear shape gaps have poor agreement.
- The results presented in Chapter 4 showed that the CFD simulations are very sensitive to the yarn porosity and yarn permeability as well as the geometric

modelling of fabrics. A small change in yarn porosity can lead to a dramatic change in the predicted through thickness air permeability of fabric.

- Using A1 fabric, with a tight structure, the significant influence of yarn porosity on fabric permeability was shown. CFD results showed good agreement with measured data for A1 fabric due to the fact that it was easy to model its unit cell. There is no good agreement for other fabrics especially for twill-weave fabrics as it was difficult to obtain an accurate unit cell geometry.
- The limitations of the TexGen/CFD approach are also presented. The difficulty of modelling very tight fabrics in TexGen is of primary concern. Current models assume an idealised shape of the yarn and use an idealised yarn path. In reality, there is a lot of mixing of fibres between the yarns within the fabric structure (see Appendix C) and often there are no distinct boundaries. The current fabric model cannot take this into consideration.
- The studies here have highlighted the strengths of using CFD simulations in comparison with the analytical approach presented in Chapter 3. It showed that TexGen can model a large range of geometries including plain-weave and twill-weave. TexGen is good at meshing the unit cell geometry. It showed that it is possible to provide a permeability prediction using CFD simulations for real fabrics in the same order of magnitude as experimental with an accurate thorough geometric model. CFD modelling can demonstrate the Forchheimer effect (non-linear relationship between flow rate and pressure) whereas the analytical model cannot do this.

Issues identified from the study of through thickness air permeability of deformed fabrics are the following based on the results from Chapter 5:

- Three common types of deformation of textile fabrics were analysed: shear, compaction and tension. An analytical model for sheared fabrics has been developed using a modified model for permeability through unsheared fabrics which was described in Chapter 3.

- Locking angle for each fabric was calculated. Two mechanisms of shear have been described: shear before and after locking. If fabric has loose fibres inside the yarns, than shear changes the permeability significantly even after locking as seen from Chomarat 800S4-F1 fabric (Chapter 5).
- An experimental set up was designed to fit the shear rig around the permeability tester to measure the through thickness air permeability of the fabric after shear. Unfortunately, only one glass-fibre fabric Chomarat 800S4-F1 was tested using the shear rig as others buckled. A more suitable rig should be developed which will include some pre-tension to prevent fabrics from buckling. Predicted results have poor agreement with measured data for all shear angles.
- Abaqus FE software was used to perform compaction simulations on U2 fabric. Results were used in an analytical model to calculate the fabric permeability after compaction. There was no experimental work done for the permeability of compacted fabrics and effect of compaction on permeability.
- Other types of deformation like tension in warp and weft directions were studied using U2 fabric. The analytical model included the results from FE simulations of tension for U2 fabric. Tension was applied in three ways: in warp direction; in weft direction; and in both warp and weft directions. The predictions showed a more significant influence of tension in the weft direction than in the warp direction on fabric permeability as there was more spacing between weft yarns than between warp yarns. More computational and experimental work should be done on all three deformation mechanisms.

Another part of the study was to develop an analytical model for thermal conductivity for fabrics (single-layer and multiple-layers) taking into consideration moisture content:

- Analytical models for thermal conductivity prediction were developed using two different approaches: rule of mixtures and thermal resistance. It was shown that the thermal resistance approach produced better agreement with experimental data than the rule of mixtures approach.

- Thermal conductivity predictions for multiple layers were shown in Chapter 6. Using experimental results, it was shown that there is little influence of thermal conductivity of the air gap on overall thermal conductivity of multiple layer fabrics.
- The influence of moisture on thermal conductivity of fabrics was studied. It is noticeable that there is no significant influence of moisture content on thermal conductivity for very tight fabrics such as A3, C3 and C9; whereas for U1 and U3 cotton fabrics there is an influence of relative humidity on thermal conductivity. This can be explained by the nature of fabrics: hygroscopic fabrics like cotton (U1 and U3) show change in thermal conductivity to convective flow at the higher humidities, due to fibre swelling and decrease in free air volume in the fabric, and possibly, some increase in fabric thickness. The fabrics which are less hygroscopic, such as polyester/cotton (C3, C9) or nylon (A3), showed much less variation with relative humidity.

7.3 RECOMMENDATIONS FOR FURTHER WORK

From the discussion of the work done, certain areas have been identified in which further research may be constructive.

- More work should be done on accurate modelling fabric geometries using TexGen. It is very difficult to model real fabrics using only the programme interface. It is recommended to use a script to model very tight and overlapping fabrics, allowing (for example) yarn cross-section to vary along the yarn length.
- There is a possibility to further develop an analytical model to predict through thickness air permeability. In the current work, gap geometry has been assumed as a straight capillary. In reality, the geometry of gap is far more complicated. More work can be done to study the real geometry of gaps between yarns.
- More work can be done to study fabric behaviour using the Forchheimer equation. More analytical and CFD modelling should be done to characterise

and explain the non-linear changing of fabric permeability under changes in pressure drop.

- Further CFD modelling could be performed to predict thermal conductivity. CFX 11.0 has several options to predict thermal conductivity of porous unit cells which need to be investigated thoroughly.
- This work made a first step to measure permeability for deformed fabrics. More work can be done to improve the current shear rig, so that different types of fabrics can be sheared without buckling.
- More analytical and CFD work should be done to predict through thickness air permeability of deformed fabrics such as compressed and sheared fabrics and fabrics under the tension. Currently there are some difficulties in transferring models of sheared or compressed fabrics back to TexGen or CFX 11.0.
- Permeability prediction as well as thermal conductivity study for multiple layer fabrics could be further developed. This work has included an experimental study of air permeability and thermal conductivity for multiple layers. More analytical and CFD work needs to be done for multiple layer fabrics.

7.4 CONCLUSIONS

The conclusions gained from this thesis are summarised below.

- Through thickness air permeability of different types of fabrics was studied using both analytical, experimental and CFD approaches. An analytical approach included two mechanisms: flow through gaps and through yarns. CFD predictions were developed using TexGen and CFX 11.0 software packages. Both analytical and CFD predictions had reasonable agreement with experimental data in some cases but they are very sensitive to the geometric modelling.
- A number of sensitivity studies for air permeability predictions were carried out. The influence of pressure drop on fabric permeability was studied. All

fabrics showed non-linear behaviour under different pressure drops which is reflected in the Forchheimer equation. Studies showed that there was also a significant influence of fabric finishing on permeability.

- Through thickness air permeability of deformed fabrics was studied. Different deformations were chosen such as shear, compression and tension. Experimental work was performed for shear deformation for glass-fibre fabric. Analytical predictions had good agreement with the experimental results.
- Experimental work for thermal conductivity of single layer and multiple layer fabrics was carried out. An analytical model was developed taking into consideration the influence of moisture content on thermal conductivity of fabrics. Thermal conductivity predictions showed fair agreement with experimental data. There was no significant influence of moisture on thermal conductivity.

REFERENCES

- [1] DAS A., ISHTIAQUE S.M. (2004). *Comfort characteristics of fabrics containing twist-less and hollow fibrous assemblies in weft*. Journal of Textile and Apparel, Technology and Management 3 (4): 1 – 5.
- [2] SENOGUZ M.T, DUNGAN F.D., SASTRY A.M., KLAMO J.T. (2001). *Simulations and experiments on low-pressure permeation of fabrics: Part 2 – The variable gap model and prediction of permeability*. Journal of Composite Materials 35 (14): 1285 – 1322.
- [3] GEBART B.R. (1992). *Permeability of unidirectional reinforcements for RTM*. Journal of Composite Materials 26 (8): 1100 – 1133.
- [4] MCCARTNEY J., HINDS B.K., SEOW B.L., GONG D. (2000). *Dedicated 3D CAD for garment modelling*. Journal of Materials Processing Technology 107: 31 – 36.
- [5] FONTANA M., RIZZI C., CUGINI U. (2005). *3D virtual apparel design for industrial applications*. Computer-Aided Design 37: 609 – 622.
- [6] WONG C.C. (2006). *Modelling the effect of textile preform architecture on permeability*. PhD thesis, University of Nottingham.
- [7] KULICHENKO A.V. (2005). *Theoretical analysis, calculation and prediction of the air permeability of textiles*. Fibre Chemistry 37 (5): 371 – 380.
- [8] CARMAN P.C. (1937). *Fluid Flow through Granular Beds*. Transactions of the Institution of Chemical Engineers (London) 15: 150-156.
- [9] BRUSCHKE M.V. AND ADVANI S.G. (1990). *A Finite Element/Control Volume Approach to Mold Filling in Anisotropic Porous Media*. Polymer Composites 11 (6): 398-405.

- [10] KULICHENKO A.V., LANGENHOVE L.V. (1992). *The resistance to flow transmission of porous materials*. Journal of Textile Institute 1: 127 – 132.
- [11] BERDICHEVSKY A.L. AND CAI Z. (1993). *Preform Permeability Predictions by Self-Consistent Method and Finite Element Simulation*. Polymer Composites 14 (2): 132-143.
- [12] CAI Z. AND BERDICHEVSKY A.L. (1993). *An Improved Self-Consistent Method for Estimating the Permeability of a Fiber Assembly*. Polymer Composites 14 (4): 314-323.
- [13] BRUSCHKE M.V., ADVANI S.G. (1993). *Flow of generalized Newtonian fluids across periodic array of cylinders*. Rheology 37 (3): 479 – 497.
- [14] VAN DER WESTHUIZEN, DU PLESSIS J. AND J.P. (1996). *An Attempt to Quantify Fibre Bed Permeability Utilizing the Phase Average Navier-Stokes Equation*. Composites Part A 27A: 263-269.
- [15] WANG C.Y. (1996). *Stokes Flow through an Array of Rectangular Fibres*. International Journal of Multiphase Flow 22 (1): 185-194.
- [16] PHELAN JR. F.R., WISE G. (1996). *Analysis of transverse flow in aligned fibrous porous media*. Composites: Part A 27A (1): 25 – 34.
- [17] SADIQ T., ADVANI S.G., PARNAS R.S. (1992). Proceedings 24th International SAMPE Technical Conference on Composite Materials, Toronto. 25-34.
- [18] DELUCA P., BENOIT Y. (2001). *LCMflot User guide*, ESI group.
- [19] SIMACEK P.E., SOZER E.M., ADVANI S.G. (1998). *User manual for Drape 1.1 and LIMS 4.0*. CCM Report 98-01. University of Delaware, USA.
- [20] HIBBITT, KARLSSON and SORENSON LTD. (1998). *Abaqus/Standard user's manual*.

- [21] FLUENT INC. (2001). *Fluent 6.0 user's manual*.
- [22] ANSYS INC. (2005). *ANSYS CFX-Solver, Release 11.0: Theory*.
- [23] SHERBURN M. (2006). *Geometric and mechanical modelling of textiles*. PhD Thesis, University of Nottingham.
- [24] LOMOV S.V., HUYSMANS G., LUO Y., PARNAS R.S., PRODROMOU A., VERPOEST I., PHELAN F.R. (2001). *Textile composites: modelling strategies*. Composites: Part A 32: 1379 – 1394.
- [25] ROBITAILLE F., LONG A.C., JONES I.A., RUDD C.D. (2003). *Automatically generated geometric descriptions of textile and composite unit cells*. Composites: Part A 34: 303-312.
- [26] BELOV E.B., LOMOV S.V., VERPOEST I., PETERS T., ROOSE D., PARNAS R.S., HOES K., SOL H. (2004). *Modelling of permeability of textile reinforcements lattice Boltzmann method*. Composites Science and Technology 64: 1069 – 1080.
- [27] SOBERA, M.P., KLEIJN, C.R., BRASSER, P., HARRY E.A. VAN DEN AKKER (2004). *A multi-scale numerical study of the flow, heat and mass transfer in protective clothing*. Computational Science – ICCS. 4th International Conference. Poland: 637-644.
- [28] WANG Q., MAZE B., VAHEDI TAFRESHI H., POURDEYHIMI B. (2006). *A note on permeability simulation of multifilament woven fabrics*. Chemical Engineering Science 61: 8085 – 8088.
- [29] LEKAKOU C., EDWARDS S., BELL G., AMICO S.C. (2006). *Computer modelling for the prediction of the in-plane permeability of non-crimp stitch bonded fabrics*. Composites: Part A 37: 820 – 825.

- [30] NORDLUND M., LUNDSTROM T.S., FRISHFELDS V., JAKOVICS A. (2006). *Permeability network model for non-crimp fabrics*. Composites: Part A 37: 826 -835.
- [31] WONG C.C., LONG A.C., SHERBURN M., ROBITAILLE F., HARRISON P., RUDD C.D. (2006). *Comparisons of novel and efficient approaches for permeability prediction based on the fabric architecture*. Composites: Part A 37: 847 – 857.
- [32] VERLEYE B., CROCE R., GRIEBEL M., KLITZ M., LOMOV S.V., VERPOEST I., ROOSE D. (2007). *Finite difference computation of the permeability of textile reinforcements with a fast Stokes solver and new validation examples*. 10th ESAFORM Conference on Material Forming. AIP Conference Proceedings, Volume 907. Spain: 945 – 950.
- [33] VERLEYE B., CROCE R., GRIEBEL M., KLITZ M., LOMOV S.V., MORREN G., SOL H., VERPOEST I., ROOSE D. (2008). *Permeability of textile reinforcements: Simulation, influence of shear and validation*. Composites Science and Technology 68: 2804 – 2810.
- [34] VAKIL A., OLYAEI A., GREEN S.I. *The Influence of Machine-Side Filaments and Jet-to-Wire Speed Ratio on the Flow Through a Forming Fabric*. TAPPI Paper Conference, 2009.
- [35] NIU J., GU Z. (2008). *Research of immersion-resistant and moisture permeable smart fabric and theoretically analysis of its immersion-resistant property*. The 86th Textile Institute World Conference, Hong Kong: 814 – 830.
- [36] JIA L.-X., WANG R., LIU J.-M. (2008). *Study on the chemical method used for decreasing the permeability of polyester fabric*. The 86th Textile Institute World Conference, Hong Kong: 596 – 602.
- [37] HUANG H., AYOUB J. (2008). *Applicability of the Forchheimer equation for non-Darcy flow in porous media*. Society of Petroleum Engineers Journal: 112 – 122.

- [38] DOUGLAS R., HUIPING M. (1992). On the derivation of the Forchheimer equation by means of the averaging theorem. *Transport in Porous media* 7: 255 – 264.
- [39] WANG X.-H., LIU Z.-F. (2004). *The Forchheimer equation in two-dimensional percolation porous media*. *Physica A* 337: 384 – 388.
- [40] CLEARMAN W.M. (2007). *Measurement and correlation of directional permeability and Forchheimer inertial coefficient of micro porous structures used in pulse-tube cryocoolers*. MSc Thesis. Georgia Institute of Technology: 14-21.
- [41] PETRASCH J., MEIER F., FRIESS H., STEINFELD A. (2008). *Tomography based determination of permeability, Dupuit-Forchheimer coefficient, and interfacial heat transfer coefficient in reticulate porous ceramics*. *International Journal of Heat and Fluid Flow* 29: 315 – 326.
- [42] KIM S.M. (2008). *Numerical investigation on laminar pulsating flow through porous media*. MSc Thesis. Georgia Institute of Technology: 2 – 9.
- [43] WONG C.C., LONG A.C. (2006). *Modelling variations of textile fabric permeability at mesoscopic scale*. *Plastics, Rubber and Composites* 35 (3): 101 – 111.
- [44] SMITH P., RUDD C.D., LONG A.C. (1997). *The effect of shear deformation on the processing and mechanical properties of aligned reinforcements*. *Composites Science and Technology* 57: 327 – 344.
- [45] BICKERTON S., SIMACEK P., GUGLIELMI S.E., ADVANI S.G. (1997). *Investigation of draping and its effects on the mold filling process during manufacturing of a compound curved composite part*. *Composites: Part A* 28A: 801 – 816.
- [46] CHEN B, CHOU T.-W. (1999). *Compaction of woven-fabric performs in liquid composite molding process: single-layer deformation*. *Composites Science and Technology* 59: 1519 – 1526.

- [47] CHEN B., CHOU T.W. (2000). *Compaction of woven-fabric performs: nesting and multi-layer deformation*. Composites Science and Technology 60: 2223 – 2231.
- [48] CHEN B., LANG E.J., CHOU T.W. (2001). *Experimental and theoretical studies of fabric compaction behaviour in resin transfer molding*. Materials Science and Engineering A317: 188 – 196.
- [49] TAKANO N., ZAKO M., OKAZAKI T., TERADA K. (2002). *Microstructure-based evaluation of the influence of woven architecture on permeability by asymptotic homogenization theory*. Composites Science and Technology 62: 1347 – 1356.
- [50] LOUIS M., HUBER U. (2003). *Investigation of shearing effects on the permeability of woven fabrics and implementation into LCM simulation*. Composites Science and Technology 63: 2081 – 2088.
- [51] ENDRUWEIT A., ERMANNI P. (2004). *The in-plane permeability of sheared textiles. Experimental and a predictive conversion model*. Composites: Part A 35: 439 – 451.
- [52] LOIX F., BADEL P., ORGEAS L., GEINDREAU C., BOISSE P., BLOCH J.-F. (2008). *Modelling of the flow of generalised Newtonian fluids through deformed textile reinforcements*. Composite Science and Technology 68: 1624 – 1630.
- [53] GOLDSTEIN R.J., ECKERT E.R.G., IBELE W.E., PATANKAR S.V., SIMON T.W., KUEHN T.H., STRYKOWSKI P.J., TAMMA K.K., BAR-COHEN A., HEBERLEIN J.V.R., DAVIDSON J.H., BISCHOF J., KULACKI F.A., KORTSHAGEN U., GARRICK S., SRINIVASAN V. (2005). *Heat transfer – a review of 2002 literature*. International Journal of Heat and Mass Transfer 48: 819 – 927.
- [54] HENRY P.S.H. (1939). *Diffusion in absorbing media*. Proc. Royal Society 171: 215 - 241.

- [55] BRAILSFORD A.D., MAJOR K.G. (1964). *The thermal conductivity of aggregates of several phases, including porous materials*. British Journal of Applied Physics 15: 313 – 319.
- [56] WATT I.C., DARCY R.L. (1979). *Water-vapour adsorption isotherms of wool*. Journal of Textile Institute 70 (7): 298 – 307.
- [57] WARREN M.R., JAMES P.H., YOUNG I.C. (1998). Handbook of heat transfer. 3rd Edition. McGraw-Hill Handbooks.
- [58] FARNWORTH, B. (1983). *Mechanisms of heat flow through clothing insulation*. Textile Research Journal 53 (12): 717-725.
- [59] LI Y., HOLCOMBE B.V. (1992). *A two-stage sorption model of the coupled diffusion of moisture and heat in wool fabric*. Textile Research Journal 62 (4): 211 – 217.
- [60] YASUDA T., MIYAMA M., MURAMOTO A. (1994). *Dynamic water vapour and heat transport through layered fabrics. Part 3: Surface temperature change*. Textile Research Journal 64 (8): 457 – 461.
- [61] LE C.V., LY N.G. (1995). *Heat and mass transfer in the condensing flow of steam through an absorbing fibrous medium*. International Journal of Heat and Mass Transfer 38 (1): 81 – 89.
- [62] GHALI K., JONES B., TRACY J. (1995). *Modelling heat and mass transfer in fabrics*. International Journal of Heat and Mass Transfer 38 (1): 13 – 21.
- [63] FOHR J.P., COUTON D., TREGUIER G. (2002). *Dynamic heat and water transfer through layered fabrics*. Textile Research Journal 72 (1): 1 – 12.
- [64] GHALI K., GHADDAR N., JONES B. (2002). *Empirical evaluation of convective heat and moisture transport coefficients in porous cotton medium*. Journal of Heat Transfer 124: 530 – 537.

[65] LUO Z., LI F., LIU Y. and LI Y. (2004). *Effect of the environmental atmosphere on heat, water and gas transfer within hygroscopic fabrics*. Journal of Computational and Applied Mathematics 163: 199 – 210.

[66] SOBERA M.P., KLEIJN C.R., BRASSER P., AKKER H. (2004). *A multi-scale numerical study of the flow, heat and mass transfer in protective clothing*. Lecture Notes in Computer Science 3039: 637 – 644.

[67] WANG J., CARSON J.K., NORTH M.F., CLELAND D.J. (2008). *A new structural model of effective thermal conductivity for heterogeneous materials with co-continuous phases*. International Journal of Heat and Mass Transfer 51: 2389 – 2397.

[68] MAXWELL J.C. (1954). *A treatise on electricity and magnetism*. Third edition, Dover Publications Inc., New York. (Chapter 9).

[69] EUCKEN A. (1940). *Allgemeine gesetzmäßigkeiten für das wärmeleitvermögen verschiedener stoffarten und aggregatzustände*. Forschung Gabiete Ingenieur 11 (1): 6 – 20.

[70] BÖTTCHER C.J.F. (1952). *Theory of electric polarisation*. Elsevier, Houston: 415 – 420.

[71] LANDAUER R. *The electrical resistance of binary metallic mixtures*. Journal of Applied Physics 23: 779 – 784.

[72] LUO X., XU Q. (2006). *A new numerical implementation on 2D heat and moisture transfer through fabric*. Applied Mathematics and Computation 174: 1135 – 1150.

[73] DIAS T., DELKUMBUREWATTE G.B. (2007). *The influence of moisture content on the thermal conductivity of a knitted structure*. Measurement Science and Technology 18: 1304 – 1314.

- [74] MIN K., SON Y., KIM C., LEE Y., HONG K. (2007). *Heat and moisture transfer from skin to environment through fabrics: a mathematical model*. International Journal of Heat and Mass Transfer 50: 5292 – 5304.
- [75] LIN L.-Y., JOU G.T. (2008). *A study on heat transfer and thermal protective properties of clothing materials for firefighters' protective clothing*. The 86th Textile Institute World Conference, Hong Kong: 331 – 346.
- [76] LITTLE T., LIU R. (2008). *Thermal and moisture performance of competition athletic wear*. The 86th Textile Institute World Conference, Hong Kong: 2058 – 2065.
- [77] HAVELKA A., KUS Z. (2008). *Transport properties of semi-permeable-barrier textile for modern sports apparel*. The 86th Textile Institute World Conference, Hong Kong: 1514 – 1523.
- [78] SARKAR M.K., FAN J.T., CHEN Q. (2008). *Transplanar water transport tester for fabrics*. The 86th Textile Institute World Conference, Hong Kong: 2041 – 2057.
- [79] DASGUPTA A., AGARWAL R.K., BHANDARKAR S.M. (1996). *Three-dimensional modelling of woven-fabric composites for effective thermo-mechanical and thermal properties*. Composites Science and Technology 56: 209 – 223.
- [80] NING Q.G., CHOU T.W. (1995). *Closed-form solutions of the in-plane effective thermal conductivities of woven-fabric composites*. Composites Science and Technology 55: 41 – 48.
- [81] WOO K., GOO N.S. (2004). *Thermal conductivity of carbon-phenolic 8-harness satin weave composites*. Composite Structures 66: 521 – 526.
- [82] HIND S., ROBITAILLE F., RAIZENNE D. (2006). *Parametric unit cell modelling of the effective transverse thermal conductivity of carbon plain weave composites*. 8th International Conference on Textile Composites (TEXCOMP-8), Nottingham: T16-1 – T16-6.

- [83] SCHUSTER J., HEIDER D., SHARP K., GLOWANIA M. (2008). *Thermal conductivities of three-dimensionally woven fabric composites*. Composites Science and Technology 68: 2085 – 2091.
- [84] MARKLUND P.-O., NILSSON L. (2002). *Simulation of airbag inflation processes using a coupled fluid structure approach*. Computational Mechanics 29 (4): 289 – 297.
- [85] British Standard BS EN ISO 9237:1995. Textiles – Determination of the permeability of fabrics of air.
- [86] Air permeability tester. FX 3300 LABOTESTER III. TEXTTEST AG, CH-8603 Schwerzenbach, Switzerland.
- [87] KAWABATA S. (1982). *The development of the objective measurement of fabric handle*, in Kawabata S., Postle R., Niwa M. (Eds), *The Textile Machinery of Japan*: 31-59, Kyoto, Japan.
- [88] International Standard ISO 8301: 1991. Thermal insulation – Determination of steady-state thermal resistance and related properties – Heat flow meter apparatus.
- [89] P.A. HILTON LTD. (1994). *Experimental operating and maintenance manual*. Thermal conductivity of building and insulating materials unit B480.
- [90] LOMOV S.V., VERPOEST I., PEETERS T., ROOSE D., ZAKO M. (2003). *Nesting in textile laminates: geometrical modelling of the laminate*. Composite Science and Technology 63: 993 – 1007.
- [91] HUST J.G., LANKFORD A.B. (1982). *Comments on the measurement of thermal conductivity and presentation of thermal conductivity integral method*. International Journal of Thermophysics 3(1): 67 – 77.
- [92] British Standard BS EN ISO 12571:2000. Hygrothermal performance of building materials and products – Determination of hygroscopic sorption properties.

[93] BLAZEK J. (2006) .Computational Fluid Dynamics: Principles and Applications, 2nd edition. Elsevier.

[94] IMAGE J SOFTWARE: <http://rsbweb.nih.gov/ij/>

[95] ENDRUWEIT A., MCGREGOR P., LONG A.C., JOHNSON M.S. (2006). *Influence of the fabric architecture on the variations in experimentally determined in-plane permeability values*. Composites Science and Technology 66 (11): 1778 – 1792.

[96] KESHAVARAJ R., TOCK R.W., HAYCOOK D. (1996). *Analysis of fabrics used in passive restraint systems – Airbags*. Journal of Textile Institute 87 (3): 554 – 571.

[97] SOUTER B.J. (2001). *Effect of fibre architecture on formability of textile performs*. PhD Thesis, University of Nottingham.

[98] LIN H., SHERBURN M., CROOKSTON J., LONG A.C., CLIFFORD M.J., JONES I.A. (2008). *Finite element modelling of fabric compression*. Modelling and Simulation in Materials Science and Engineering 16 (3).

[99] LIN H., CLIFFORD M.J., LONG A.C., SHERBURN M., RAMGULAM R., POTLURI P. (2008). *Finite element modelling of fabric tensile behaviour using automated modelling approach*. Proc. 86th Textile Institute World Conference. Hong Kong.

APPENDIX A PUBLICATIONS

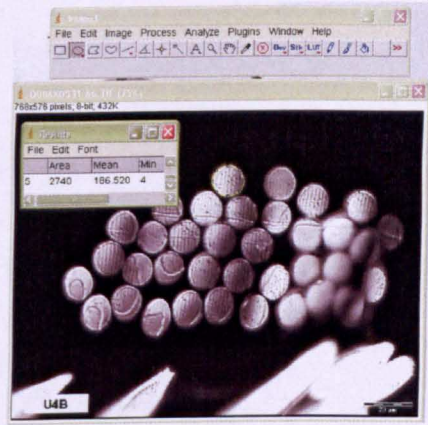
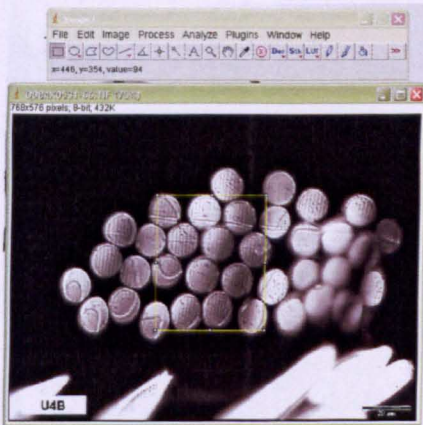
E.SALDAEVA, X.ZENG, M.J.CLIFFORD, H.LIN, A.C.LONG, S.WATSON AND N.RUDDOCK. *Permeability prediction of textiles using analytical methods and computational fluid dynamics.* (in preparation).

APPENDIX B IMAGE J

Figure B.1 shows Image J software window. It is possible to calculate fibre volume fraction using Image J by selecting a certain part of yarn on the image. Image J calculates the area of the yarn part and also the area of each fibre and number of fibres. For each fabric three measurements in different places of images were made to get more accurate results. Then fibre volume fraction is calculated using the following equation:

$$V_f = \frac{\text{Fibre area}}{\text{Yarn area}} \text{Number of fibres (B.1)}$$

U4



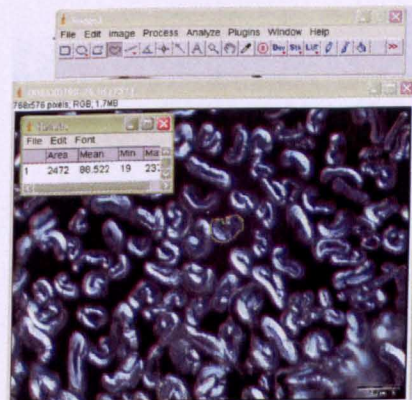
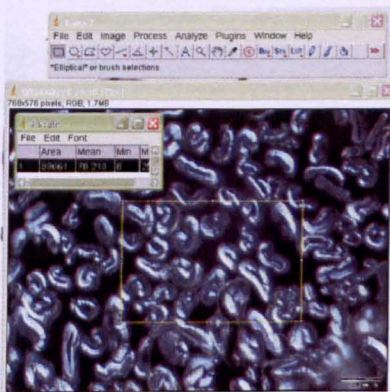
Yarn area = 52530pixel

Fibre area = 2740pixel

Number of fibres = 13

$V_f = 0.68$

U1



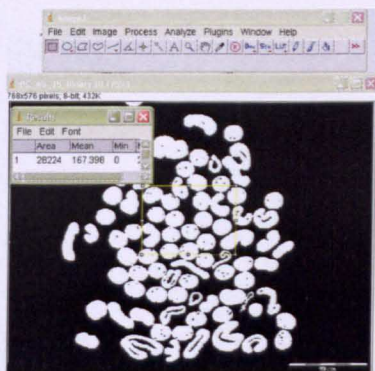
Yarn area = 89661pixel

Fibre area = 2472pixel

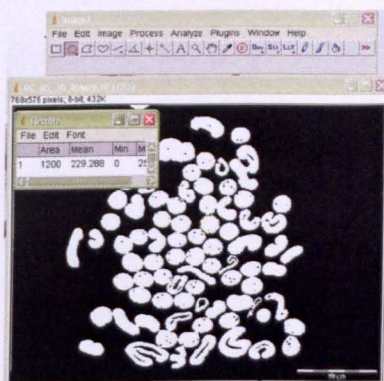
Number of fibres = 21

$V_f = 0.57$

U2



Yarn area = 28224pixel

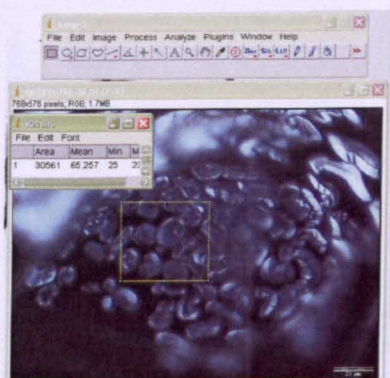


Fibre area = 1200pixel

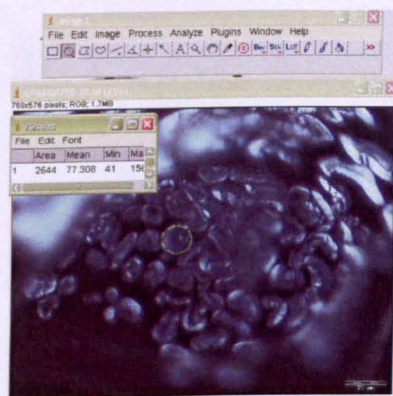
Number of fibres = 14

$$V_f = 0.59$$

U3



Yarn area = 30561pixel

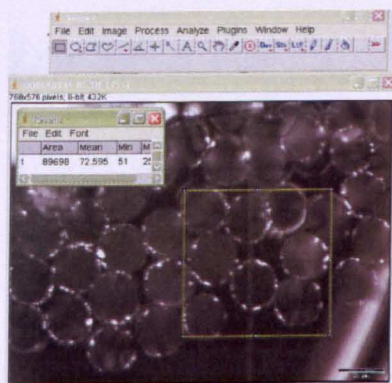


Fibre area = 2644pixel

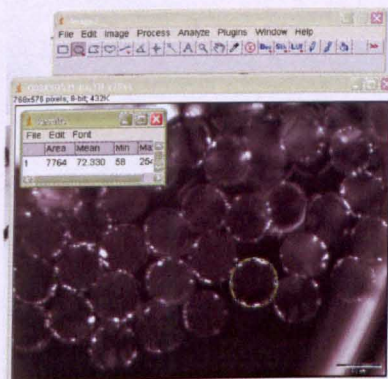
Number of fibres = 8

$$V_f = 0.69$$

A3



Yarn area = 89698pixel

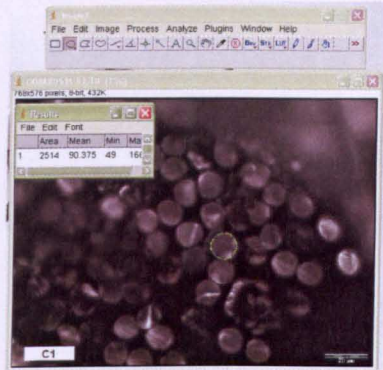
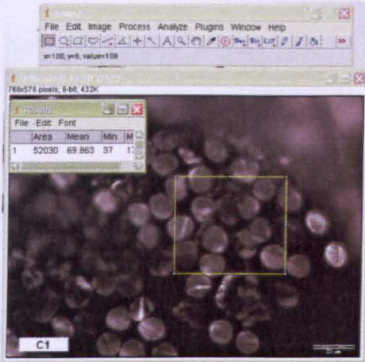


Fibre area = 7764pixel

Number of fibres = 8

$$V_f = 0.69$$

C1



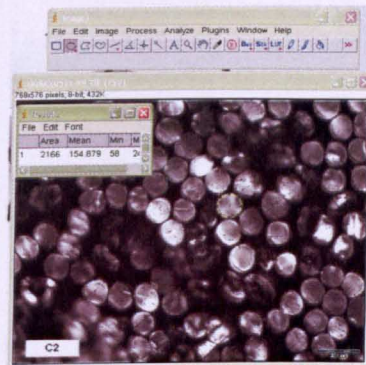
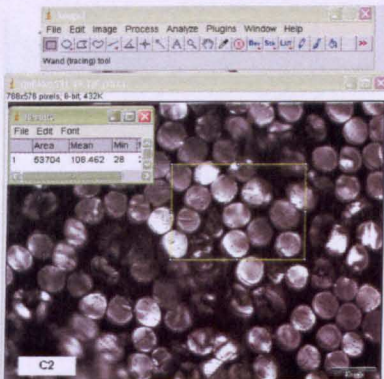
Yarn area = 52030pixel

Fibre area = 2514pixel

Number of fibres = 12

$$V_f = 0.57$$

C2



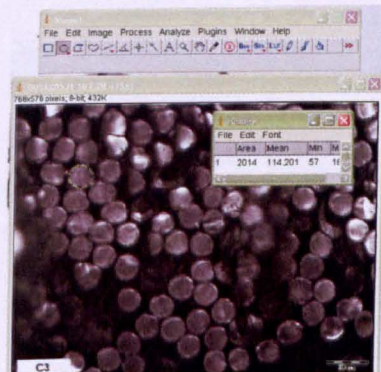
Yarn area = 53704pixel

Fibre area = 2166pixel

Number of fibres = 15

$$V_f = 0.60$$

C3



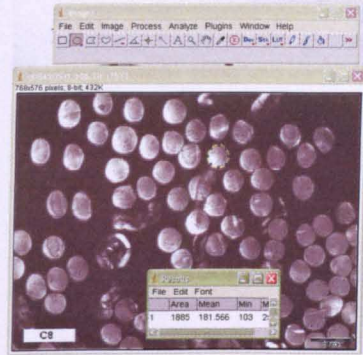
Yarn area = 25398pixel

Fibre area = 2014pixel

Number of fibres = 8

$$V_f = 0.63$$

C8



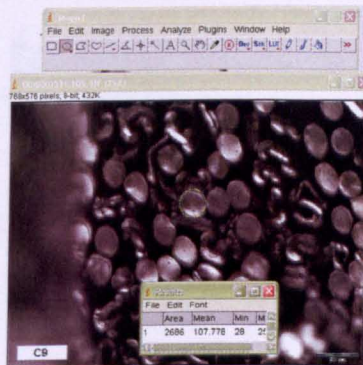
Yarn area = 62329pixel

Fibre area = 1885pixel

Number of fibres = 18

$$V_f = 0.54$$

C9



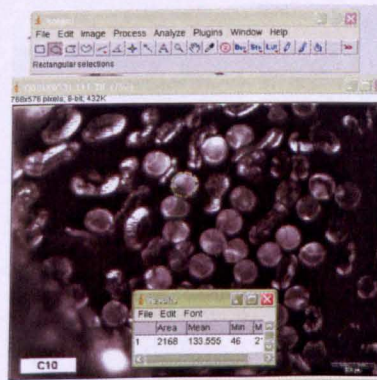
Yarn area = 49887pixel

Fibre area = 2686pixel

Number of fibres = 12

$$V_f = 0.64$$

C10



Yarn area = 64491pixel

Fibre area = 2168pixel

Number of fibres = 16

$$V_f = 0.54$$

Figure B.1 Image J software for fibre volume fraction calculations for selected fabrics

Table B.1 Fibre volume fraction and fibre radius for selected fabrics measured using

Image J

Fabric code	Fibre volume fraction V_f	Fibre radius r μm
U1	0.56	4.3
U2	0.58	5.4
U3	0.64	5.3
U4	0.66	5.8
A3	0.7	10.3
C1	0.56	5.9
C2	0.63	5.9
C3	0.57	5.5
C8	0.61	5.7
C9	0.67	5.6
C10	0.56	5.7

Fibre radius was obtained from as a half of fibre diameter measurements using Image J.

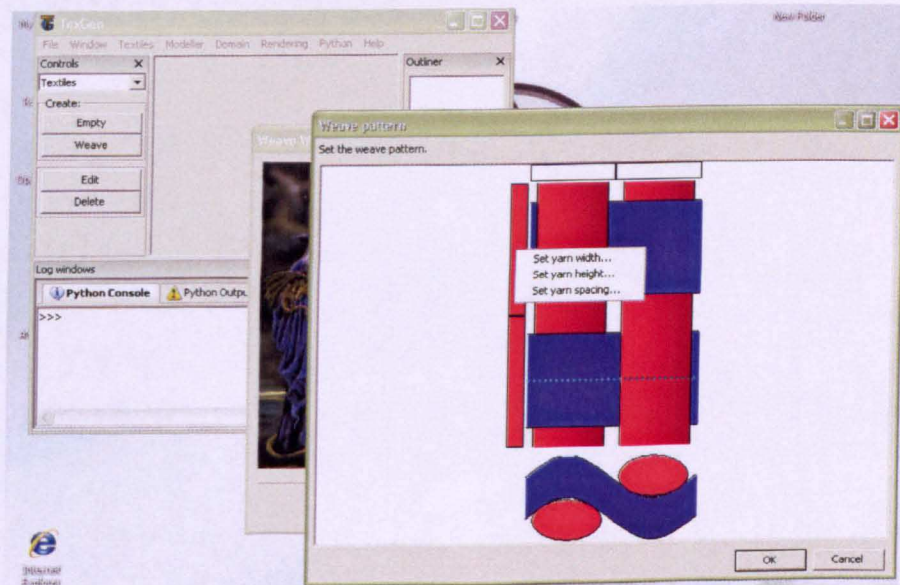
APPENDIX C TEXGEN MODELS

TexGen is software which helps to create unit cell geometry using measured geometric parameters of real fabric. Figure C.1 presents a step by step guide to create unit cell geometry based on geometric parameters for U2 fabric.

Firstly, the number of warp and weft yarns, yarn spacing and yarn width, fabric thickness and gap size were input.



Secondly, if fabric is unbalanced, yarn width, spacing and height need to be chosen separately for warp and weft yarns.



When all geometric parameters are input, TexGen generates the geometric model.

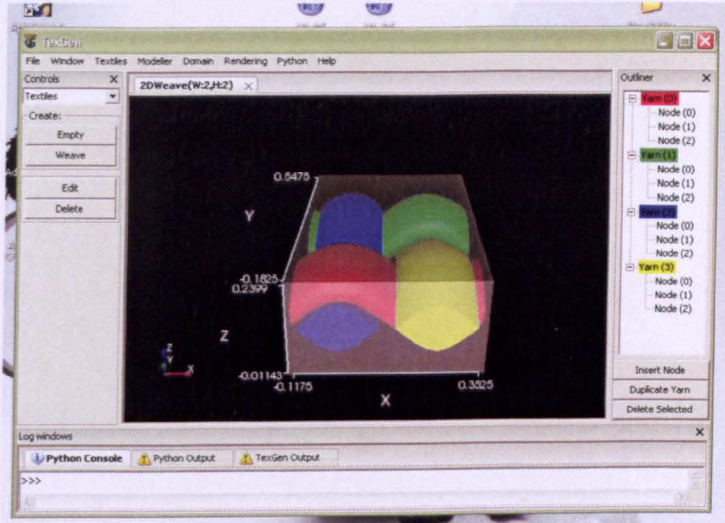
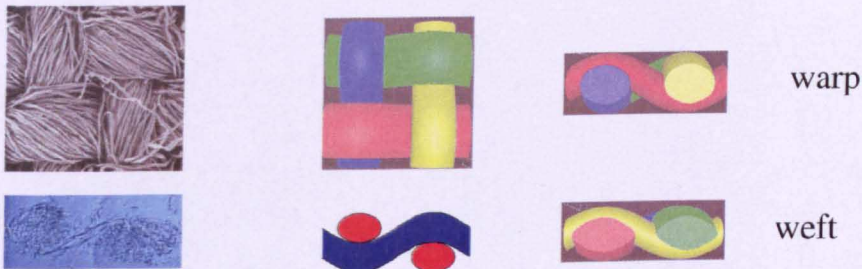
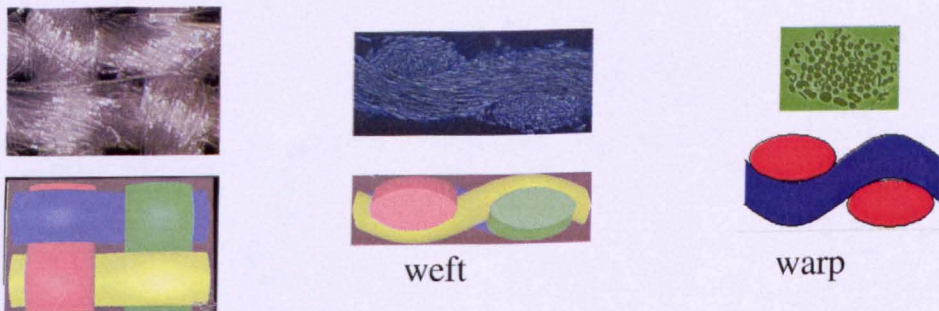


Figure C.1 Creating unit cell geometry for U2 fabric using TexGen

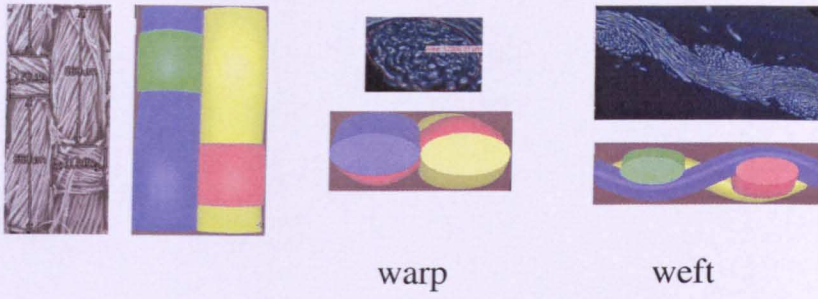
Figure C.2 compares unit cell geometries from microscopic images with ones created in TexGen as described above.



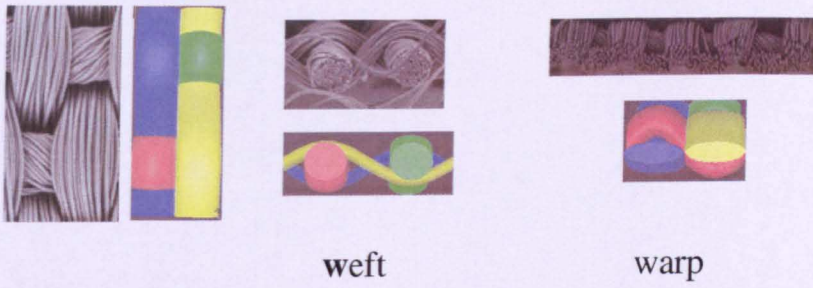
U1



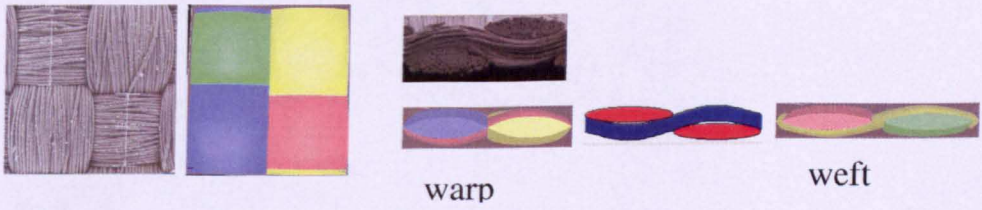
U2



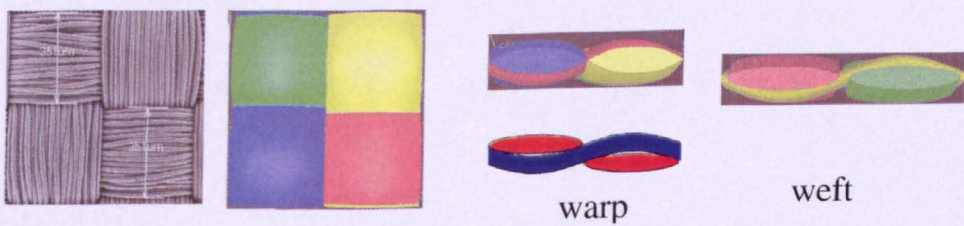
U3



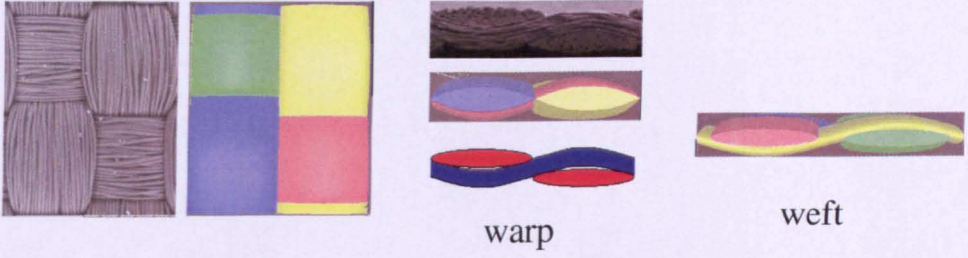
U4



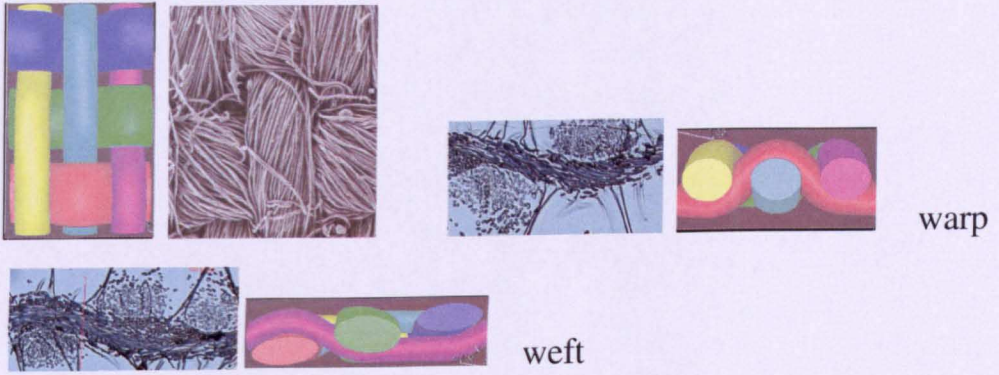
A1



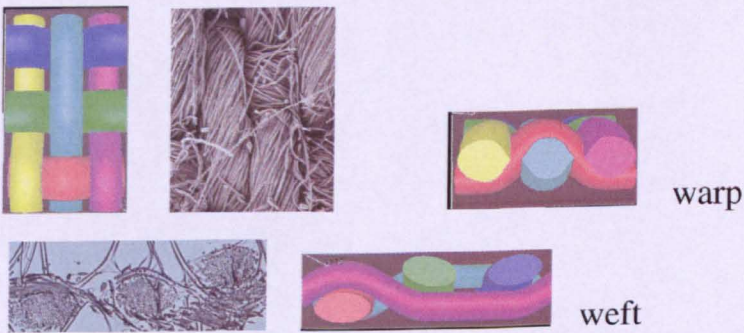
A3



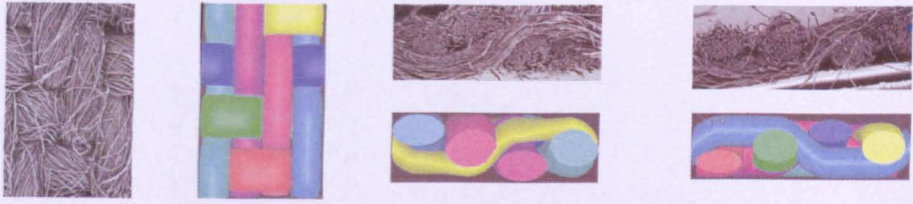
A4



C2



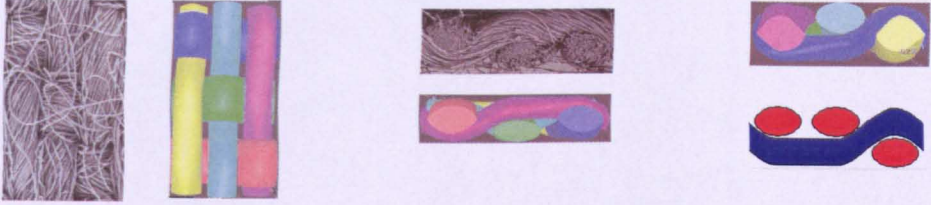
C3



warp

weft

C5



weft

warp

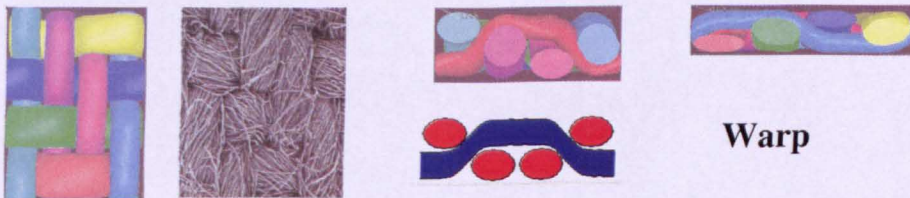
C7



warp

weft

C8



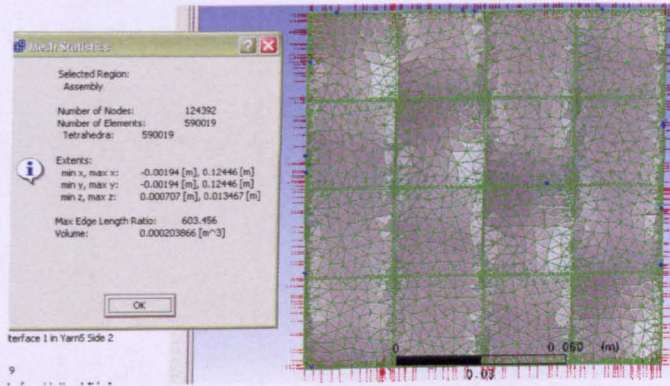
Weft

Warp

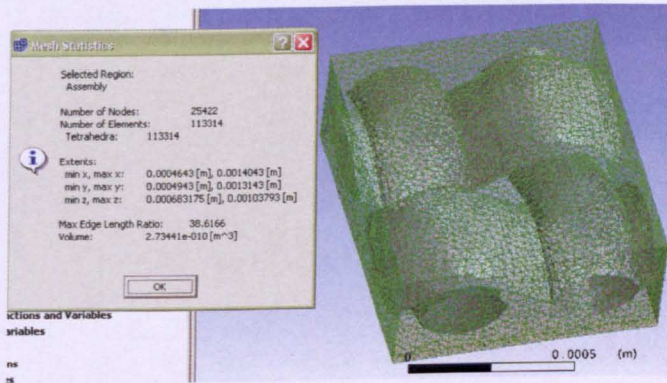
C9

Figure C.2 TexGen modelling of unit cell geometry for selected fabrics.

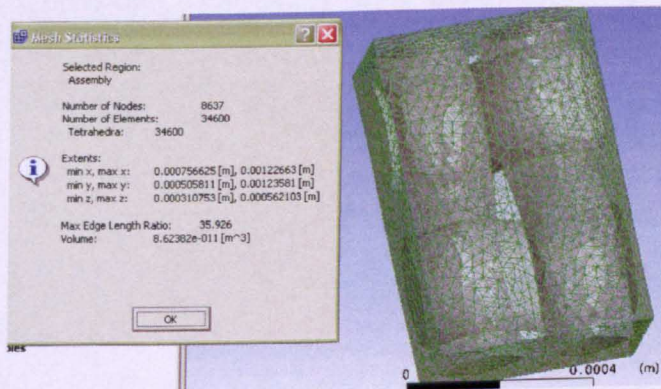
TexGen was used to mesh the unit cell geometries. Figure C.3 shows meshed unit cell geometries with mesh statistics for selected fabrics. Because it is not possible to view meshed geometry in TexGen directly after meshing, CFX 11.0 is used to view the mesh quality and mesh statistics.



Glass fibre



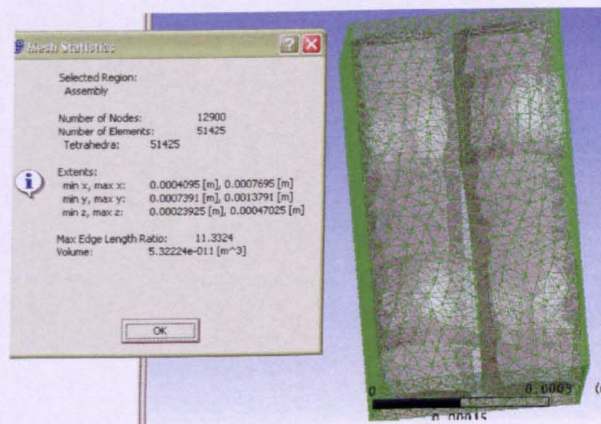
UI



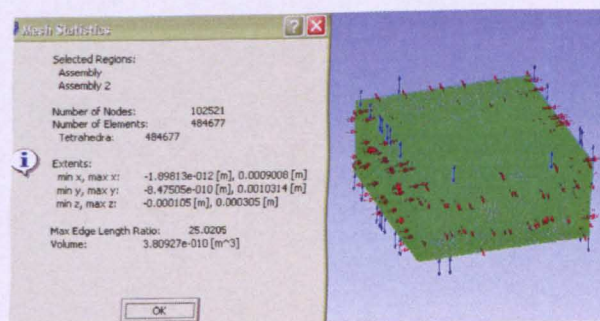
U2



U3

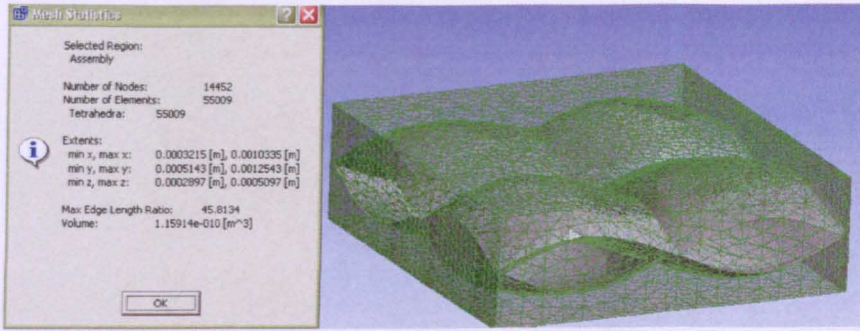


U4

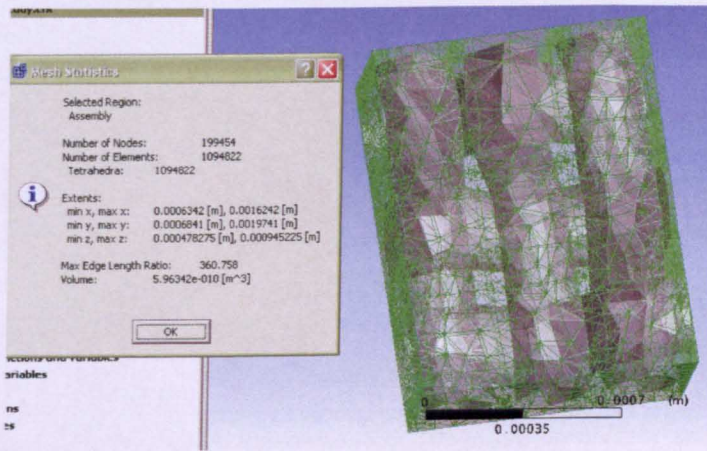


A1

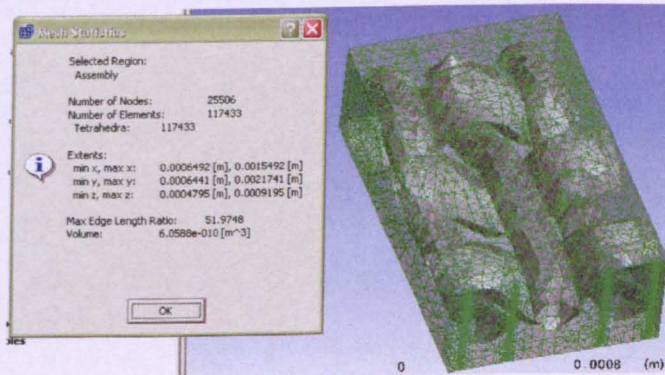
Through thickness air permeability and thermal conductivity analysis for textile materials



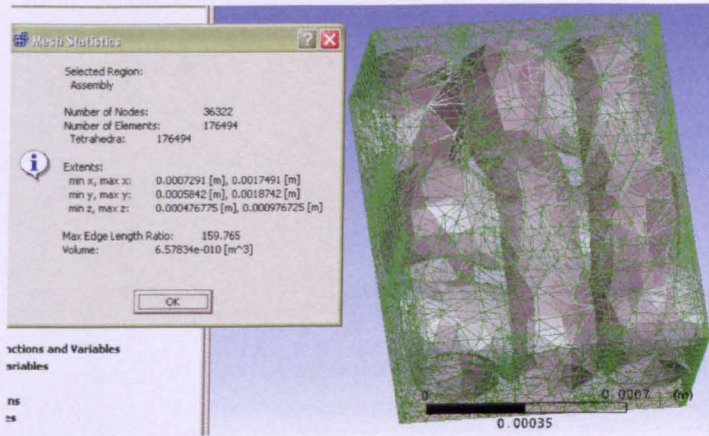
A3



C2



C3



C8

Figure C.3 Meshed geometries of unit cells for selected fabrics

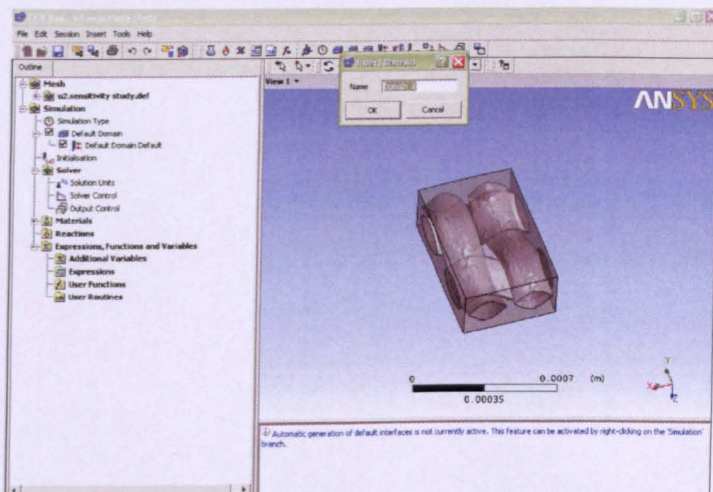
Through thickness air permeability and thermal conductivity analysis for textile materials

APPENDIX D CFX 11.0 SOFTWARE

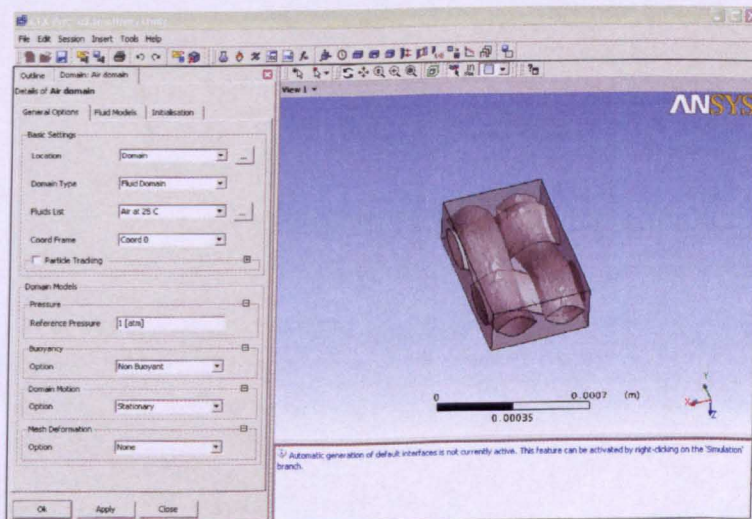
D.1 CFX 11.0 PRE-PROCESSOR

CFX 11.0 Pre-processor allows creating domains, input boundary condition, set up properties of liquid and porous regions. Figure D.1 presents a step by step guide for creating boundary conditions for U2 fabric.

Firstly, the air domain was created with all main parameters input.



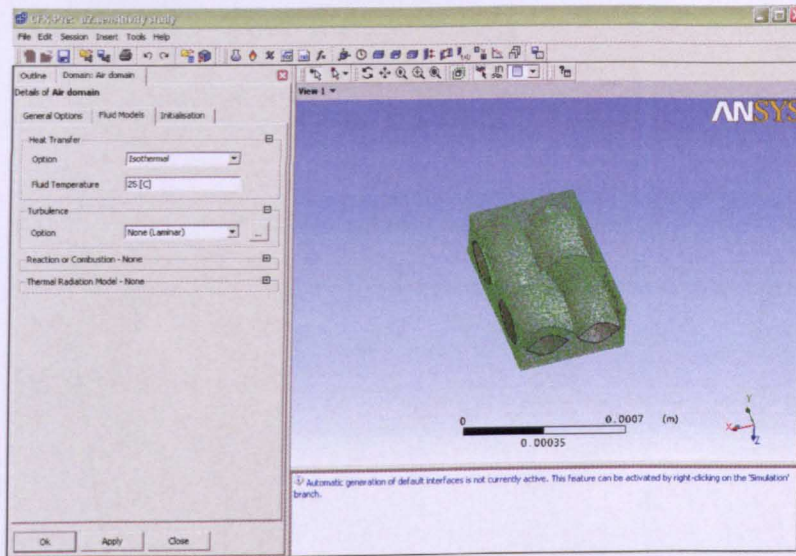
In general options location of the domain, its type and fluid type was chosen.



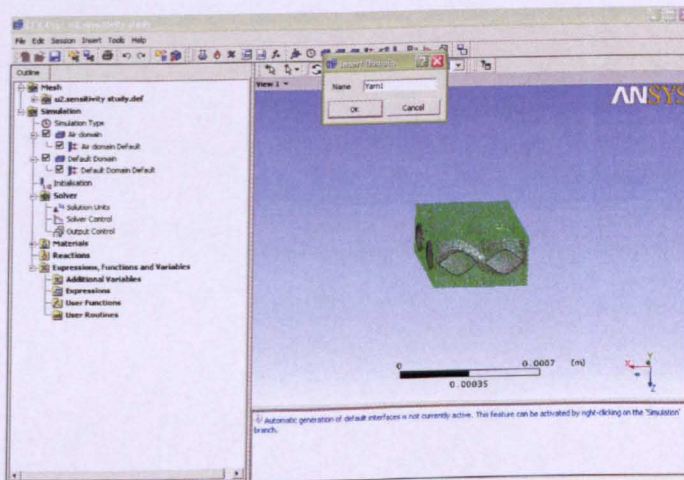
Through thickness air permeability and thermal conductivity analysis for textile materials

In Fluid model options Isothermal condition with fluid temperature 25°C was input.

Turbulence was chosen as “none” which means laminar flow.

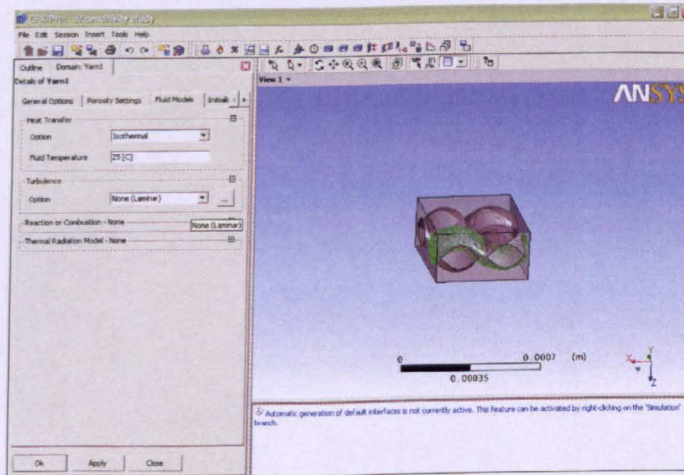
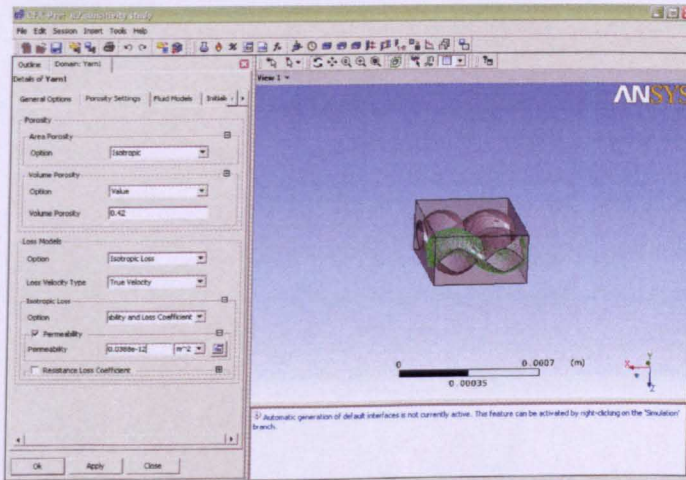
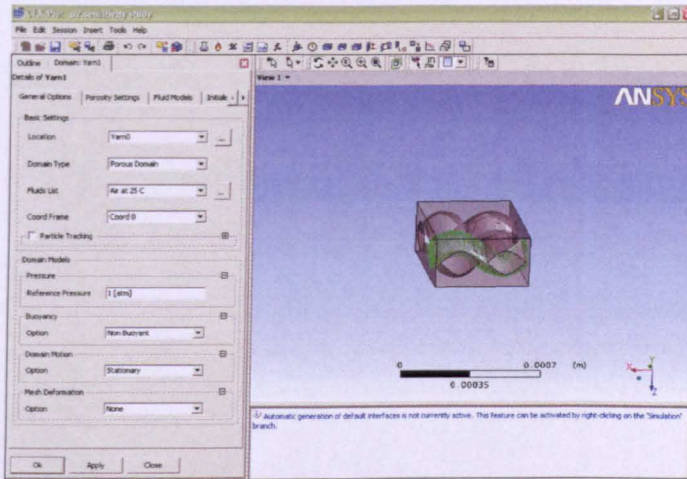


Next yarn domains were created.



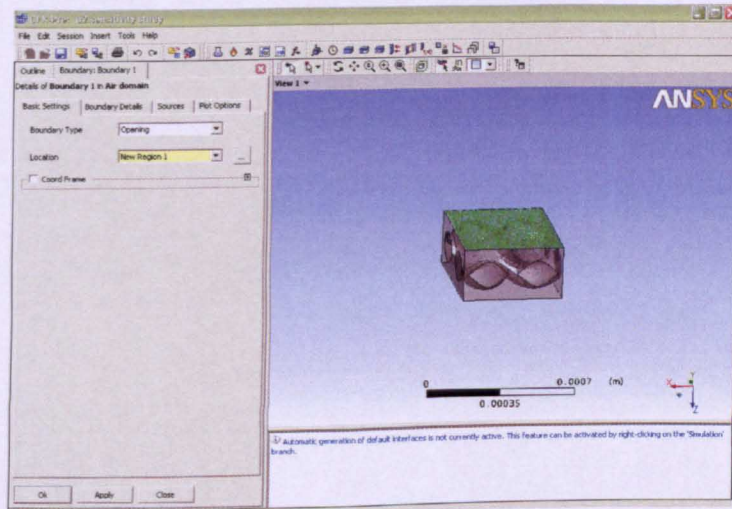
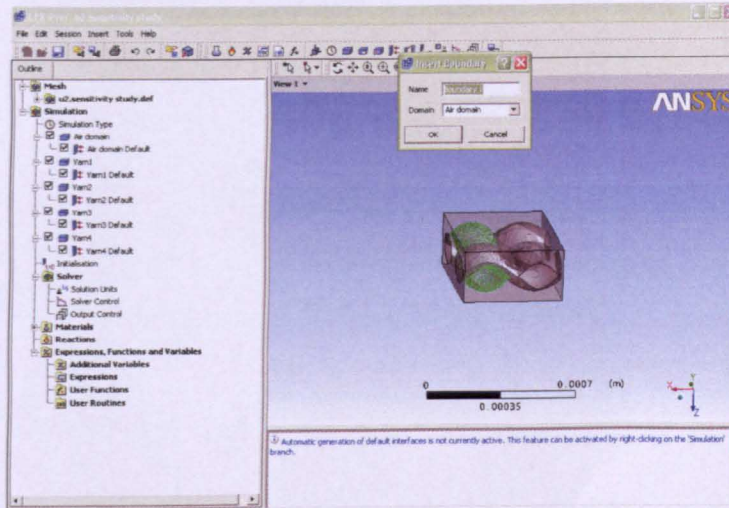
Yarn location and type were chosen. Yarn porosity and yarn permeability were input as calculated in Chapter 3 using Gebart's equation. Fluid model was chosen similar to the model for air domain with laminar flow.

Through thickness air permeability and thermal conductivity analysis for textile materials

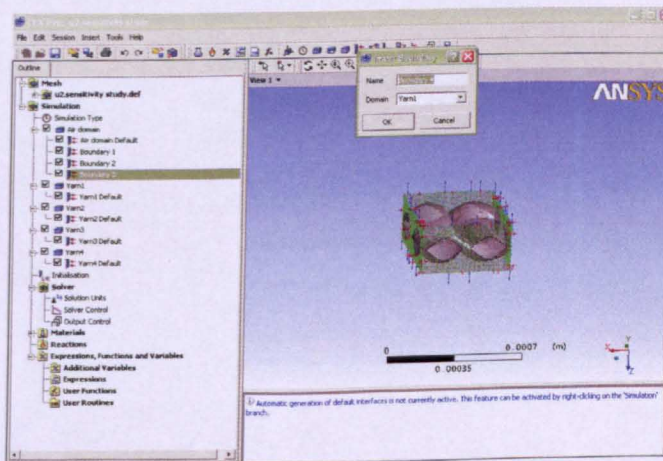
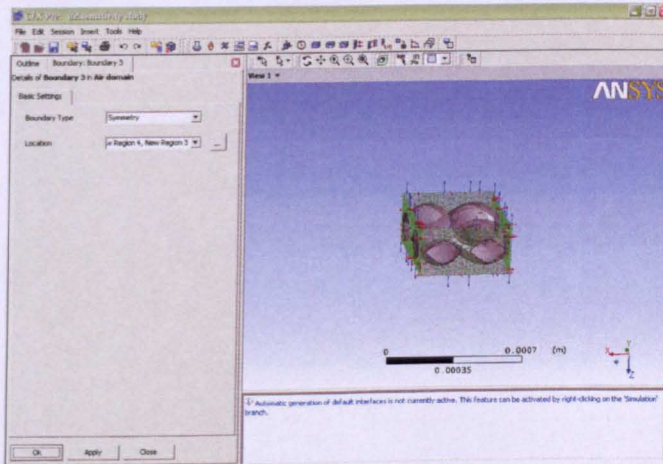
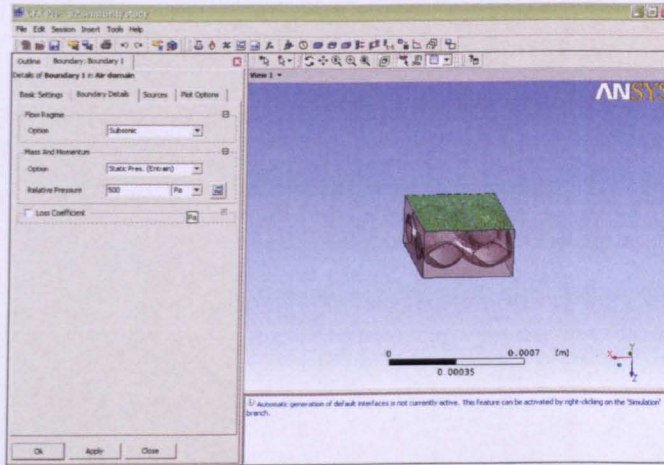


Through thickness air permeability and thermal conductivity analysis for textile materials

Next step was to create boundary conditions for air domain. Opening boundary conditions were chosen for inlet and outlet of air domain, and symmetry boundary conditions for four walls. Inlet pressure was set to 500Pa and outlet pressure – 0Pa.

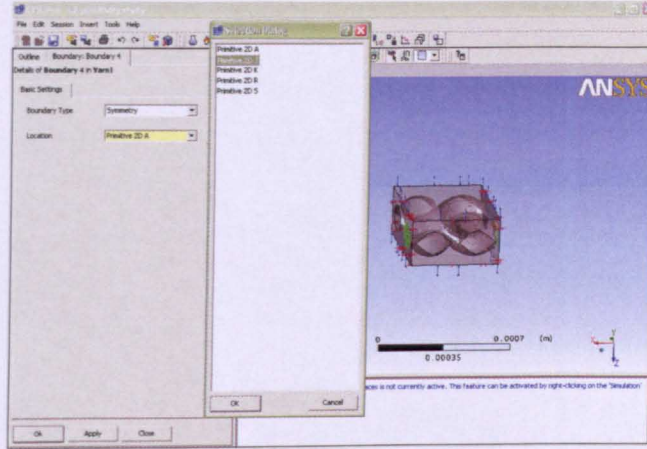


Through thickness air permeability and thermal conductivity analysis for textile materials

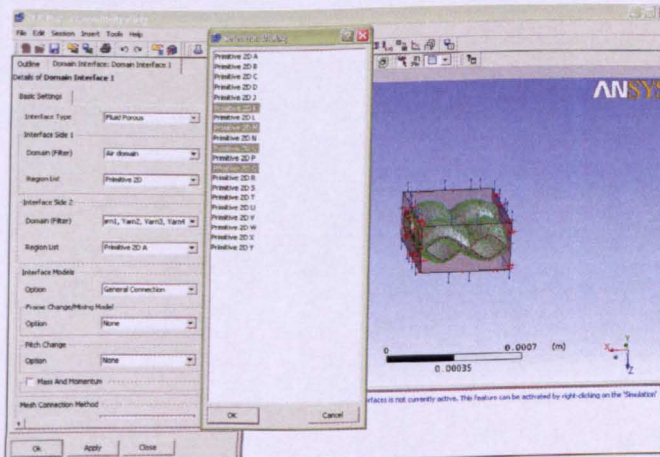
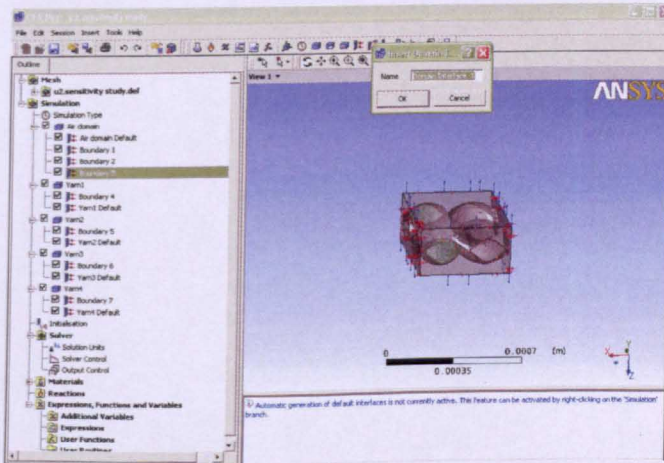


Through thickness air permeability and thermal conductivity analysis for textile materials

Then boundary conditions for the yarns were allocated as symmetry for two vertical sides of the yarns.



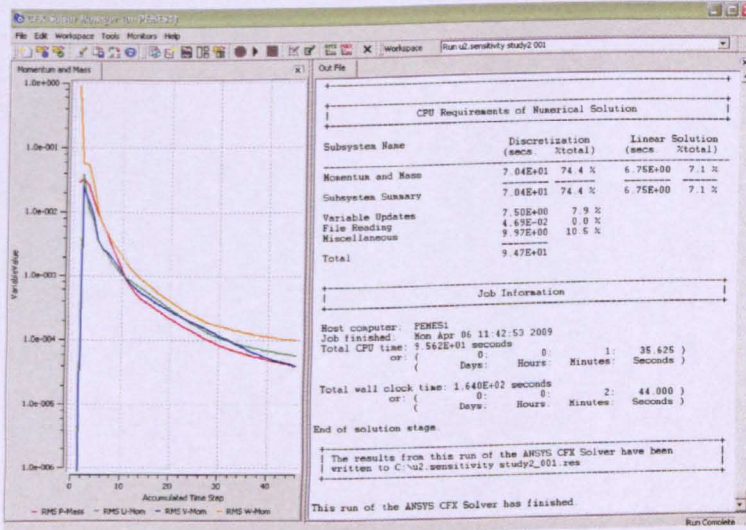
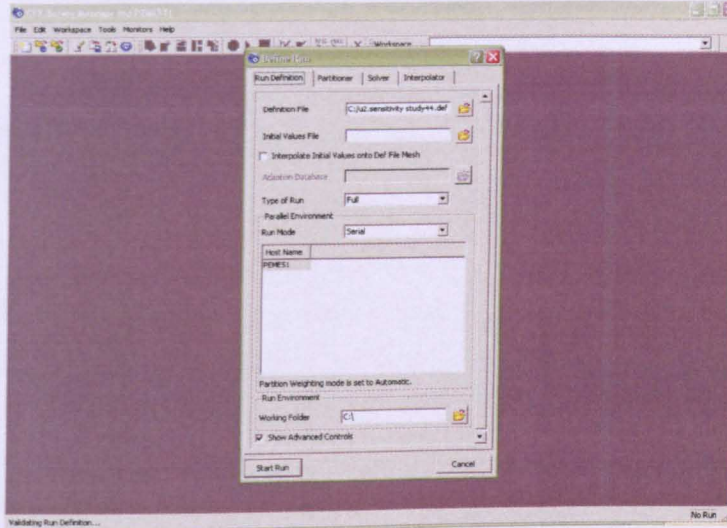
Then interface between air and yarn domains was input.



Through thickness air permeability and thermal conductivity analysis for textile materials

D.2 CFX 11.0 SOLVER

CFX SOLVER opens in new window. Simulation time takes between 30minutes and 10hours depends on number of elements. At the end of simulation solver shows if there is any errors and opens results in new window (CFX Post-processor).



Through thickness air permeability and thermal conductivity analysis for textile materials

```

+-----+
|                               |
|                               |
|                               |
|                               |
+-----+
+-----+
|                               |
|                               |
+-----+
Run mode:    serial run
Host computer: PEMES1
Job started:  Fri Aug 07 12:38:09 2009
+-----+
|   Memory Allocated for Run (Actual usage may be less)   |
+-----+
Data Type   Kwords  Words/Node  Words/Elem   Kbytes  Bytes/Node
Real        28095.4  3252.91    812.01    109747.7  13011.65
Integer     7544.7   873.53    218.05    29471.4   3494.12
Character   2886.6    334.21    83.43     2818.9    334.21
Logical     65.0     7.53     1.88     253.9     30.10
Double     115.8    13.41     3.35     904.7     107.26

```

```

+-----+
|                               |
|                               |
+-----+

```

Domain Name : Air domain

```

Total Number of Nodes           =    4739

Total Number of Elements         =    17966
  Total Number of Tetrahedrons   =    17966

Total Number of Faces           =    6886

Minimum Orthogonality Angle [degrees] =    6.5 !
Maximum Aspect Ratio            =    35.0 OK
Maximum Mesh Expansion Factor    =    62.1 !

```

Domain Name : Yarn1

```

Total Number of Nodes           =    976

Total Number of Elements         =    4259
  Total Number of Tetrahedrons   =    4259

```


Through thickness air permeability and thermal conductivity analysis for textile materials

Total Number of Faces	=	932
Minimum Orthogonality Angle [degrees]	=	42.4 ok
Maximum Aspect Ratio	=	3.9 OK
Maximum Mesh Expansion Factor	=	4.7 OK

Domain Name : Yarn2

Total Number of Nodes	=	959
Total Number of Elements	=	4174
Total Number of Tetrahedrons	=	4174
Total Number of Faces	=	916
Minimum Orthogonality Angle [degrees]	=	42.4 ok
Maximum Aspect Ratio	=	3.6 OK
Maximum Mesh Expansion Factor	=	4.4 OK

Domain Name : Yarn3

Total Number of Nodes	=	979
Total Number of Elements	=	4086
Total Number of Tetrahedrons	=	4086
Total Number of Faces	=	1034
Minimum Orthogonality Angle [degrees]	=	45.4 ok
Maximum Aspect Ratio	=	4.2 OK
Maximum Mesh Expansion Factor	=	4.1 OK

Domain Name : Yarn4

Total Number of Nodes	=	984
Total Number of Elements	=	4115
Total Number of Tetrahedrons	=	4115
Total Number of Faces	=	1036
Minimum Orthogonality Angle [degrees]	=	36.9 ok
Maximum Aspect Ratio	=	4.1 OK
Maximum Mesh Expansion Factor	=	4.6 OK

Through thickness air permeability and thermal conductivity analysis for textile materials

Global Statistics :

Global Number of Nodes	=	8637
Global Number of Elements	=	34600
Total Number of Tetrahedrons	=	34600
Global Number of Faces	=	10804
Minimum Orthogonality Angle [degrees]	=	6.5 !
Maximum Aspect Ratio	=	35.0 OK
Maximum Mesh Expansion Factor	=	62.1 !

Domain Interface Name : Domain Interface 1

Non-overlap area fraction on side 1	=	3.35E-01
Non-overlap area fraction on side 2	=	3.35E-01

CFD Solver started: Fri Aug 07 12:39:24 2009

```

+-----+
|           Convergence History           |
+-----+
=====
|           Timescale Information          |
+-----+
| Equation | Type      | Timescale |
+-----+-----+-----+
| U-Mom-Air domain | Auto Timescale | 1.80845E-05 |
| V-Mom-Air domain | Auto Timescale | 1.80845E-05 |
| W-Mom-Air domain | Auto Timescale | 1.80845E-05 |
| U-Mom-Yarn1      | Auto Timescale | 1.80845E-05 |
| V-Mom-Yarn1      | Auto Timescale | 1.80845E-05 |
| W-Mom-Yarn1      | Auto Timescale | 1.80845E-05 |
| U-Mom-Yarn2      | Auto Timescale | 1.80845E-05 |
| V-Mom-Yarn2      | Auto Timescale | 1.80845E-05 |
| W-Mom-Yarn2      | Auto Timescale | 1.80845E-05 |
| U-Mom-Yarn3      | Auto Timescale | 1.80845E-05 |
| V-Mom-Yarn3      | Auto Timescale | 1.80845E-05 |
| W-Mom-Yarn3      | Auto Timescale | 1.80845E-05 |
| U-Mom-Yarn4      | Auto Timescale | 1.80845E-05 |
| V-Mom-Yarn4      | Auto Timescale | 1.80845E-05 |
| W-Mom-Yarn4      | Auto Timescale | 1.80845E-05 |
+-----+-----+-----+

```

Through thickness air permeability and thermal conductivity analysis for textile materials

=====

OUTER LOOP ITERATION = 1 CPU SECONDS = 8.281E+00

Equation	Rate	RMS Res	Max Res	Linear Solution
U-Mom	10.00	4.2E-08	3.5E-07	1.4E+04 ok
V-Mom	10.00	3.9E-08	3.9E-07	1.4E+04 ok
W-Mom	10.00	7.7E-01	3.9E+00	3.7E-03 OK
P-Mass	10.00	4.1E-02	2.0E-01	9.1 2.4E-02 OK

=====

OUTER LOOP ITERATION = 2 CPU SECONDS = 1.053E+01

Equation	Rate	RMS Res	Max Res	Linear Solution
U-Mom	99.99	3.2E-02	3.9E-01	1.3E-02 OK
V-Mom	99.99	2.1E-02	2.4E-01	3.9E-02 OK
W-Mom	10.07	5.0E-02	5.9E-01	3.9E-02 OK
P-Mass	10.77	3.1E-02	4.9E-01	5.1 7.0E-02 OK

=====

OUTER LOOP ITERATION = 3 CPU SECONDS = 1.244E+01

Equation	Rate	RMS Res	Max Res	Linear Solution
U-Mom	10.66	2.1E-02	5.1E-01	2.2E-02 OK
V-Mom	10.87	1.8E-02	2.5E-01	2.8E-02 OK
W-Mom	11.01	5.0E-02	3.7E-01	2.6E-02 OK
P-Mass	10.83	2.6E-02	3.9E-01	5.1 6.5E-02 OK

=====

OUTER LOOP ITERATION = 63 CPU SECONDS = 1.234E+02

Equation	Rate	RMS Res	Max Res	Linear Solution
U-Mom	10.99	5.0E-05	2.4E-03	2.8E-03 OK
V-Mom	10.98	1.9E-05	6.9E-04	1.1E-02 OK
W-Mom	11.00	1.0E-04	3.8E-03	1.4E-03 OK
P-Mass	10.98	2.5E-05	4.5E-04	5.1 1.6E-02 OK

Through thickness air permeability and thermal conductivity analysis for textile materials

=====

OUTER LOOP ITERATION = 64 CPU SECONDS = 1.253E+02

Equation	Rate	RMS Res	Max Res	Linear Solution
U-Mom	10.99	14.9E-05	12.4E-03	2.7E-03 OK
V-Mom	10.98	11.9E-05	16.8E-04	1.1E-02 OK
W-Mom	11.00	11.0E-04	13.8E-03	1.3E-03 OK
P-Mass	10.98	2.4E-05	4.5E-04	5.1 1.6E-02 OK

CFD Solver finished: Fri Aug 07 12:41:24 2009

CFD Solver wall clock seconds: 1.2000E+02

Average Scale Information

Domain Name : Air domain

Global Length = 3.4796E-04
 Minimum Extent = 2.5135E-04
 Maximum Extent = 7.3000E-04
 Density = 1.1850E+00
 Dynamic Viscosity = 1.8310E-05
 Velocity = 7.3744E+00
 Advection Time = 4.7185E-05
 Reynolds Number = 1.6607E+02

Domain Name : Yarn1

Global Length = 2.2388E-04
 Minimum Extent = 2.2586E-04
 Maximum Extent = 4.7000E-04
 Density = 1.1850E+00
 Dynamic Viscosity = 1.8310E-05
 Velocity = 9.0753E-03
 Advection Time = 2.4669E-02
 Reynolds Number = 1.3150E-01

Domain Name : Yarn2

Global Length = 2.2387E-04
 Minimum Extent = 2.2587E-04
 Maximum Extent = 4.7000E-04
 Density = 1.1850E+00
 Dynamic Viscosity = 1.8310E-05
 Velocity = 9.4740E-03
 Advection Time = 2.3630E-02

Through thickness air permeability and thermal conductivity analysis for textile materials

Reynolds Number = 1.3727E-01

Domain Name : Yarn3

Global Length = 2.2129E-04
Minimum Extent = 1.9500E-04
Maximum Extent = 7.3000E-04
Density = 1.1850E+00
Dynamic Viscosity = 1.8310E-05
Velocity = 1.9107E-02
Advection Time = 1.1582E-02
Reynolds Number = 2.7363E-01

Domain Name : Yarn4

Global Length = 2.2125E-04
Minimum Extent = 1.9500E-04
Maximum Extent = 7.3000E-04
Density = 1.1850E+00
Dynamic Viscosity = 1.8310E-05
Velocity = 1.7971E-02
Advection Time = 1.2312E-02
Reynolds Number = 2.5733E-01

-----+
| Job Information |
-----+

Host computer: PEMES1

Job finished: Fri Aug 07 12:41:26 2009

Total CPU time: 1.285E+02 seconds

or: (0: 0: 2: 8.484)

(Days: Hours: Minutes: Seconds)

Total wall clock time: 1.970E+02 seconds

or: (0: 0: 3: 17.000)

(Days: Hours: Minutes: Seconds)

End of solution stage.

Through thickness air permeability and thermal conductivity analysis for textile materials

D.3 CFX 11.0 POST-PROCESSOR

The results of the simulation can be seen in CFX 11.0 Post processor. It is possible to create a streamline to see the behaviour of the flow. It is also possible to see the whole report of the current simulation and calculate velocity or pressure drop in the unit cell.

